Ministry of Higher Education and Scientific Research

Monastir University

THESIS

Presented to fulfill the doctor degree requirements from the

FACULTY OF SCIENCES OF MONASTIR
In Physics

By Kaouther Ben Ltaifa

Heat transfer by a flow of a Nanofluid in a porous system

Publicly defended on December 29, 2022

Jury Members

Mr. Adel Kalboussi	**Professor**	**FSM, faculty of Science of Monastir, Monastir**	**Chair**
Mr. Ammar Hidouri	**Associate-Professor**	**Faculty of Science of Gafsa, Gafsa**	**Reviewer**
Mr. Gazzeh Hichem	**Associate-Professor**	**FSM, faculty of Science of Monastir, Monastir**	**Reviewer**
Mr.Rachid Said	**Professor**	**IPEIM ,Monastir**	**Examinator**
Mr. Hacen Dhahri	**Professor**	**ENIM, Monastir**	**Supervisor**

Laboratory for the Study of Thermal and Energy Systems (LESTE) LR99ES31

Acknowlagement

I wish to express deep gratitude to my supervisor **Hacen Dhahri**, professor at ENIM National Engineering School of Monastir University of Monastir, Tunisia, for his invaluable supervision and insight throughout the research process and for all the patience and support you gave me since the first day of my thesis completion. His consistent trust during my thesis work is greatly appreciated.

I would like to thank **Annunziata D'Orazio**, associate professor at University of Rome Sapienza, Italy, for accepting me as a visitor scholar and researcher in his Laboratory and the useful advice and support, for co-supervising, generously providing guidance and for all the patience and support you gave me. She was always there to lend a helping hand in this thesis.

I would like to thank **Arash Karimipour**, professor at Islamic Azad University, Najafabad, Iran, for his help, advice and support.

I would like to thank **Hassane Naji**, professor at University of Artois and University of Lille, France, for his help, advice and support.

I would like to thank **Adel kalboussi**, professor at Faculty of sciences of Monastir, University of Monastir, who has kindly accepted to be the president of the jury evaluating my thesis work.

I would thank also my committee members **Ammar Hidouri,** associate-Professor at FSG faculty of sciences of Gafsa, University of Gafsa, and **Mohamed Hichem Gazzeh,** associate-rofessor at FSM, Faculty of sciences of Monastir, University of Monastir, for accepting to review my thesis. Their critical reviews and evaluations of my work resulted in the success of this PhD thesis.

Many thanks are also addressed to **Rachid Said**, professor at IPEIM preparatory institute for engineering studies of Monastir, University of Monastir, for accepting to examine this thesis.

I dedicate this thesis to the memory of my father **Abdelaziz**.

Special thanks to my family, words cannot express how grateful I am to my Mother **Souad,** my mother in law **Fouzia,**my sister in law **Akila,** my husband **Mohamed Essayed** and my daughter **Lina** for unconditional support, prayers for me all the time and encouragement to pursue my interests. This thesis is dedicated to them. No dedication can express the love, esteem, dedication and respect that I have always had for you. Nothing in the world is worth the efforts provided day and night for my education and my well-being. This work is the fruit of your sacrifices that you have made for my education and training.

I am deeply thankful to my sister **Manel** and my brothers **Mahmoud**, **Haytherm** and **Gassene** for their supports, sacrifices and help throughout my life. You have always been a major source of support when things would get a discouraging.

A special dedication for my nieces **Nour**, **Kenza** and **Lynda**. No words could express my love and my attachment to you. Certainly it seems fast but I had the privilege and the luxury to attend your birth and I felt full of feelings and love for you from the first day .I will never stop watching over you, playing with you, and taking care of you. I love you my princesses.
Without family kind support, it would be impossible for me to complete my PhD.

Table of Contents

List of Figures

List of Tables

General introduction

Recently, large attention is focused on fabrication and use of micro devices. The small structure properties as well as high efficiency of these systems – such as microsensors, microvalves and micro pumps – are some of the benefits of using MEMS and NEMS (Micro and Nano Electro Mechanical Systems).MEMS are mechanical systems comprising at least one component of micrometric size. This component can be a pipe, the seat of a flow, the dimension of which is of the order of a few microns.

In the case of flows in micro channels (**figure.1.1**), many effects can no longer be neglected as is often the case on a macroscopic scale. These effects include: viscous dissipation, slip velocity and temperature jump at the top-bottom walls, the zone of simultaneous development of thermal and dynamic boundary layers, owing to the large surface / volume ratio in these micro systems. In particular, because of the confinement, the friction of the fluid induces a release of heat such as to modify the thermal field.

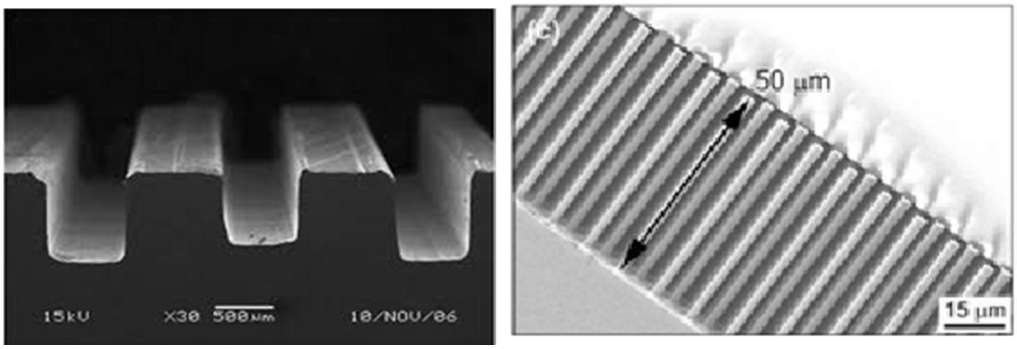

Figure 1. 1: Photos of the micro-channels taken under an electron microscope [1,2]

The classification of different gas of the flow regimes is as follows:

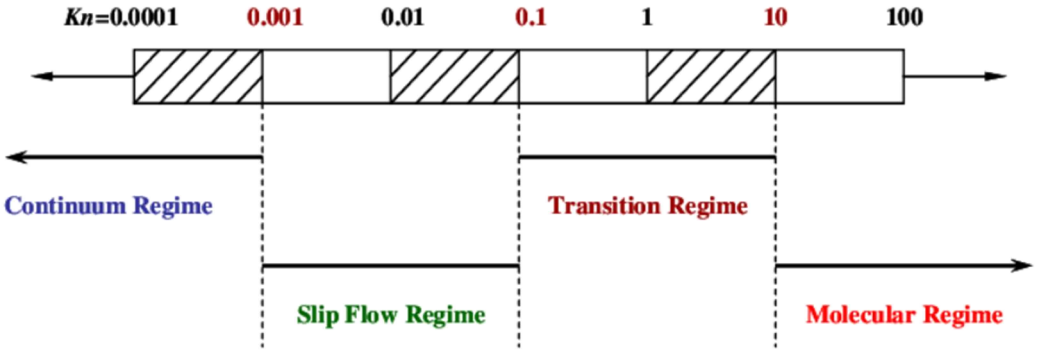

Figure 1. 2: Classification of flow regimes with Knudsen number [3]

Due to the phenomenon of dilution (high Knudsen number), the gaz density changes along the channel and the velocity of flow near the wall is different from to the velocity at the wall. This means that there is a certain slippage on the rigid borders. Due to the slip condition the flow rate is greater than a certain amount which is predicted by the Navier-Stokes equation with the slip

boundary condition.

The need to improve the heat transfer of fluids gave rise to the development of a new class, called nanofluids. These are solutions containing nanoparticles suspended in a base fluid. Thanks to their properties which improve thermal performance.

The main objectives of this thesis reside in the study of the flow and heat transfer under local thermal equilibrium conditions taking into account the viscous dissipation effects. In addition, the improve of the performance of a system through a comprehensive minimization of adverse effects is done. The latter is a thermodynamic approach that is used to optimize thermally engineered devices for high energy efficiency. Optimization can therefore be performed to reduce the production of entropy in the system, which leads to the optimum engineering design that makes the process of thermodynamics and heat transfer more applicable.

This thesis is laid out as follows:

Chapter 1 Microfluids systems, nanofluids and porous media.

This chapter covrs a bibliographical analysis on the notion of the micro system, nanofluid and porous media. Admittedly, the characteristics and textures of these flows constitute a basis for the study of transport phenomena in thermal systems.

Chapter 2 Forced convection heat transfer by a flow of nanoffluid in a micro-channel using the lattice Boltzmann method.

The second chapter deals with heat transfer in a micro-channel by a flow of a nanofluid. The partial differential equations which govern this physical phenomenon are solved by the Lattice Boltzmann method. The numerical results relating to the dynamic and thermal fields are presented and analyzed.

Chapter 3 Heat transfer by a flow of nanofluid in a porous macro-channel

A fine thermal analysis must be based on a mesoscale approach applied at a micro scale level constitues the third chapter. The thermal Lattice Boltzmann method (TLBM) of multi distribution functions (MDF) was used to treat the convective heat flux and entropy generation in a channel with high-low isothermal walls and filled with a nanofluid (Cu/Water). It has been extended to simulate the flow governed by the Darcy brinkmann forchheimer (BFD) using the hypothesis of local termal equilibrium (LTE). The effects of nanoparticle volume fraction, Darcy number, porosity, heat capacity ratio and thermal conductivity ratio on heat transfer; entropy generation, average Nusselt number and Bejan number are studied.

Chapter 4 Mixed convection heat transfer in a rectangular inclined microchannel totally filled with nanofluid

A numerical analysis has been carried out of the heat transfer by mixed convection for a laminar

flow in an inclined rectangular microchannel completely filled with a nanofluid Al2O3 / Water represents the continuation of this fourth chapter. The conservation equations are translated the thermal relaxation time and it modifies Boltzmann's lattice method with dual distribution functions. Viscous dissipation effects are adapted to the energy equation. Effects of nanoparticle volume fractions and inclination angles on the Nanofluid flow and heat transfer are studied. The results obtained are presented in terms of streamlines, isotherms, slip velocity, wall temperature, and Nusselt number. The results show that the higher values of the volume fraction of Al2O3 and the higher values of inclination angles improve the rate of heat transfer.

References

[1] DE LOOS, S. R. A., VAN DER SCHAAF, J., TIGGELAAR, Roald M., et al. Gas–liquid dynamics at low Reynolds numbers in pillared rectangular micro channels. Microfluidics and nanofluidics, 2010, vol. 9, no 1, p. 131-144.

[2]PRAKASH, Shashi et KUMAR, Subrata. Fabrication of microchannels: a review. Proceedings of the Institution of Mechanical Engineers, Part B: Journal of Engineering Manufacture, 2015, vol. 229, no 8, p. 1273-1288.

[3] DONGARI, Nishanth, SHARMA, Ashutosh, et DURST, Franz. Pressure-driven diffusive gas flows in micro-channels: from the Knudsen to the continuum regimes. Microfluidics and nanofluidics, 2009, vol. 6, no 5, p. 679-692.

Chapter 1: Microfluids systems, nanofluids and porous media

1. Introduction

Microfluidics is a novel topic. It really appeared as a discipline in the 2000s with a dazzling rise in innovative constructions and in the number of publications. This development is caused by the demand in many life science fields such as medicine, chemistry and the environment. They can be represented either as a science (study of the performance of fluids in micro-channels) and as a technology for manufacturing systems for laboratories on chips ("lab on chip") in the field of physics, chemistry and biology. These devices incorporate a number of miniaturized components permitting the study and analysis of chemical or biological samples. True “microprocessors for biology”, they allow bulky and very expensive instruments to be replaced. Microfluidics represents for biology and chemistry a revolution similar to that brought by microprocessors to electronics and data processing. [1-3].

For ten years or so, man has imitated nature by producing objects crossed by micrometric flows. In general, the micron-scale handling makes it possible to work faster, at lower cost, in a suitable and safer environment. There are different forms and applications of microfluidics systems (**figure.1.3** and **table 2.1**).

Nevertheless, progress in the various fields of microfluidics is still quite heterogeneous. The first ones devices offered commercially or in laboratories generally perform only one standard operation at a time, whether of biological, chemical or even physical benefit. There are thus several prototypes of microfluidic devices for PCR (polymerase chain reaction), immunological analysis or electrophoresis. Numerous “technological bricks” concerning different issues of microfluidic analysis and manipulation, such as micro fabrication and rapid prototyping [4–6], mixers (diffusive, chaotic,..), pumps, valves and many more are being developed in research laboratories. Research is also focused on devices with a limited number of functionalities, but interested in diversifying the problems and the subjects of study, in particular in the direction of proteomic analysis, and cell culture or analysis.

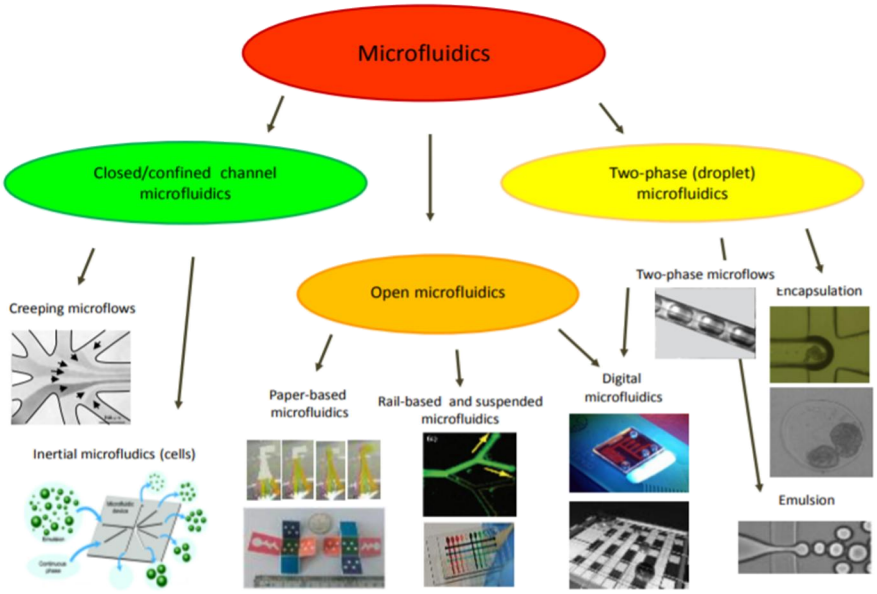

Fig.1. 3 Different forms of microfluidics and their different applications

Table 1.1: Applications of microfluidics systems

Areas of application	**Applications**
Automobile	Air-bag, puncture detection, syst. Anti-collision. Injection pressure, traction control, active suspensions. Air conditioning locks,..
Medical	Administration of substances. Accelerometer for pacemakers, Monitoring (blood gas sensor...). Biological analysis. Minimally invasive surgery.
Aeronautics and Defense	Instrumentation: gyrometer, altimeter ... Guidance systems, missiles and ammunition
Electro / Domotique	Electro / Home automation Intrusion security, gas leak, ambient sensor...
Environment	Physico-chemical sensors, water control ...
Instrumentation	Instrumentation Measurements of physical quantities: Ph, Nose eln, humidity, preventive maintenance
Equipment multimedia	Multimedia equipment Inkjet cartridges, mobiles, camcorder stabilization, …

1.1 Specificity of gaseous micro-flow: effects of rarefaction

In microfluidics, knowledge of gaseous micro-flows is currently more advanced than that of liquid micro-flows. With regard to gases, the problem is indeed more clearly identified: the main micro-effect resulting from the high containment is the rarefaction of the flow (reducing sizes in microsystems). This generates a thermodynamic imbalance because the mean free path λ (average distance traveled by the molecule between 2 successive collisions) is no longer

negligible compared to the characteristic length Lc of the microsystem. For a low level of rarefaction, this thermodynamic imbalance essentially results in a not inconsiderable temperature jump and slip velocity at the top-bottom walls. The corresponding regime is called the slip regime (**figure 1.4**). For a more marked rarefaction, the thermodynamic imbalance is no longer confined to the walls but concerns the entire flow. The interest in rarefied flows was originally linked to studies of low pressure flows in the upper atmospheric layers for space applications [7]. The level of rarefaction is quantified by a dimensionless number, the Knudsen number:

$$K_n = \frac{\lambda}{L_c} \qquad \textbf{(1.1)}$$

Where L_c represents a dimension characteristic of the volume in which the molecules are contained. More L_c decreases, more the rate of rarefaction increases.

The mean free path λ represents the mean distance traveled by a molecule between two successive shocks.

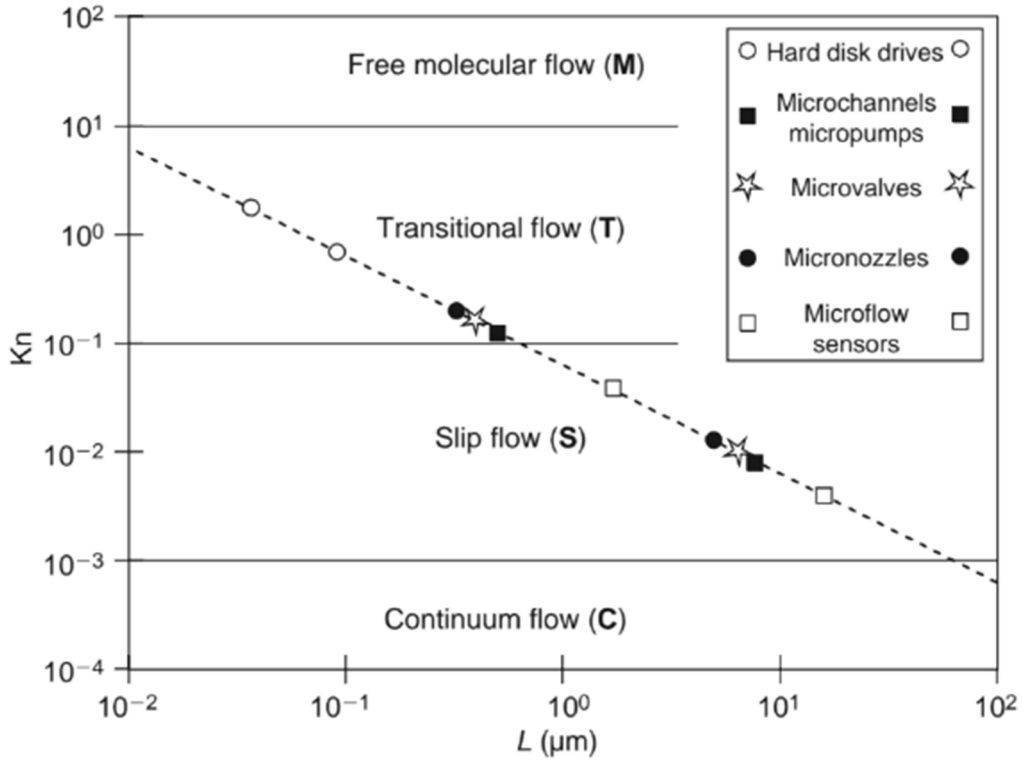

Fig.1. 4: Gaz flow régimes for usual microsystems [8]

1.2 The different flow regimes vs. the Knudsen number (Kn)

The modeling of gas flows in microchannels depends on the level of rarefaction which is qualified by the number of Knudsen. In these flows, the slip regime is most often encountered. It can be described by analytical and semi-analytical models [9], the gas being considered as an ideal gas. For the different flow regimes classified by the Knudsen number

in **figure 1.4**, here the basic model is presented in the literature for each regime (**figure. 1.5**).

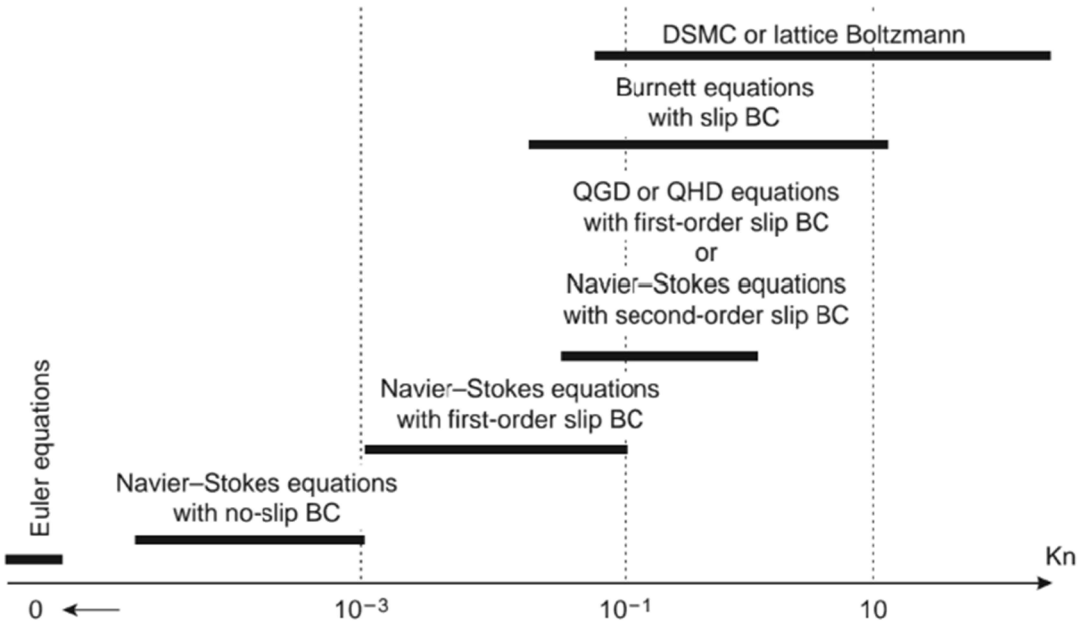

Figure 1. 5. Gaz Flow regimes and main models according to the Knudsen number [8]

It is however convenient to differentiate the flow regimes according to Kn, and the following classification, tinged with empiricism, is conventionally adopted (**figures 1.4 et 1.5**) [7].

- For$Kn<10^{-3}$, the regime is continuous (**figure.1.4.C**), with adhesion to the wall, the Navier – Stokes equations associated with the classical conditions of continuity, temperature and velocity at the walls.
- For$10^{-3}<Kn<10^{-1}$, it is the continuous regime with wall slip (**figure1.4.S**) : the Navier-Stokes equations remain valid but specific boundary conditions must be used,
- For $10^{-1}<Kn<10$,it is the transition regime (**figure.1.4.T**) : it is a regime out of thermodynamic equilibrium, in which the intermolecular collisions and with the wall must be taken into account;
- For Kn>10, it is the free molecular regime (**figure1.4.M**) where the interactions between the gas molecules are negligible compared to the collisions on the walls.

1.3 Knudsen layer and slip conditions

1.3.1 Modeling of the Knudsen layer

In continuous regime (as in slip regime), there exists in the vicinity of the walls a region where the gas is in imbalance thermodynamic. This region is called the Knudsen layer. Under continuous conditions, the effect of this layer is negligible. In slip regime, the Knudsen layer must be taken into account. This layer can be studied and simulated from a microscopic approach such as the kinetic theory of gases, molecular dynamics or direct Monte Carlo simulations

(DSMC, [10]) of Boltzmann equations. According to the microscopic approach used, the thickness of the Knudsen layer varies between 0.9 λ and 4.9 λ, most of the results giving values between λ and 3 λ [11].

On the other hand, for $10^{-3}<Kn<10^{-1}$, it is considered that the flow regime is continuous with slip, i.e. the continuous approach can be used to model the flow (the equations of Navier-Stokes are valid) but that it is necessary to introduce specific boundary conditions (dynamic slip conditions and temperature jump) to approximate what happens in the Knudsen layer and correctly model the flow outside this layer (**Fig.1.6**).

d :molecular average diameter

δ : molecular average spacing

λ :average free path

L : characteristic length of the flow

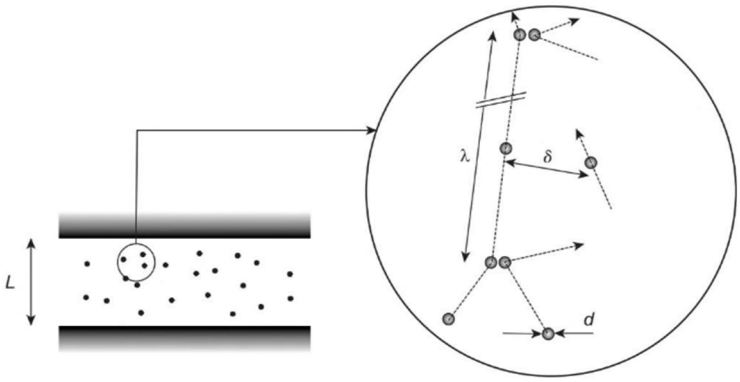

Figure 1. 6. Main caracteristic length scales to take into account at the molecular level [12]

1.3.2 Dynamic slip conditions

For Kn =0.1, the models based on the Navier-Stokes equations remain the most efficient but, for them to be precise enough, it is necessary to capture most of the physical phenomena present in the Knudsen layer. The use of boundary conditions for slip and in the Knudsen layer were introduced by Navier and then taken up by Maxwell in 1879 [13].

The simplified form of the dynamic slip condition proposed by Navier and Maxwell [13] is written:

$$u_g - u_p = L_g \left.\frac{\partial u}{\partial n}\right|_p \qquad \textbf{(1.2)}$$

Where :

u is the gas velocity component tangent to the wall,

u_g is the slip velocity of the gas on the wall,

u_p is the wall velocity and n is the normal to the wall

L_g is the slip length (**figure 1.7**). It is an empirical quantity, proportional to λ which depends on

the surface roughness, the nature of the gas, that of the wall and the gas / wall interaction. This length must be accurately evaluated for u_g to provide a correct approximation of the velocity profile outside the Knudsen layer. There are many formulations of L_g in the literature and its evaluation is subject to many discussions. Some formulations are a function of a viscous slip coefficient, σ_μ, others function of an accommodation coefficient, σ_T (Tangential Momentum Accommodation Coefficient : TMAC) and others are still different [11, 14].

The general form proposed by Maxwell [13] can be written [11, 14]:

$$u_g - u_p = \sigma_\mu \lambda \left(\frac{\partial u}{\partial n} + \frac{\partial v}{\partial t} \right)\Bigg|_p + \sigma_T \frac{\mu_r}{p} \frac{\partial T}{\partial t}\Bigg|_p \qquad \textbf{(1.3)}$$

Where u and v are the tangential and normal components of the velocity vector.

T is the gas temperature. σ_μ is the viscous slip coefficient, σ_T is the thermal slip coefficient. $\sigma_\mu = (2-\sigma_v)/\sigma_v$ where σ_v is the dynamic accommodation coefficient. σ_v represents the fraction of tangential momentum to the wall so that the incident gas molecules have transferred on average to the wall following collisions: σ_v =1 in the case of a wall with diffuse reflection and $\sigma_v \to 0$ in the case of a wall with specular reflection. The last term of equation (1.3) reflects transpiration or thermal pumping, ie the presence of an axial flow generated by a longitudinal temperature gradient, the flow evolves from cold sides temperatures towards hot areas. A dimensional analysis will show that this term is second order in Knudsen number. It will therefore be negligible in most of the time, before the first term of the right hand side of equation (1.3). The boundary condition (1.3) on a flat and smooth wall simply becomes:

$$u_g - u_p = \sigma_\mu \lambda \frac{\partial u}{\partial n}\Bigg|_p \qquad \textbf{(1.4)}$$

Where

$$L_g = \sigma_\mu \lambda \qquad \textbf{(1.5)}$$

According to Colin [15], the dynamic slip conditions (1.3) - (1.5) are also often written, in the first order in Kn, in the form

$$u_g - u_p = \frac{2-\sigma_v}{\sigma_v} \lambda \frac{\partial u}{\partial n}\Bigg|_p \qquad \textbf{(1.6)}$$

$$L_g = \frac{2-\sigma_v}{\sigma_v} \qquad \textbf{(1.7)}$$

Formulation (1.6) of the dynamic slip condition is compatible with formulation (1.4)

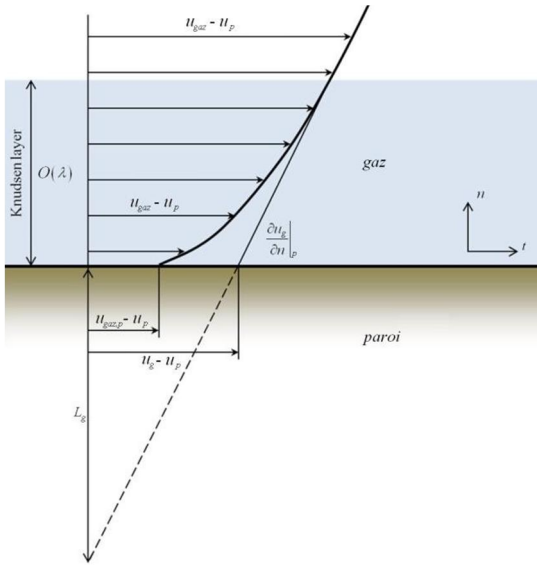

Figure 1. 7. Ideal velocity profile (noted $u_{gaz} - u_p$) and profile approximated by slip boundary conditions (noted $u_g - u_p$) in the Knudsen layer. u_p is the wall velocity, u_{g_p} is the true slip velocity, u_g is the artificial slip velocity and L_g is the slip length

1.3.3 Temperature jump conditions

Smoluchowski [16] introduced the equivalent conditions to describe the temperature jump at the wall. The conditions equivalent to (1.4) and (1.6) are written for the temperature, in the first order in Kn [11, 14]:

$$T_g - T_p = \xi_T \lambda \left.\frac{\partial T}{\partial n}\right|_P \tag{1.8}$$

$$T_g - T_p = \frac{2-\sigma_T}{\sigma_T}\frac{2\beta}{\beta+1}\frac{\lambda}{\mathrm{Pr}}\left.\frac{\partial T}{\partial n}\right|_P \tag{1.9}$$

Where T_g is the gaz temperature at the wall, T_p is the wall temperature, ξ_T is the temperature jump coefficient , σ_T is the thermal accommodation coefficient , $\beta = C_p / C_v$ is the isentropic coefficient representing the ratio between specific heat at constant pressure, C_p ,and specific heat at constant volume, C_v , and Pr is the Prandtl number.

2. Nanofluids

With recent progress in nanotechnology, particles with nanometer size have been obtained. Therefore, the idea of integrating these nanoparticles in a base liquid is used to enhance the thermal conductivity of the medium. A suspension of nanoparticles in a base fluid is called a nanofluid. This term was proposed by Choi [16] in 1995 in the Argonne national laboratory. The base fluid is usually water, oil or ethylene glycol (EG). (Cooling system, microelectronics, ..)

Nanoparticles are fine nanometric particles: their diameter is a few nanometers (<50nm). In general, nanoparticles can be classified according to their shape into two main categories:

- ✓ Spherical nanoparticles for which several types of materials can be used for their manufacture. These spherical nanoparticles can thus be based on metals (copper Cu, iron Fe, gold Au, silver Ag ...) or copper oxides (aluminum oxide Al2O3, copper oxide CuO, titanium oxide TiO2 ...).
- ✓ Nanotubes (NTC carbon nanotubes, titanium TiO2 nanotubes, silicon nanotube, ..)

Many experimental studies have shown that this type of solution can have thermodynamic characteristics very different from those that can be predicted by macroscopic models, generally used to characterize composites with a particle size equal to or greater than the micrometer scale. Furthermore, experimental studies in forced convection seem to show an additional effect on the exchange coefficient, which cannot be directly attributed to the increase in thermal conductivity. In addition, Brownian agitation, linked to the nanometric size of the particles, minimizes the sedimentation problems encountered with larger particles.

2.1 Thermophysical properties

The thermophysical characteristics (thermal conductivity, dynamic viscosity and kinetics, specific heat capacity,..) of solutions are profoundly modified by the addition of nanoparticles and a large number of parameters can have an important impact on this deviation (the material, the size, the aspect ratio, the concentration of particles in suspension, the conductivity of the base fluid, the temperature of the medium, ..)

2.1.1 Thermal conductivity

In the lack of experimental data and of founded theory allowing the determination of the thermal conductivity of a nanofluid, relations used previously for computing the thermal conductivity of a suspension of particles of larger size of the order of micrometers or millimeters in a fluid, have been adopted to calculate the thermal conductivity of nanofluids.Among these relations, it can cite the following models:

Maxwell model

He assumed that the particles are separated a sufficient distance leading to no mutual interaction between them, no contact between the particles [17].

$$\frac{k_{nf}}{k_f} = \frac{k_s + 2k_f - 2\varphi\left(k_f - k_s\right)}{k_s + 2k_f - \varphi\left(k_f - k_s\right)} \qquad \textbf{(1.10)}$$

With

k_{nf} : the thermal conductivity of the nanofluid ;

k_f : the thermal conductivity of the base fluid ;

k_s : the thermal conductivity of the solid particle ;

Modèle de Hamilton

Is an extension of Maxwell's model. It concerns particles of any shape defined as follows [18]:

$$\frac{k_{nf}}{k_f} = \frac{k_s + (n-1)k_f - (n-1)(k_f - k_s)\varphi}{k_s + (n-1)k_f + \varphi(k_f - k_s)} \quad \textbf{(1.11)}$$

With n an empirical form factor (n = 3 for spherical particles and n = 6 for cylindrical particles)

Modèle de Yu et Choi

They proposed to model nanofluids as a base liquid and solid particles separated by a nanometric layer, this layer acts as a thermal bridge between the fluid and the nanoparticles [19]

$$\frac{k_{nf}}{k_f} = \frac{k_s + 2k_f - 2(1+\beta)^3(k_f - k_s)\varphi}{k_s + 2k_f + (1+\beta)^3(k_f - k_s)\varphi} \quad \textbf{(1.12)}$$

With β: The ratio of the thickness of the nanoscale layer to the radius of the particles.

2.1.2 Dynamic viscosity

Viscosity characterizes the ability of a fluid to flow. His knowledge is fundamental for all applications involving the transport of fluids. The addition of nanoparticles rises and enhances the thermal conductivity of the nanofluid but it can also cause an unfavorable increase in dynamic viscosity. Numerous theoretical and experimental studies have been carried out in order to estimate or measure the dynamic viscosity of nanofluids and to quantify the importance of main parameters that influence it. Various theoretical models have been developed to analyse the evolution of the dynamic viscosity of suspensions under certain conditions.

Modèle d'Einstein

For a mixture containing dilute suspensions of spherical and rigid fine particles is as follows [20]:

$$\mu_{nf} = \mu_f(1 - 2.5\varphi) \quad \textbf{(1.13)}$$

With

μ_{nf} : The dynamic viscosity of the nonofluid;

μ_f : The dynamic viscosity of the base fluid;

φ : The volume fraction of nanoparticles;

Einstein's formula has since been proved experimentally and is considered adequate for very dilute suspensions of spherical particles (Brownian or non-Brownian), typically for volume concentrations of less than 1%. It should be noted that this model does not take into consideration the effects of particle dimension and inter-particle interactions.

Brinkman model

Brinkman's [21] formula complements Einstein's model up to a volume concentration of less than 4%.

$$\mu_{nf} = \frac{\mu_f}{(1-\varphi)^{2.5}} \tag{1.14}$$

Batchelor Model

Has shown that viscosity is not only a linear function of φ, as indicated by Einstein's relation, but a non-linear function of φ [22].

$$\mu_{nf} = \mu_f \left(2.6\varphi^2 + 2.5\varphi + 1\right) \tag{1.15}$$

2.1.3 Heat capacity

dynamic viscosity and Thermal conductivity are the two most studied thermophysical characteristics in the case of nanofluids. The specific heat of nanofluids, for its part, is very rarely studied, especially at the experimental level. Specific heat is the heat capacity per unit mass of a substance or a homogeneous system, is defined by the amount of energy to be supplied by heat exchange to increase by one degree Kelvin substance. This quantity is incorporated into the energy equation, and then needs to be determined in a rigorous way. Most of the studies carried out in the literature use one of two models:

model of pak [23] and model of XUA [24]:

Model of PAK :

$$\left(C_p\right)_{nf} = (1-\varphi)\left(C_p\right)_f + \varphi\left(C_p\right)_s \tag{1.16}$$

Model of XUA :

$$\left(\rho C_p\right)_{nf} = \frac{(1-\varphi)\left(\rho C_p\right)_f + \varphi\left(\rho C_p\right)_s}{(1-\varphi)\rho_f\left(C_p\right)_f + \varphi\rho_s} \tag{1.17}$$

With

$\left(C_p\right)_{nf}$: Specific heat of the nanofluid;

$\left(C_p\right)_f$: Specific heat of the base fluid;

$\left(C_p\right)_s$: Specific heat of nanoparticles;

2.1.4 Density

The volume fraction of particles and the density of nanofluids are proportional. Thereby, the density of nanofluids augments with the addition of nanoparticles. In the literature, and in the absence of experimental results, the density of nanofluids is often calculated from the mixing law in which, as for specific heat, the nanofluid is assumed to be homogeneous.

$$\rho_{nf} = \left(1-\varphi\right)\rho_f + \varphi\rho_s \tag{1.18}$$

The volume fraction of the nanoparticles (φ) denotes the ratio of the volume of the nanoparticles to the total volume (fluid + solid).

$$\varphi = \frac{V_s}{V_s + V_f} \tag{1.19}$$

(V_s : solid volume and $V_f + V_s$: Total volume of nanofluid)

With

ρ_{nf} : Density of the nanofluid;

ρ_f : Density of the base fluid;

ρ_s : Density of solid nanoparticles;

2.1.5 Thermal expansion Coefficient

The variation in density under the temperature changes is depicted by the thermal expansion coefficient also named the isobaric coefficient of expansion [25]

$$\beta = \frac{1_s}{\rho}\left(\frac{\partial\rho}{\partial T}\right) \tag{1.20}$$

The determination of the value of this coefficient for nanofluids is determined by analogy with the relation (1.18) which expresses the density of the nanofluid.

$$\beta_{nf} = \left(1-\varphi\right)\rho\beta_f + \varphi\beta_s \tag{1.21}$$

2.2 The applications of nanofluids (Soufi, 2013) [26]

Among the applications of nanofluids, these examples below can be cited:

- The heat exchanger ;

- Cooling of electronic elements (producing a stable nanofluid that is compatible with electronic circuits and components) ;
- Nanoparticles for refrigerator efficiency (formulation of lubricants and coolants mixed with nanoparticles could result in increased energy efficiency of refrigerators) ;
- Aeronautics and space ;
- Cooling of nuclear systems ;
- Transport (cooling management / combustion engine vehicle) ;
- Other applications (fuel cells, solar water heating, drilling, thermal storage) ;

The advantages and disadvantages of nanofluids are mentioned in detail in this reference [26]

3. Flow in porous media

Porous media designate materials for which the solid phase, strongly imbricated with the fluid phase, is fixed. There are many natural materials in this category: soils, sedimentary layers, most rocks, as well as some living materials. Some artificial materials require to be porous either in the manufacturing process or in their purpose to play a filter role or provide specific macroscopic properties (thermal conductivity for example). Fluid flows through a porous medium are found in a wide variety of fields of science and technology. For instance, it can cite the problems of water purification, soil remediation, oil and gas extraction, geophysical problems, [27].

3.1 Characteristic of a porous medium

The porous medium is composed of a solid matrix, inside which there are pores which are interconnected or possibly isolated. In general, porous media are defined by two criteria.

- Unconsolidated solid matrices where the solid phase is formed of grains (for example sand, gravel, glass balls, steel ...).
- Consolidated solid matrices (for example limestone, clay, wood, biological tissue, sandstone,..).

Figure 1. 8. a. Consolidated porous medium [28]

Figure 1. 9.b. Unconsolidated porous medium [28].

A porous medium is characterized mainly by two interrelated macroscopic properties which are porosity and permeability. Since the formulation at the microscopic scale of heat and / or mass transfers in porous media is inapplicable in practice, geometric phase distributions are generally unknown. Consequently, the boundary conditions cannot be known in their details.

The modeling of the phenomena in such porous media is generally carried out by a change of scale: it is a question of going from the microscopic scale where the size of the representative elementary volume (REV) is small compared to those of the pores to the 'macroscopic scale where the size of the VER is large compared to those of the pores. By means of this change of scale, it can go from a discontinuous real porous medium to a fictitious continuous medium.

3.1.1 Representative elementary volume

Solving differential equations requires a continuous medium to establish partial differential relations. The characteristics of a medium such as porosity and permeability are discontinuous at the microscopic level. It would then be appropriate to deal with the flow problem by introducing a new concept called representative elementary volume (REV). Within this volume, the average properties of the fluid and the material are considered to be uniform and continuous. In this context, certain hypothesis must be satisfied (figure 1.7). On the one hand, the dimensions of the (REV) must be generally large in relation to those of the grain size. The REV scale must check:

$$d << l << L \qquad \textbf{(1.22)}$$

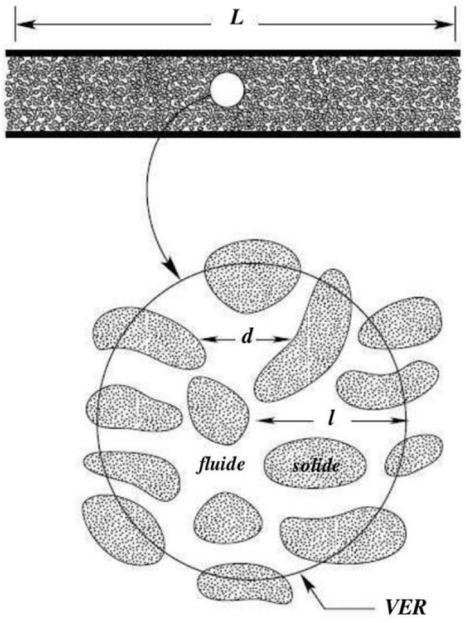

Figure 1. 10. Representative elementary volume REV

One thus obtains the characteristic quantities of the velocity, the pressure and the temperature, by averaging them on the REV. This makes it possible to represent a point in a new fictitious continuous medium by changing the scale. It is equivalent to the porous domain studied but on a macroscopic scale. When the local properties, defined on the REV, are independent of its position, the medium is said to be homogeneous, at the macroscopic scale.

3.1.2 Porosity

The porosity of such a medium represents a consequence of the presence of empty spaces within the solid matrix. The porosity ε is considered as the ratio of the empty volume occupied by the pores V_p, on the total volume V_t

$$\varepsilon = \frac{V_p}{V_t} \tag{1.23}$$

Depending on the pores, it can be considered [29]:

- **Interstice porosity:**

The interstice porosity represents the voids around the solid particles more or less bound to each other.

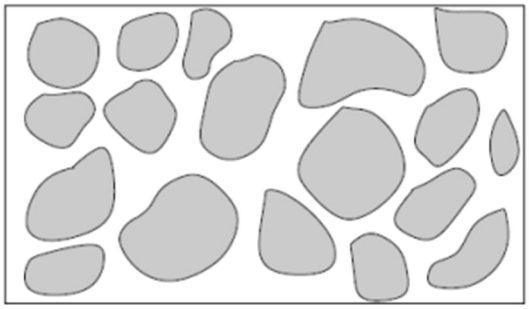

Figure 1. 11. Interstice porosity [29]

❖ **Crack porosity:**

Crack porosity is fractures (cracks) in the matrix.

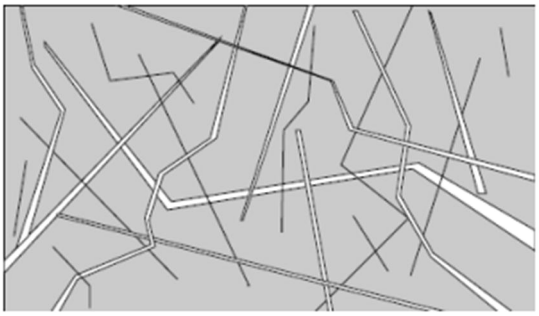

Figure 1. 12. Crack porosity [29]

3.1.3 Permeability

The permeability K refers to the capacity of the porous medium to allow the fluid to pass inside the pores. This parameter is related to the size and connection of the pores between them.

According to Darcy's law (1856), the permeability K measures the conductance of the flow of a porous matrix:

$$K = -\frac{(\mu u_D)}{\left(\frac{dp}{dx}\right)} \tag{1.24}$$

Where μ, u_D and $\frac{dp}{dx}$ are respectively the dynamic viscosity of the fluid, filtration velocity (or Darcian) and the pressure gradient. The unit of permeability is m^2, but it is often expressed in Darcy:

1 Darcy $= 9.87 \times 10^{-13} \mathrm{m}^2$.

3.1.4 Specific surface

The specific surface is a property which results from the geometric parameters of a porous medium. This quantity plays a suitable role in the phenomena of heat transfer between the

fluid and the solid phases. It is defined as the ratio of the total surface area of the fluid-solid interface A_{sf} by the volume of the sample V:

$$\alpha = \frac{A_{sf}}{V} \tag{1.25}$$

3.1.5 Effective thermal conductivity and diffusivity

The effective thermal conductivities depend on the relative proportions of each phase, their geometric distributions and the flow for the case of porous media saturated with a single fluid phase. Since, under forced convection into a porous matrix, heat transfer occurs in a parallel fashion in both solid and fluid phases. Thus, the effective thermal conductivity K_{eff} can be written as follows:

$$k_{eff} = \varepsilon k_f + (1-\varepsilon) k_s \tag{1.26}$$

- k_f and k_s are respectively the thermal conductivities of the fluid and solid phase ;
- ε porosity.

It can also define another parameter which characterizes the heat propagation velocity in a porous medium called effective thermal diffusivity, written as:

$$\alpha_{eff} = \frac{k_{eff}}{(\rho C_p)_{eff}} \tag{1.27}$$

This parameter represents the ratio of the heat which passes through the porous medium by the heat which is stored there. It is directly related to the inertia of this medium. Therefore, heat easily propagates in porous media with high conductivity and low heat capacity. $(\rho C_p)_{eff}$ represents the effective specific heat which varies according to the volume fractions of the different phases as indicated by the following relationship:

$$(\rho C_p)_{eff} = (1-\varepsilon)(\rho C_p)_s + \varepsilon (\rho C_p)_f \tag{1.28}$$

It is important to mention that these two sizes, k_{eff} and α_{eff} do not link to the distribution of the pore but of the evaporation zone [30].

3.2 Flow models in the porous medium

The porous medium that was used is saturated with a pure fluid, subjected to a uniform flow. The fluid has kinematic viscosity ν_f, a dynamic viscosity μ_f, a density ρ_f, and a thermal conductivity k_f .The quantities are averaged over a REV. Moreover, the homogenization

method [31] allows the change scale to obtain new continuous quantities of a fictitious continuous porous medium. It is essentially based on asymptotic expansions of the velocity and pressure at the pore scale, then by an application of a mean integration operator; it can go to the macroscopic scale. Therefore, the fluid velocity V_f which corresponds to the average velocity of the fluid taken on a REV is introduced. The interstitial velocity which represents the average velocity of the fluid but inside pores is defined as V_p. This real velocity can be much higher than V_f, because only a part of the total volume of the porous media is available for fluid transport. By taking the model of the porous medium, in the form of parallel capillaries, we easily verify that:

$$\left|\vec{V}_p\right| = \frac{1}{\varepsilon}\left|\vec{V}_f\right| \tag{1.29}$$

Based on the average pore size d and the interstitial velocity $\vec{V}_p$, the Reynolds number Rep is constructed as follows:

$$\mathrm{R}_{e_p} = V_p \frac{d_p}{V_f} \tag{1.30}$$

According to Dybbs and Edwards, there are three types of R_{e_p} :

- For $R_{e_p} < 1$, the regime is laminar, thereby large viscous forces compared to the inertial forces, Darcy's law is valid.
- For $1 < R_{e_p} < 150$, the regime of the boundary layers develop at the level of the solid walls Outside this boundary layer, there is no longer proportionality between the gradient of pressure and the velocity of the fluid: Darcy's law is no longer applicable. This laminar steady flow regime persists until $R_{e_p} = 150$.
- For $150 < R_{e_p} < 300$, an unsteady laminar flow regime is developing.
- For $R_{e_p} > 300$,it is the presence of a turbulent flow.

To describe the flow in porous media, different models have been developed. The first model was established by Darcy (1856), and since then several other models have been proposed to take into account certain effects neglected by the last.

3.2.1 Darcy's law

The dynamics of homogeneous fluids in porous media is described by Darcy's law [32], established in 1856 on experimental bases. This law, established from unidirectional flows

over sand columns, demonstrated the proportionality of the pressure gradient applied and the water flow through the sand column. Since then, hydrogeological sciences have been based on Darcy's law even for multidirectional flows [33]. It is written:

$$\nabla p = -\frac{\mu_f}{K}\vec{V} + \rho_f \vec{g} \qquad \textbf{(1.31)}$$

Where $\frac{dp}{dx}$ is the pressure gradient, K is the permeability, μ_f is the dynamic fluid viscosity and $\vec{V}$ is the velocity filtration.

It is necessary to indicate that Darcy's law becomes inadequate in certain flow and heat transfer situations, as the filtration rate increases, there is a deviation which caused by to the combined effects of inertia (owing to the presence of solid obstacles) and viscosity, both of which form resistance to flow. To take all these effects into account, other models have been proposed and used.

3.2.2 Forchheimer's empirical model

Forchheimer (1901) was the first author who proposed an empirical modification of Darcy's law to account for non-negligible forces of inertia when the velocity of the fluid becomes important.

The most commonly used Darcy-Forchheimer formulation, the flow of an incompressible fluid, through a homogeneous and isotropic porous medium in steady state is written in the presence of gravity as follows:

$$\nabla p = -\frac{\mu_f}{K}\overrightarrow{V_f} + \rho_f \vec{g} - \frac{\rho_f F}{\sqrt{K}}\left|\overrightarrow{V_f}\right|\overrightarrow{V_f} \qquad \textbf{(1 .32)}$$

Where F (empirical coefficient) depends on the permeability, porosity and microstructure of the porous medium.

3.2.3 Brinkman's empirical model

When the porosity of the medium becomes high (of the order of 0.8), Darcy's law becomes insufficient to portray the flow of the fluid within the porous medium. Indeed, must be considered, in this case, the effects of viscous diffusion created by the friction at the level of the walls containing the porous medium. In this context, Brinkman (1947) [34] extended Darcy's law by introducing a term equivalent to the viscous diffusion term in Stokes' law:

$$\nabla p = -\frac{\mu_f}{K}\overrightarrow{V_f} + \rho_f \vec{g} + \mu_{eff}\nabla^2\overrightarrow{V_f} \qquad \textbf{(1.33)}$$

This empirical law is known as the Darcy-Brinkman formulation. The first term on the right in equation (1.33) is the Darcy term and the second is called the Brinkman term. Brinkman justifies this empirical law by the fact that, for low values of the permeability K, equation (1.33) degenerates into Darcy's law, equation (1.31), and when the permeability tends to infinity, the Stokes equation is obtained. The difficulty in using this model resides in evaluating the equivalent viscosity.

3.2.4 General model or Darcy-Brinkman-Forchheimer model

Darcy Forchheimer's law applies to an environment that meets specific characteristics. However, when the permeability of the medium is large, Darcy's law is not sufficient because it is necessary to take into account the viscous shear forces, which can be of the same order of magnitude as the resistance, introduced by the porous matrix, when the permeability is high. Indeed, for a more general study, it needs to take into consideration all the effects that may occur during the flow. Brinkmann was the first to consider these effects. The pressure gradient in this case is expressed by a law known as the Darcy-Binkman- Forchheimer law (DBF):

$$\nabla p = -\frac{\mu_f}{K}\overrightarrow{V_f} + \rho_f \vec{g} - \frac{\rho_f F}{\sqrt{K}}\left|\overrightarrow{V_f}\right|\overrightarrow{V_f} + \mu_{eff}\nabla^2\overrightarrow{V_f} \qquad \textbf{(1.34)}$$

μ_{eff} is an effective viscosity equal to the ratio of the viscosity of the fluid to the porosity ε.

4. Conclusion

The present chapter introduced a review on advanced research study in the scientific community regarding the application of nanofluids in porous systems. Several models aspects were discussed: models to handle nanofluids heat transfer and nanofluids flow phenomenon in porous supports. Numerical models are reviewed to deal with these mechanisms. This chapter allows us to highlight the various relevant parameters in the study of heat flow and transfer in microsystems, porous media and nanofluids. Given the wide range of nanofluid applications, we are focused on developing this research theme. Therefore, the study of such a parameter of either porous structure (e.g. porosity) or nanofluids (e.g. concentration) on the heat transfer performances is the key of this thesis. To this end, the Lattice Boltzmann method was selected and adopted for the discretization of the governing equations. Thus, more details on this numerical approach and models deemed herein are depicted in the following chapters.

References

[1] YANG, Yong, CHEN, Yong, TANG, Hao, et al. Microfluidics for biomedical analysis. Small methods, 2020, vol. 4, no 4, p. 1900451.

[2] HO, Chih-Ming et TAI, Yu-Chong. Micro-electro-mechanical-systems (MEMS) and fluid flows. Annual review of fluid mechanics, 1998, vol. 30, p. 579-612.

[3] A. Manz, H. Becker, Microsystem Technology in Chemistry and Life Science, Springer, Berlin, 1999.

[4] SANDERS, Giles HW et MANZ, Andreas. Chip-based microsystems for genomic and proteomic analysis. TrAC Trends in Analytical Chemistry, 2000, vol. 19, no 6, p. 364-378.

[5] STONE, Howard A. et KIM, S1. Microfluidics: basic issues, applications, and challenges. American Institute of Chemical Engineers. AIChE Journal, 2001, vol. 47, no 6, p. 1250.

[6] HANSEN, Carl et QUAKE, Stephen R. Microfluidics in structural biology: smaller, faster… better. Current opinion in structural biology, 2003, vol. 13, no 5, p. 538-544.

[7] S. Colin and L. Baldas, Rarefaction effects in gaseous microflows [rarefaction effects in gaseous micro-flows]. Comptes Rendus Physique, 2004, vol. 5, pp. 521-530.

[8] KARNIADAKIS, George Em, BESKOK, Ali, et GAD-EL-HAK, M. Micro flows: fundamentals and simulation. Appl. Mech. Rev., 2002, vol. 55, no 4, p. B76-B76.

[9] C. Aubert, Ecoulements compressibles de gaz dans les microcanaux : effets de raréfaction, effets instationnaires. Thèse de Doctorat, Université Paul Sabatier, 1999.

[10] G. A. Bird, Molecular gas dynamics and the direct simulation of gas flows. Clarendon Press, Oxford, 1994

[11] W. M. Zhang, G. Meng and X. Wei, A review on slip models for gas microflows. Microfluidics and Nanofluidics, 2012, vol. 13, pp. 845-882.

[12] Kandlikar S, Garimella S, Li D, Colin S, King MR. Heat transfer and fuid fow in minichannels and microchannels. 1st ed. NY: Rochester Institute of Technology; 2005.

[13] J. C. Maxwell, On stresse in rarified gases arising from inequalities of temperature. Philosophical Transactions of the Royal Society of London, 1879, vol. 170, pp. 231-256.

[14] S.G. Kandlikar, S. Colin, Y. Peles, S. Garimella, R.F. Pease, J.J. Brandner and D.B. Tuckerman. Heat transfer in microchannels - 2012 status and research needs. J. Heat Transf. , 2013, vol. 135.

[15] S. Colin, Gas microflows in the slip flow regime: A critical review on convective heat

transfer. J. Heat Transf.,2012, vol. 134, pp. 020908.

[16] Choi, S. U., & Eastman, J. A. (1995). Enhancing thermal conductivity of fluids with nanoparticles (No. ANL/MSD/CP-84938; CONF-951135-29). Argonne National Lab.(ANL), Argonne, IL (United States).

[17] Maxwell, J. C. (1873). A treatise on electricity and magnetism (Vol. 1). Clarendon press.

[18] HAMILTON, R. L et CROSSER, O. K. Thermal conductivity of heterogeneous two-component systems. Industrial & Engineering chemistry fundamentals, 1962, vol. 1, no 3, p. 187-191.

[19] YU, W. et CHOI, S. U. S. The role of interfacial layers in the enhanced thermal conductivity of nanofluids: a renovated Maxwell model. Journal of nanoparticle research, 2003, vol. 5, no 1, p. 167-171.

[20] A. Einstein. Investigations on the Theory of the Brownian Movement.Dover Publications, New York, 1956

[21] BRINKMAN, Hendrik C. The viscosity of concentrated suspensions and solutions. The Journal of chemical physics, 1952, vol. 20, no 4, p. 571-571.

[22] BATCHELOR, GK406082. Brownian diffusion of particles with hydrodynamic interaction. Journal of Fluid Mechanics, 1976, vol. 74, no 1, p. 1-29.

[23] PAK, Bock Choon et CHO, Young I. Hydrodynamic and heat transfer study of dispersed fluids with submicron metallic oxide particles. Experimental Heat Transfer an International Journal, 1998, vol. 11, no 2, p. 151-170.

[24] XUAN, Yimin et ROETZEL, Wilfried. Conceptions for heat transfer correlation of nanofluids. International Journal of heat and Mass transfer, 2000, vol. 43, no 19, p. 3701-3707.

[25] Stéphane FOHANNO, Guillaume POLIDORI, Catalin POPA. Nanofluides et transfert de chaleur par convection naturelle. Université de Reims ChampagneArdenne, France2012.

[26] Soufi, E., H., (2013): Application des nanofluides pour le refroidissement : étude d'un cas d'une géométrie simple, Thèse de Master en Génie Chimique, Université Kasdi Merbah d'Ouargla.

[27] D. A. Nield and A. Bejan, Convection in Porous Media. Springer-Verlag, New York, second edition, 1999

[28] KASDI, Jugurtha. Simulation of the oil-water immiscible displacement interface in a

porous medium. 2012. Doctoral thesis. Mouloud Mammeri Tizi-Ouzou University.

[29] LOMINÉ, Franck et OGER, Luc. Dispersion of particles by spontaneous interparticle percolation through unconsolidated porous media. Physical Review E, 2009, vol. 79, no 5, p. 051307.

[30] H. V. Thai, Influence of pore size distribution on drying behaviour of porous media by a continuous model. Thése de doctorat, Université de Magdebourg, 2006.

[31] E. Sanchez-Palencia, Local and macroscopic behavior of a type of physical environment heterogeneous. Int. J. Engng. Sc., 1980, vol. 12, pp. 331-351.

[32] H. Darcy, Les fontaines publiques de la ville de Dijon. Dalmont, Paris, 1856.

[33] H. Dhahri, Study of heat transfers by a pulsating or oscillating flow in a cylinder containing a porous medium. Doctoral thesis, University of Monastir, 2005

[34] BRINKMAN, Hendrik C. A calculation of the viscous force exerted by a flowing fluid on a dense swarm of particles. Flow, Turbulence and Combustion, 1949, vol. 1, no 1, p. 27-34.

Chapter 2: Forced convection heat transfer by a flow of nanoffluid in a micro-channel using the lattice Boltzmann method

1. Introduction

Recent miniaturization techniques have led to the growing development of MEMS (Micro Electro- mechanical Systems) used in different sectors (medicine, biology, industry, etc.). MEMS are mechanical systems comprising at least one micrometric size component. This component can be a pipe, the seat of a flow, the dimension of which is of the order of a few microns. However, to design and manufacture such systems, it is necessary to fully understand and characterize the flows as well as the heat transfers in these small scales. Heat transfers in fluids led to many practical and industrial applications, including transportation (combustion engines), energy supply, air conditioning, and electronics cooling…

The recent considerable development of research treating with nanofluid is due to the fact that it is possible, for certain applications, to increase appreciably the heat transfers by introducing into a pure fluid a low concentration of nanoparticles. The intensity of heat transfer strongly depends on the conductivity and thermal capacity of the heat transfer fluids. Remember that nanofluids are colloidal solutions obtained by dispersing solid particles of nonmetric size in a base fluid. At very low concentrations, some of these solutions have been found to be very effective in improving heat transfer under certain conditions. There are several works regarding nanofluid in different geometries, many publications have reported the heat transfer for nanofluid flow in microchannels [1–4]. Thus, Karimipour et al. [5] numerically investigated the Cu-water nanofluid in a microchannel for slip condition. Authors used the Lattice Boltzmann approach to handle the physical probem. They proved the robust ability of LBM to simulate nanofluid heat transfer into mico-channel subjected to forced convection. In addition, they found that the temperature jump strongly affected the heat transfer.

On the other hand, Hussein et al. [6] reviewed the applications of nanofluids to enhance the thermal and heat performance of such a system. They noted that numerical and experimental works found that the most important property of nanofluids is its high volume fraction which improves the heat transfer in car radiators.

Sheikholeslami and Bhatti [7] reported the nanfluid incorporated into porous semi-annulus maintained under forced convective heat transfer in presence of constant magnetic field. They used the Control volume based finite element method (CVFEM) for numerical simulations. Findings showed that the increase in Darcy and Reynolds numbers, accelerate the nanofluid velocity. In addition, as the nanofluid volume fraction, Darcy, and Reynolds numbers increase, the heat transfer enhances. However, the increase in Lorentz forces, mitigates the Nusselt number.

Hussein et al. [8] carried out both a numerical and experimental study on heat transfer performance of the SiO2 nanoparticle addition in a car radiator. They take into consideration the friction forces and forced convection. Results depicted that the use of SiO2 nanofluid with small concentration enhances the heat transfer rate with a rise of 50% compared to the pure water.

In general, the Lattice Boltzmann Method (LBM) represents a suitable approach for simulating nanofluids heat transfer phenomena through microchannel [9, 10]. This tool is based on mesoscopic, microscopic and macroscopic models to discretize the governing equations. For example, Ma et al. [11] used the Lattice Boltzmann method to simulate the nanofluid heat transfer in a bent channel under forced convection.

Sheikholeslami [12] adapted the LBM to handle three dimensional porous structure composed of nanofluid and maintained under forced convection and Lorentz forces.

Thereby, the main task in this chapter is to numerically handle the heat transfer performances in a two-dimensional rectangular micro-channel fully filled with Ag/Water subjected to laminar forced convection. Where, slip/jump boundary conditions and their effects are considered. The Single Relaxation Time (T- SRT) model modified Lattice Boltzmann Method (LBM) with double distribution functions (DDFs) is adapted to deal with the physical problem. The findings were studied in terms of thermal and dynamic behavior along the channel.

The structure of this chapter is as follows: After the introduction in section 1, the physical geometry is described in section 2. Then, the section 3 presented the numerical method used (LBM). Section 4 presents a definition of nanofluids and their expressions of thermophysical properties. In section 5 the boundary conditions of the physical problem are outlined. Section 6 portrays the grid independence test and model validation. The results of simulations are written in section 7. Finally, the main findings are summarized in section 8.

2. Problem statement and assumptions

The two-dimensional (2D) open-ended channel completely filled with a Ag/Water nanofluid subjected to laminar forced convection, is the interest domain for this work, as schematically illustrated in (**Figure 2.1**).The rectangular channel length is L and it height is H. As seen, both upper and lower channel walls are imposed to temperature of the wall Tw. The fluid flow enters the channel with a uniform and constant temperature Ti and a uniform initial velocity Ui. The exit conditions are supposed to be fully developed.

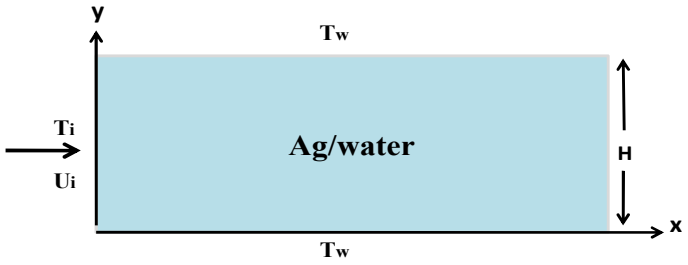

Figure 2. 1. Geometric configuration

In this analysis, the following assumptions are considered: The Ag/water nanofluid is assumed to be homogeneous, isotropic Newtonian and incompressible; and obey to local thermal equilibrium (LTE) taking into account viscous dissipation; the thermophysical properties of both fluid and solid phases are constant. It is also assumed that the fluid circulates in the slip-flow regime.

Governing equations:

Given the assumptions adopted, the system of equations describing the problem is written, in Cartesian coordinates, as follows

Continuity equation

$$\nabla.\mathrm{u} = 0 \tag{2.1}$$

Momentum equation

$$\frac{\partial \mathrm{u}}{\partial \mathrm{t}} + \mathrm{u}.\nabla\mathrm{u} = -\frac{1}{\rho_{\mathrm{nf}}}\nabla\mathrm{p} + \nu_{\mathrm{nf}}\nabla^2\mathrm{u} \tag{2.2}$$

Energy equation

$$\frac{\partial \mathrm{T}}{\partial \mathrm{t}} + \nabla(\mathrm{u}.\mathrm{T}) = \alpha_{\mathrm{nf}}\nabla^2\mathrm{T} + \phi \tag{2.3}$$

Where **u**, **p** and **T** are the velocity vector, the pressure and the temperature , respectively. Density ρ_{nf} and viscosity of the nanofluid μ_{nf} can be estimated by Eqs. (**2.18**) and (**2.21**) using nanoparticles volume fraction φ ; while the subscripts **f**, **s** and **nf** represent the base-fluid, solid nanoparticles and nanofluid, respectively.

ϕ is the source term corresponding to the dissipation function , α_{nf} is the thermal diffusivity of nanofluid and ν_{nf} is the nanofluid kinematic viscosity.

The use of reduced variables in the equations makes it possible to illustrate the reality of physical phenomena. Indeed, their existence and their evolution are independent of the

system of measurement units used. Moreover, these variables make it possible to obtain general information, which plays a major role in the similarities. Thus, for bring back the phenomenological equations in a dimensionless form, it is necessary to define, by means of characteristic quantities, changes of variables. The equations that describe the present problem are rendered dimensionless using the following reference quantities:

$$\theta = \frac{T - T_i}{T_w - T_i}, (X, Y) = \left(\frac{x}{H}, \frac{y}{H} \right), \quad \textbf{(2.3. a)}$$

$$P = \frac{p}{\rho U_0^{\,2}}, \tilde{t} = \frac{tU_0}{H}, (U, V) = \left(\frac{u}{U_0}, \frac{v}{U_0} \right) \quad \textbf{(2.3. b)}$$

3. Lattice Boltzmann approach

The system of equations which governs the phenomenon of forced convection in a micro channel filled with a nanofluid was solved numerically by the modified Lattice Boltzmann method with a single relaxation time (SRT) from the BGK model (using the second order accurate strategy). This method has the advantage of following the evolution of sample particles during convection due to his kinetic theory and the equation by Boltzmann. During the discretization, the sample is assumed to consist of a fine number of nodes, each of them is assimilated to a particle which propagates with a well determined velocity then it collides with neighboring nodes.

In this study, the D2Q9 arrangement is used (**figure 2.2**).This type of model is generally the most used given their stability and their precision compared to other type of Lattice model. The resolution process is done in two steps:

A collision step which consists in calculating in each node all the functions of distribution of the network model at the instant $t + \Delta t$. A second stage called propagation which consists in calculating the distribution functions by each node according to the neighboring nodes of the spatial grid.

The numerical simulation of a flow by the modified Lattice Boltzmann method consists in solving a system of Boltzmann equations on a well-defined network:

$$\tilde{f}_i(\vec{x} + \vec{c}_i dt, t + dt) - \tilde{f}_i(\vec{x}, t) = -\frac{dt}{\tau_f + 0.5dt}\left(\tilde{f}_i - f_i^e\right) \quad \textbf{(2.4)}$$

$$\tilde{g}_i(\vec{x} + \vec{c}_i dt, t + dt) - \tilde{g}_i(\vec{x}, t) = -\frac{dt}{\tau_g + 0.5dt}\left(\tilde{g}_i - g_i^e\right) - \frac{\tau_g dt}{\tau_g + 0.5dt} f_i Z_i \quad \textbf{(2.5)}$$

f and g indicated the density momentum and internal energy distribution functions respectively .The discrete distribution function $\tilde{f}_i$ and $\tilde{g}_i$ with velocity c_i at position x and time t are given by **[**13**]:**

$$\widetilde{f}_i = f_i + \frac{dt}{2\tau_f}\left(f_i - f_i^e\right) \tag{2.6}$$

$$\tilde{g}_i = g_i + \frac{dt}{2\tau_g}\left(g_i - g_i^e\right) + \frac{dt}{2} f_i Z_i \tag{2.7}$$

$$Z_i = \left(\vec{c}_i - \vec{u}\right).D_i\vec{u},\ D_i = \partial_t + \vec{c}_i.\nabla \tag{2.8}$$

Z_i and D_i represent the effect of heat dissipation and the material derivative along the direction $\vec{c}_i$, τ_f and τ_g are the hydrodynamic and thermal relaxation times, respectively.

f_i^e and g_i^e are the equilibrium distribution function.

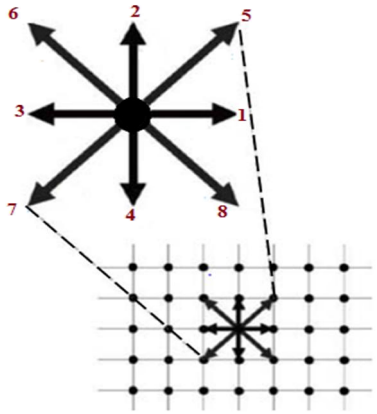

Figure 2. 2.**Lattice structure for distribution function**

According to the D2Q9 model, the equilibrium distribution functions are expressed as follows:

$$f_i^e = \omega_i \rho\left[1 + \frac{3\vec{c}_i.\vec{u}}{c^2} + \frac{9\left(\vec{c}_i.\vec{u}\right)^2}{2c^4} - \frac{3\left(u^2+v^2\right)}{2c^2}\right] \tag{2.9}$$

$$g_0^e = -\omega_0\left[\frac{3\rho e\left(u^2+v^2\right)}{2c^2}\right] \tag{2.10}$$

$$g^e_{1,2,3,4} = \omega_i \rho \left[1.5 + 1.5\frac{\vec{c}_i.\vec{u}}{c^2} + 4.5\frac{(\vec{c}_i.\vec{u})^2}{c^4} - 1.5\frac{(u^2+v^2)}{c^2} \right] \quad \textbf{(2.11)}$$

$$g^e_{5,6,7,8} = \omega_i \rho \left[3 + 6\frac{\vec{c}_i.\vec{u}}{c^2} + 4.5\frac{(\vec{c}_i.\vec{u})^2}{c^4} - 1.5\frac{(u^2+v^2)}{c^2} \right] \quad \textbf{(2.12)}$$

Where

$\vec{u} = (u,v), \vec{x} = (x,y)$, $\rho e = \rho RT$, $c^2 = 3RT$ and T is the temperature, w_i are set as : $w_0 = 4/9$, $w_{1,4} = 1/9$ and $w_{5,8} = 1/36$.The D2Q9-discret velocity model is given as[14]:

$$\begin{aligned} &\vec{c}_o = (0,0). \\ &\vec{c}_i = \left(\cos\frac{i-1}{2}\pi, \sin\frac{i-1}{2}\pi \right) c, i = 1,2,3,4 \\ &\vec{c}_i = \sqrt{2}\left(\cos\left(\frac{i-5}{2}\pi + \frac{\pi}{4}\right), \sin\left(\frac{i-5}{2}\pi + \frac{\pi}{4}\right) \right) c, i = 5,6,7,8 \end{aligned} \quad \textbf{(2.13)}$$

The expression of hydrodynamic and thermal variables is written as follows [**15**]:

$$\rho = \sum_i \tilde{f}_i \quad \textbf{(2.14)}$$

$$\rho\vec{u} = \sum_i \vec{c}_i \tilde{f}_i \quad \textbf{(2.15)}$$

$$\rho e = \sum_i \tilde{g}_i - \frac{dt}{2}\sum_i f_i Z_i \quad \textbf{(2.16)}$$

The hydrodynamic and thermal relaxation times are used to estimate the kinematics viscosity and thermal diffusivity:

$$\nu = \tau_f RT \;\; \alpha = 2\tau_g RT \quad \textbf{(2.17)}$$

RT is supposed as 1/3 in LBM so that the value of hydrodynamic relaxation time and its corresponded kinematic viscosity is estimated; then thermal diffusivity is achieved by the definition of Prandtl number as Pr=υ/α. It means the amount of thermal relaxation time can now be estimated by Eq. **(2.17).**

4. Nanofluid

The properties of the nanofuid are obtained using the following relations [**16]**:

$$\rho_{nf} = \varphi\rho_s + (1-\varphi)_{\rho_f} \quad \textbf{(2.18)}$$

$$(\rho c_p)_{nf} = \varphi(\rho c_p)_s + (1-\varphi)(\rho c_p)_f \quad \textbf{(2.19)}$$

$$\alpha_{nf}=k_{nf}/\left(\rho c_p\right)_{nf} \tag{2.20}$$

Where C_p denoted nanofluid specific heat capacity.

Using the Brinkman model [16**]** the effective dynamic viscosity is:

$$\mu_{nf}=\mu_f/(1-\varphi)^{2.5} \tag{2.21}$$

The nanofluid thermal conductivity as a function of liquid k_f and solid conductivities k_s is expressed as following [16**]**:

$$k_{nf}=k_f\left[1+\frac{k_s}{k_f}\frac{A_s}{A_f}+Ck_sP_e\frac{A_s}{k_fA_f}\right] \tag{2.22}$$

Where

$$\frac{A_s}{A_f}=\frac{d_f}{d_s}\frac{\varphi}{1-\varphi}\quad P_e=\frac{u_Bd_s}{\alpha_f}\quad u_B=\frac{2k_BT}{\pi\mu_fd_s^{\,2}}\quad k_B=1.3807\times10^{-23}J/K\quad C=36000 \tag{2.23}$$

Where water molecule diameter is considered as d_f and d_p is the nanoparticle molecule diameter. P_e is the Peclet number with the Brownian motion velocity of nanoparticles u_B, k_B is the constant of Boltzmann and C is an experimental constant.

5. Boundary condition

Non-equilibrium bounce back model, normal to the boundary, is used for inlet and outlet hydrodynamic boundary conditions. In this model, distribution functions are reflected in suitable ways to satisfy the equilibrium conditions and improve accuracy.

$$\begin{aligned}\tilde{f}_1&=\tilde{f}_3+\frac{2}{3}\rho_{in}u_{in}\\ \tilde{f}_5&=\tilde{f}_7+\frac{1}{2}\left(\tilde{f}_4-\tilde{f}_2\right)+\frac{1}{6}\rho_{in}u_{in}\\ \tilde{f}_8&=\tilde{f}_6-\frac{1}{2}\left(\tilde{f}_4-\tilde{f}_2\right)+\frac{1}{6}\rho_{in}u_{in}\end{aligned} \tag{2.24}$$

$$\begin{aligned}\tilde{f}_3&=\tilde{f}_1-\frac{2}{3}\rho_{out}u_{out}\\ \tilde{f}_7&=\tilde{f}_5-\frac{1}{2}\left(\tilde{f}_4-\tilde{f}_2\right)-\frac{1}{6}\rho_{out}u_{out}-\frac{1}{2}\rho_{out}u_{out}\\ \tilde{f}_6&=\tilde{f}_8+\frac{1}{2}\left(\tilde{f}_4-\tilde{f}_2\right)-\frac{1}{6}\rho_{out}u_{out}+\frac{1}{2}\rho_{out}u_{out}\end{aligned} \tag{2.25}$$

The different thermal distribution functions at the exit and entrance region have determined using the bounce back model [17, 18]:

$$\tilde{g}_1 = \frac{6\rho_{in}e_{in} + 3dt\sum_i\left[f_i Z_i - 6\left(g_0 + \tilde{g}_2 + \tilde{g}_3 + \tilde{g}_4 + \tilde{g}_6 + \tilde{g}_7\right)\right]}{2 + 3u_{in} + 3u_{in}^2}\left[1.5 + 1.5u_{in} + 3u_{in}^2\right]\frac{1}{9}$$

$$\tilde{g}_5 = \frac{6\rho_{in}e_{in} + 3dt\sum_i\left[f_i Z_i - 6\left(\tilde{g}_0 + \tilde{g}_2 + \tilde{g}_3 + \tilde{g}_4 + \tilde{g}_6 + \tilde{g}_7\right)\right]}{2 + 3u_{in} + 3u_{in}^2}\left[3 + 6u_{in} + 3u_{in}^2\right]\frac{1}{36} \qquad \textbf{(2.26)}$$

$$\tilde{g}_8 = \frac{6\rho_{in}e_{in} + 3dt\sum_i\left[f_i Z_i - 6\left(\tilde{g}_0 + \tilde{g}_2 + \tilde{g}_3 + \tilde{g}_4 + \tilde{g}_6 + \tilde{g}_7\right)\right]}{2 + 3u_{in} + 3u_{in}^2}\left[3 + 6u_{in} + 3u_{in}^2\right]\frac{1}{36}$$

$$\tilde{g}_6 = \frac{6\left(\tilde{g}_1 + \tilde{g}_5 + \tilde{g}_8\right) - 3dt\sum_i\left(\frac{c_{ix}}{c}\right)f_i Zi - 6\left(\rho e u_{out}\right)}{2 - 3u_{out} + 3u_{out}^2}\left[3 - 6u_{out} + 6v_{out} + 3\left(u_{out}^2 + v_{out}^2\right) - 9u_{out}v_{out}\right]\frac{1}{36}$$

$$\tilde{g}_3 = \frac{6\left(\tilde{g}_1 + g_5 + \tilde{g}_8\right) - 3dt\sum_i\left(\frac{c_{ix}}{c}\right)f_i Zi - 6\left(\rho e u_{out}\right)}{2 - 3u_{out} + 3u_{out}^2}\left[1.5 - 1.5u_{out} + 3u_{out}^2 - 1.5v_{out}^2\right]\frac{1}{9} \qquad \textbf{(2.27)}$$

$$\tilde{g}_7 = \frac{6\left(\tilde{g}_1 + g_5 + \tilde{g}_8\right) - 3dt\sum_i\left(\frac{c_{ix}}{c}\right)f_i Zi - 6\left(\rho e u_{out}\right)}{2 - 3u_{out} + 3u_{out}^2}\left[3 - 6u_{out} - 6v_{out} + 3\left(u_{out}^2 + v_{out}^2\right) + 9u_{out}v_{out}\right]\frac{1}{36}$$

Concerning the boundary conditions at the walls of microchannels, the sliding boundary is applied for the hydrodynamic field. The slip length coefficient, β, is used to define the slip velocity u_s for the liquid (Ngoma and Erchiqui [19]) and as written us follows:

$$u_s = \pm\beta\frac{\partial u_{fluid}}{\partial y}\Big|_{y=0,h} \qquad \textbf{(2.28)}$$

Where u_s is the slip velocity of the liquid on the wall. The dimensionless form is written as:

$$U_s = \pm B\frac{\partial U}{\partial Y}\Big|_{Y=0,1} \qquad \textbf{(2.29)}$$

To define the slip velocity in LBM, the specular reflective bounce back model (combination of bounce back and specular boundary condition) is applied in this work. For example for the bottom wall, the unknown distribution functions are approximated by:

$$\begin{aligned}\tilde{f}_2 &= \tilde{f}_4\\ \tilde{f}_5 &= r\tilde{f}_7 + (1-r)\tilde{f}_8\\ \tilde{f}_6 &= r\tilde{f}_8 + (1-r)\tilde{f}_7\end{aligned} \qquad \textbf{(2.30)}$$

The accommodation factor, r, is chosen appropriately [**20**].

The temperature jump can be expressed asfollows [**21**]:

$$\Delta T_w = T_{fluid}\left(y \to wall\right) - T_w = \zeta \frac{\partial T_{fluid}}{\partial y}\Big|_w \tag{2.31}$$

Where ζ is the temperature jump distance.

The dimensionless temperature at the wall can be obtained from the expression bellow

$$\theta - \theta_w = \frac{B}{\Pr}\frac{\partial \theta}{\partial y}\Big|_{Y=0,1} \tag{2.32}$$

The temperature jump at the bottom wall is written based on the internal energy distribution function [22]:

$$\tilde{g}_{2,5,6} = \frac{3}{\rho_w e} g^e{}_{2,5,6}\left(\rho_w u_w e_w\right)\left(\tilde{g}_4 + \tilde{g}_7 + \tilde{g}_8\right) \tag{2.33}$$

By semilarity, top wall temperature jump is determined.

The local Nusselt number is given as [5] :

$$Nu_x = \left(\frac{k_{nf}}{k_f}\right)\frac{q_y D_H}{\Delta T k} = \left(\frac{k_{nf}}{k_f}\right)\frac{D_H\left(\partial T/\partial y\right)_w}{\left(T_w - T_{bulk}\right)} \tag{2.34}$$

6. Grid Independence and validation

Trial computations have been performed using three mesh sizes, i.e. 700×35, 800×40 and 900×45 for nanoparticles concentration φ = 0 and slip coefficient B = 0.01. The numerical results for different grids are shown in Table 1, due to small difference between the results of the last two grid sizes, a uniform grid with 800×40 was chosen to obtain the best agreement between accuracy and computation time.

To validate the developed code, the comparison of the values obtained by Santra et al. [23] for the average Nusselt number (for different Reynolds number: Re=50, Re=100and Re=200) of a forced convection of cold Cu–water nanofluid in a macro channel with hot walls. The **figure2.3** demonstrated good agreement with those of Santra et al. [23].In the present computation, the Reynolds number and the Prandtl number are chosen to be $\mathrm{Re} = \rho_{nf} u_{nf} D_H / \mu_{nf}$, $\Pr = \upsilon_{nf} / \alpha_{nf}$ and are calculated for the nanofluid mixture at φ= 0% (pure water), φ = 2% and φ = 4%, and the Reynolds number is fixed 1. The effects of slip Velocity on the walls and heat transfer are examined, the slip Velocity coefficient is chosen from 0.005 to 0.02.

Table 2. 1: Thermophysical properties of Ag (Argent) as the nanoparticles and water as the base fluid (at average temperature from 27 to 34,7 °C)

	ρ(kg/m^3)	K(W/mK)	μ (Pa.s)	Cp(J/KgK)
Ag	10500	429	-	235
water	997.1	0.613	$8.9x10^{-4}$	4179

Table 2. 2: Grid Independency for Re = 1, Pr = 0.7, φ = 0 and B = 0.015

	Grids		
	700x35	800x40	900x45
Nu	7.18	7.23	7.25
$C_f\,Re$	21.04	21.10	21.13

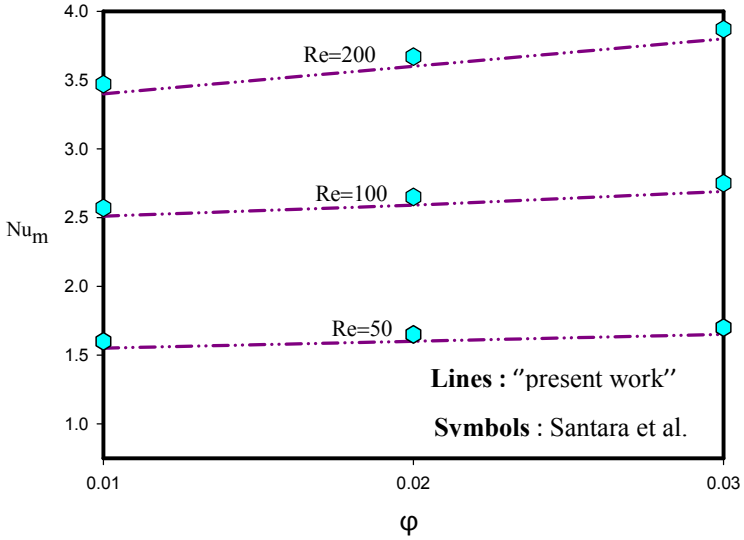

Figure 2. 3. Obtained numerical results of the averaged Nusselt number vs. the results of Santra et al. [23].

7. Results and discussion

Figure2.4. examines the horizontal dimensionless velocity profiles, $U = u/\mathrm{u_i}$ .Along the microchannel wall at B=0.005for φ=0and φ=0.04.The fully developed condition is seen at x=0.08L and x=0.16L after a short entrance length(x=0.02L and x=0.04L).Moreover, it can be observed that the nanoparticles volume fraction do not have significant effects on U. The slip coefficient (B) leads to generate the slip velocity at Y =0 and Y=1 which is well obvious in **Figure2.4**. However, it has the maximum value at entrance and then decreases along the microchannel.In contrary of usual flows in channels (at macro scales), the maximum value of U is less than 1.5 in fully developed region due to slip velocity on the walls.**Figure2.5** Depicts the dimensionless temperature profiles, $\theta = T/\mathrm{T_i}$ along the

microchannel at B=0.005 and for φ=0 and φ=0.04.The nanofluid temperature increases along the microchannel so that at x=0.16L, its temperature approaches almost to that of the wall. Moreover, the significant temperature jump is observed at inlet which decreases moderately along the walls to the outlet. However, there is very small value of temperature jump in fully developed region.

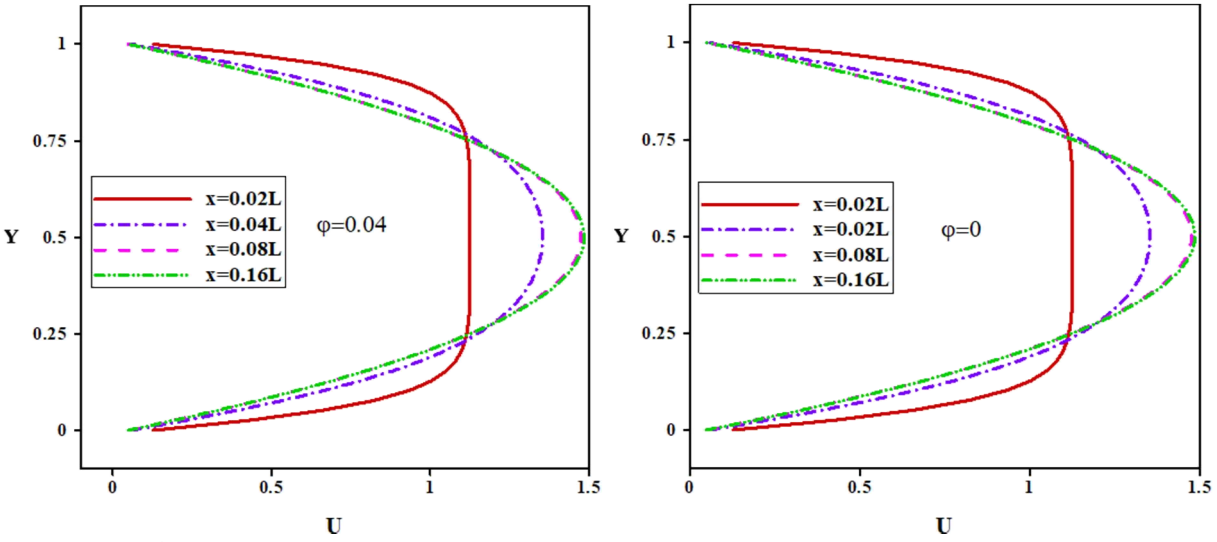

Figure 2. 4. Horizontal dimensionless velocity profiles *U* along the microchannel at B = 0.005 for φ= 0 and φ= 0.04

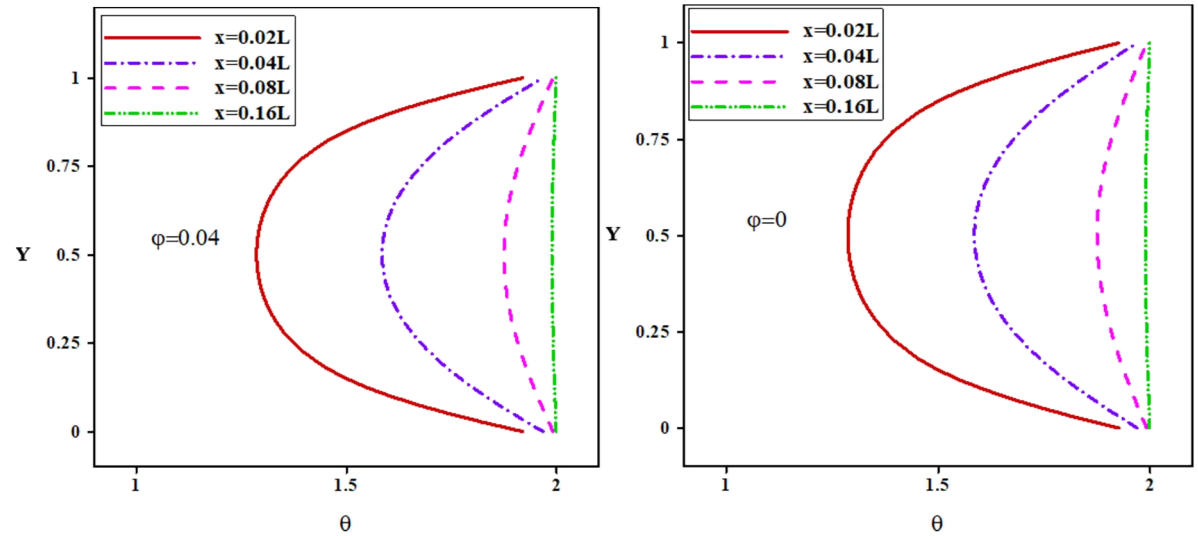

Figure 2. 5. Dimensionless temperature profiles θ ,along the microchannel at B = 0.005 for φ= 0 and φ= 0.04

Figure.2.6 presents the streamlines and isotherms of nanofluid inside the microchannel at B=0.005(line) and B=0.02(dash) for φ=0.04.Nanofluid enters the microchannel from the left and after cooling the walls, it leaves from the right side. So there will be symmetric and horizontal streamlines along the microchannel.

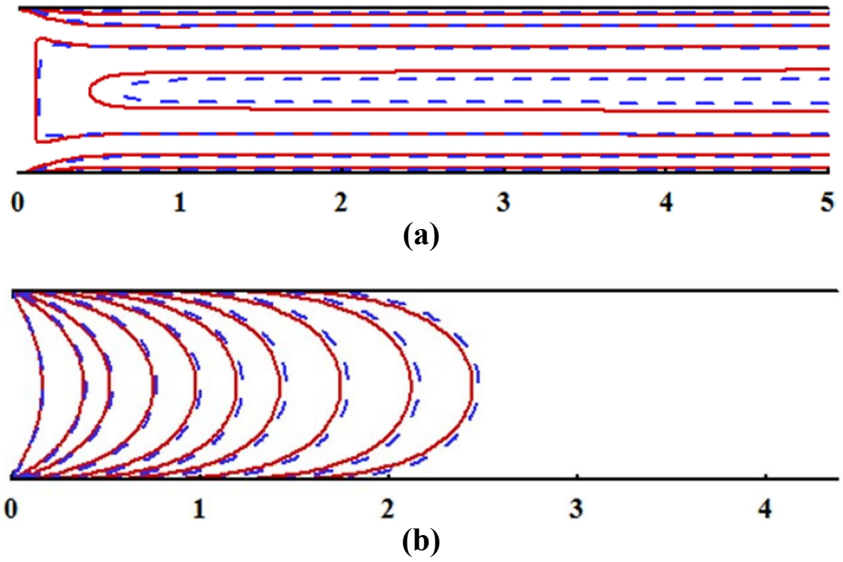

Figure 2. 6.Streamlines (a) and isotherms (b) of the nanofluid for φ=0.04(- B=0,005 and ---B=0, 02)

Figures.2.7 and **2.8** portray the effect of B on U_s and θ_s along the microchannel's walls. It is to highlight that on the inlet region, the slip velocity and temperature jump rushed their maximum values and decreases to attain constant values. Large values of B induce an improvement in both U_s and θ_s.

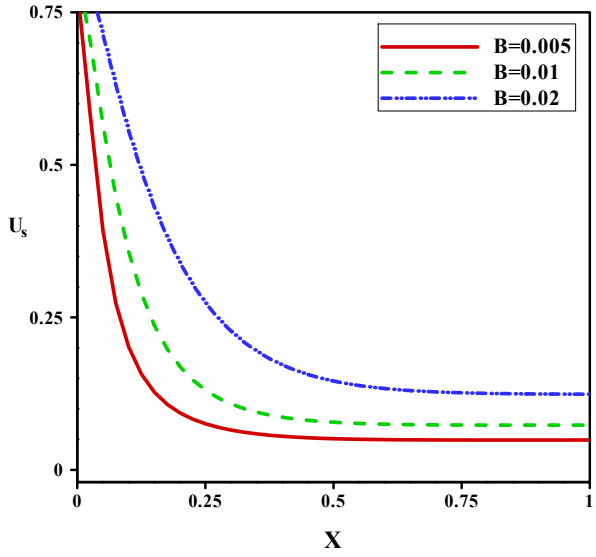

Figure 2. 7.Effects of B on U_s for φ= 0.04

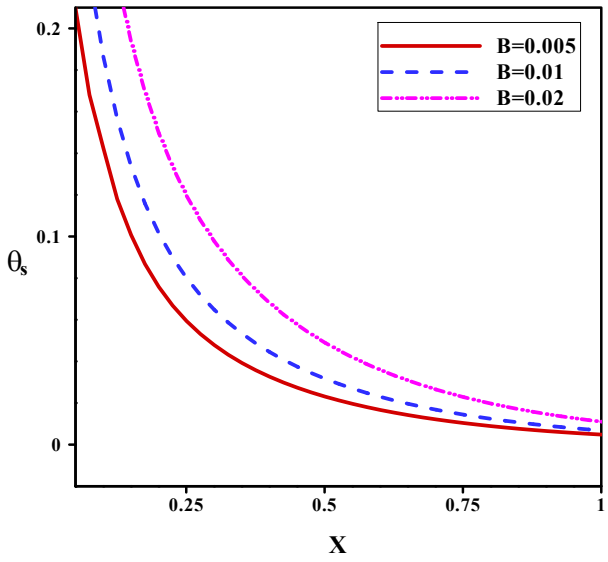

Figure 2. 8.Effects of B on θ_s for φ= 0.04

Figures.2.9 and **2.10** demonstrate the effect of φ on local Nusselt number and temperature jump at fixed value of B. Then, they start with largest value at entrance and they decrease to reach an asymptotic value. For large value of φ, N_{ux} and θ_s are improved. However, this effect is more pronounced for N_{ux}. The temperature jump around the entrance region occurs a higher values (**Figure.2.10)**.Near the wall, the obtaining thermal boundary layer is accentuated.

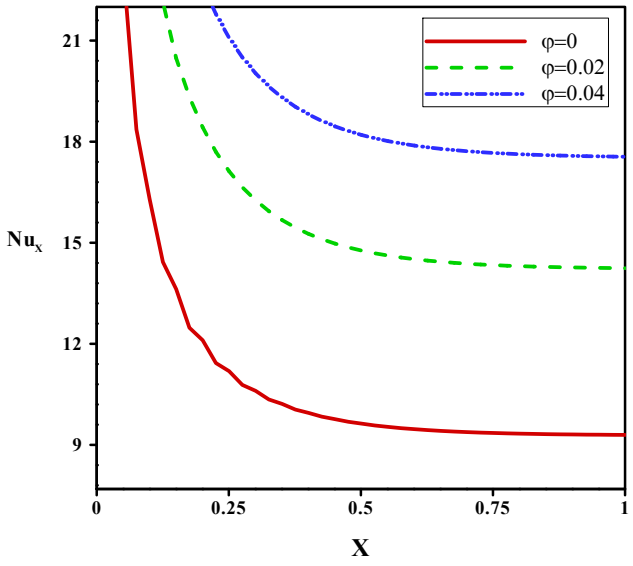

Figure 2. 9.Effect of φ on Nu_x for B = 0.005

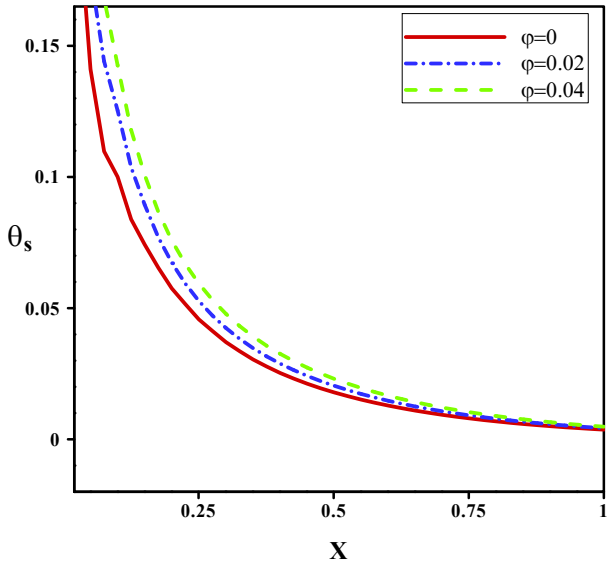

Figure 2. 10. Effect of φ on θ_s for B = 0.005

Figure 2.11. demonstrates the variations of N_{ux} along the microchannel walls at B = 0.005, B = 0.01 and B = 0.02 for φ = 0, φ = 0.02 and φ = 0.04. It can be noted that N_{ux} augments with φ; but declines with B. Temperature gradient between the nanofluid particles on the wall and their neighbor ones adjacent to the wall, diminishes at larger B; as a result N_{ux} becomes less amount at recent case.

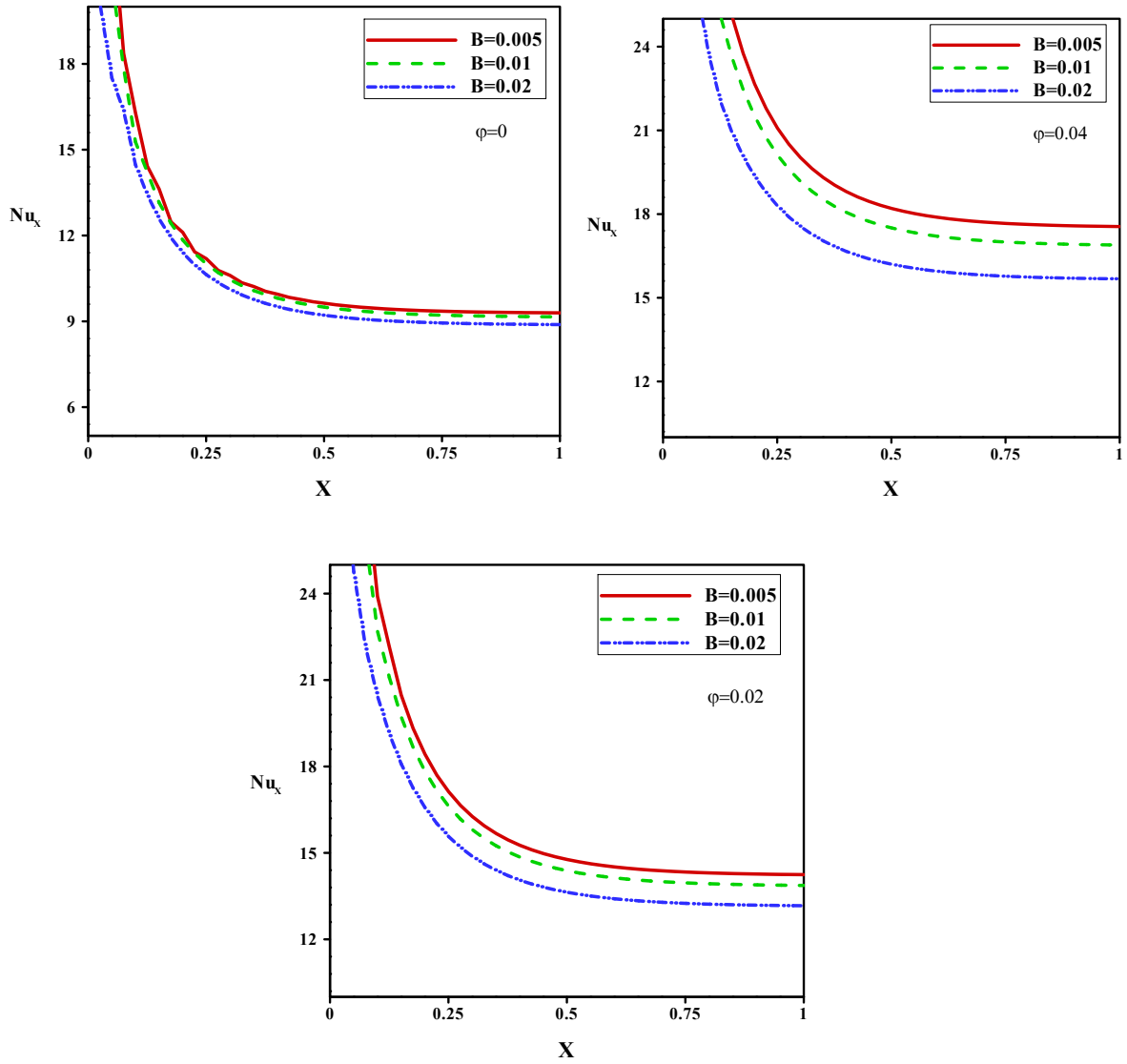

Figure 2. 11. Effect of φ and B on Nu_x

8. Conclusion

Laminar forced convection heat transfer of Ag–water nanofluid in a microchannel is simulated using a double population LBM–BGK method. The effects of different volume fractions of Argon nanoparticles and slip coefficient were investigated on the slip velocity, temperture jump and Nusselt number For Re=0.01.

- The lattice Boltzmann approach is able to handle the nanofluid heat transfer phenomena in micro-channel.
- The numerical obtained results confirmed higher φ corresponds to larger N_{ux} number.
- The larger values of B induces a decreasing in N_{ux} and larger values of Us and θs .

- At the entrance region, the temperature jump reaches a high values along the microchannel walls especially which has the most temperature gradient between the walls and nanofluid.
- To increase N_{ux} in micro liquid flows, it is recommended to use nanofluid with $\varphi = 4\%$ and at low values of slip coefficient as like $B = 0.005$.
- The effect of φ is more pronounced compared to B.
- The Decrease in the values of slip coefficient enhances the convective heat transfer coefficient and consequently the Nusselt number (Nu).

References:

[1] S.M. Aminossadati, A. Raisi, B. Ghasemi, Effects of magnetic field on nanofluid forced convection in a partially heated microchannel, Int. J. Non-Linear Mech. 46 (2011) 1373–1382.

[2] M. Kalteh, A. Abbassi, M. Saffar-Avval, J. Harting, Eulerian–Eulerian twophase numerical simulation of nanofluid laminar forced convection in a microchannel, Int. J. Heat Fluid Flow 32 (2011) 107–116.

[3] M. Mital, Semi-analytical investigation of electronics cooling using developing nanofluid flow in rectangular microchannels, Appl. Therm. Eng. 52 (2013) 321–327.

[4] M. Mital, Analytical analysis of heat transfer and pumping power of laminar nanofluid developing flow in microchannels, Appl. Therm. Eng. 50 (2013) 429–436

[5]Arash Karimipour,Alireza Hossein Nezhad,Annunziata D'Orazio,Mohammad Hemmat Esfe,Mohammad Reza Safaei,Ebrahim Shirani, Simulation of copper–water nanofluid in a microchannel in slip flow regime using the lattice Boltzmann method,European Journal of mechanics B/Fluids 49 (2015) 89-99.

[6] Hussein, Adnan M., et al. "A review of forced convection heat transfer enhancement and hydrodynamic characteristics of a nanofluid." Renewable and Sustainable Energy Reviews 29 (2014): 734-743.

[7] Sheikholeslami, M., and M. M. Bhatti. "Forced convection of nanofluid in presence of constant magnetic field considering shape effects of nanoparticles." International Journal of Heat and Mass Transfer 111 (2017): 1039-1049.

[8] Hussein, Adnan M., R. A. Bakar, and K. Kadirgama. "Study of forced convection nanofluid heat transfer in the automotive cooling system." Case Studies in Thermal Engineering 2 (2014): 50-61.

[9] C. Ay, C.W. Young, C.F. Young, Application of lattice Boltzmann method to the fluid analysis in a rectangular microchannel, Comput. Math. Appl. 64 (2012) 1065–1083.

[10] Y.T. Yang, F.H. Lai, Numerical study of flow and heat transfer characteristics of alumina-water nanofluids in a microchannel using the lattice Boltzmann method, Int. Commun. Heat Mass Transfer 38 (2011) 607–614.

[11] Ma, Yuan, et al. "Study of nanofluid forced convection heat transfer in a bent channel by means of lattice Boltzmann method." Physics of Fluids 30.3 (2018): 032001.

[12] Sheikholeslami, Mohsen. "Magnetohydrodynamic nanofluid forced convection in a porous lid driven cubic cavity using Lattice Boltzmann method." Journal of Molecular Liquids 231 (2017): 555-565.

[13] Bird, Graeme A. "Molecular gas dynamics and the direct simulation of gas flows." Molecular gas dynamics and the direct simulation of gas flows (1994).

[14] Z. Guo, T.S. Zhao, Lattice Boltzmann model for incompressible flows through porous media, Physical Review E 66 (2002) 036304/1-9.

[15] A.D'Orazio, S. Succi, Simulation two-dimensional thermal channel flows by means of a lattice Boltzmann method with new boundary conditions,Future Genet. Comput. Syst. 20 (2004) 935-944.

[16] Brinkman H C 1952 The viscosity of concentrated suspensions and solutions J. Chem. Phys. 20

[17] A. D'Orazio, S. Succi, C.Arrighetti, Lattice Boltzmann simulation of open flows with heat transfer , Phys, Fluids 15 (2003) 2778-2781.

[18]] A. D'Orazio, M. Cercione, G.P. Celata, Application to naturel convection enclosed flows of a lattice Boltzmann BGK model coupled with a general purpose thermal boundary condition, Int. J. Therm. Sci. 43 (2004) 575-586.

[19] Ngoma, Guyh Dituba, and Fouad Erchiqui. "Heat flux and slip effects on liquid flow in a microchannel." International Journal of Thermal Sciences 46.11 (2007): 1076-1083.

[20] Karniadakis, George Em, Ali Beskok, and M. Gad-el-Hak. "Micro flows: fundamentals and simulation." Appl. Mech. Rev. 55.4 (2002): B76-B76.

[21] A. Akbarinia, M. Abdolzadeh, R. Laur, Critical investigation of heat transfer enhancement using nanofluids in microchannels with slip and non-slip flow regimes, Appl. Therm. Eng. 31 (2001) 556-565.

[22] Niu, X. D., C. Shu, and Y. T. Chew. "A thermal lattice Boltzmann model with diffuse scattering boundary condition for micro thermal flows." Computers & Fluids 36.2 (2007): 273-281.

[23] A.K. Santara, S. Sen, N. Chakraborty, Study of heat transfer due to laminar flow of copper –water nanofluid through two isothermally heated parallel plates, Int. J. Therm. Sci. 48 (2009) 391-400.

Chapter3: Heat transfer in a porous macro-channel filled with nanofluid

1. Introduction

Investigations on fluid flow and forced-convective heat transfer in porous systems has raised in last years through their wide range of applications in science, engineering and industry such as heat exchangers, solar porous receivers, thermal insulation and cooling of stored grains, food processing, the cooling system of electronic equipment, nuclear waste storage, etc., and the heat transfer in soil and other media(environmental fluid flows) [1]. Besides, despite the prompt rise of microsystems technology involving nano/micro cooling systems for aircraft and aerospace vehicles, medical engineering, automotive industries, power generation, solar technologies, and so on, thermal cooling technology faces huge challenges, especially regarding overall size, energy saving and cost reduction. Further, the constant need for miniaturization is highly sought after in these areas for more space saving. Such miniaturized systems typically involve an extended length and time scale, which can pose modeling and simulation challenges to capture the physics of flows at different scales. Thereby, research attention is increasingly focused on the heat transfer field to optimize energy devices (miniature or not) performance through heat transfer enhancement. This approach is certainly set to be pursued relentlessly in the future.The dispersion of solid nanoparticles in common working fluids such as water is one of the methods that can be implemented in improving the thermal performance of energy systems, and their application is prospective in this area [2]. These nanofluids (nanosuspensions), first conceptualized and pioneered by Choi and Eastmanin [3]and since widely accepted [4] to name a few, consist mainly of two components including a base fluid and solid nanoparticles. Due to their higher thermal conductivity than usual liquids, it has been turned out that these fluids can have irrefutable potential for improving the heat transfer rate in engineering systems compared to pure liquids, especially for cooling electronic devices among others. Thereby, many groups around the world are currently working in this vast field [2, 4] for developing appropriate techniques for improving heat transfer [5, 6] to cite a few. On the other hand, porous supports' use in thermal systems is an additional technique to raise thermal efficiency as they provide a high contact surface which helps to improve the heat transfer rate.

Alhajaj et al. [7] performed a numerical study of different configurations (porous block, porous straight channel and porous wavy channels) setups using four different types of nanofluids mainly, namely 0.5% vol Al_2O_3/water, 0.5% vol TiO_2/water, 0.5% vol Al_2O_3/Ethylene Glycol and 0.5% vol TiO_2/Ethylene Glycol. They demonstrated that each nanofluid behaves differently from the others in terms of performance and found that the efficiency index is improved for the nanofluid by 0.5% by volume of water-based Al_2O_3.

Maghrebi et al. [8] investigated numerically heat transfer by nanofluids flowing through a 2D porous channel. They have pointed that the heat transfer rate in porous medium decreases for large values of the Lewis number, which is independent of the volume fraction distribution. Heat transfer and fluid flow of Cu (Copper), CuO (Copper oxide), TiO_2(Titanium dioxide) and Al_2O_3 (aluminum oxide) nanoparticles over permeable surface have been handled in the presence of injection and suction by Maleki et al. [9]. These authors demonstrated that the non-Newtonian nanofluid shows better heat transfer performance compared to the Newtonian nanofluid. However, they observed that in injection, the use of non-Newtonian nanofluid can decrease heat transfer. Akinshilo [10] studied the geometry effects of different nanoparticles on heat transfer of nanofluid through porous channel using the homology perturbation method. From the analysis performed, it turned out that the lamina-shaped nanoparticles have a higher temperature and thermal conductivity compared to those of cylindrical and spherical shapes. Zhao et al. [1] numerically investigated the effects of nanoparticle volume fraction, Darcy number on heat exchange performance and flow in a porous channel within three heated blocks. Their outcomes showed that the addition of nanoparticles greatly improves the average Nusselt (Nu) number on the surface of heated sources. Besides, they stated that this parameter and the heat exchange performance drop with rising the Darcy number. Mahdavi et al. [11] achieved a numerical study on the heat transfer and entropy generation rate in flow through an isothermal pipe partially filled with porous medium. They seeked the optimized position and porous medium characteristics in the pipe that lead to higher heat transfer and lower entropy generation rate. Xu et al. [12] conducted a numerical study on the transfer of heat by forced convection of a fluid with nanoparticles in a metallic-foam duct via the local thermal non-equilibrium (LTNE) model. The effects of some key parameters on the flow and heat transfer of the nanofluid in porous media were analyzed along with mechanisms for improving heat transfer. Alihosseini and Jafari [13] used a 3D numerical model of fluid dynamics to examine the heat transfer of water-based nanofluids and Al_2O_3 in different configurations of porous media including different cylinders. They found that the fully porous cylinder exhibited the maximum improvement in Nu number and enhancement parameter over the empty cylinder. Needless to say, the efficient use of energy is and remains a major objective in the design of engineering systems. This requires the application of the second law of thermodynamics since the amount of available work is intimately linked the entropy amount production (e.g. Bejan [14], to name a few). Ellahi et al. [15] have studied numerically a pressure-driven flow of aluminum oxide-water based nanofluid with the combined effect of entropy generation and radiative electro-magneto-hydrodynamics filled

with porous media inside a symmetric wavy channel. It was found that, due to thermal buoyancy, the Darcy number, radiation parameter, electromagnetic parameter and temperature profile increase with the magnetic field parameter.Shah et al. [16] numerically examined the behavior of a hybrid nanomaterial in a permeable container due to Lorentz forces, constant heat flow and porosity. They found that increasing buoyancy and average porosity improve convective flow and lower temperature.

Although there have been some advances in numerical and experimental approaches that deal with heat transfer via nanofluids in porous media, the forced convective flows analysis in open-ended porous channels still remains an open and challenging topic. In this context a numerical study on nanofluid forced flow and heat transfer in an open-ended porous channel was performed via thermal lattice Boltzmann method (TLBM) at the representative elementary volume (REV) scale. Indeed, in recent years, the LBM has been used more and more to study heat exchanges within nanofluids at the REV scale. In addition, the forced convection of nanofluids in porous media can be analyzed numerically at either the domain scale, the pore scale or the REV scale. It is this last approach which is retained herein since it combines the balance between the porous domain size to be deemed and the computation cost.Such an approach has achieved great success in studying complex problems across a wide range of scales [17, 18], as well as nanofluid flows [19 - 24] to name a few.

It is worth noting that computation at finer resolutions can only be achieved by simulation techniques such as LBMs, molecular dynamics (MD) and Monte Carlo (MC) methods and that due to the simplifications and empiricalmodifications often made, the traditional methods (FVM, FEM, etc.) become less suitable for handling nanofluid flows with or without heat transfer in porous media, miniaturized or not.

Seta et al. [25] studied natural convection in a square cavity filled with a porous medium using the Brinkman-Forchheimer model and provided thermal behavior influenced by porosity, Darcy number (Da), and Rayleigh number. Mohebbi et al. [26] applied a LB method to simulate forced convection in an extended surface channel deeming three different nanofluids. They highlighted the effect of changing different parameters such as the solid volume fraction, the *Re* number, and the relative height of extended surfaces. Zhao et al. [27] analyzed the impacts of the nanoparticles volume fraction and Da number on the fluid and heat exchange performance in a porous channel using a nonorthogonal multiple-relaxation time (MRT)-LBM. They noticed the conspicuous influence of heat exchange by forced convection of fluid flow and thermal conduction.

As heat transfer is one of the key parameters in the aerospace industry, many techniques for improving heat have loomed up with the primary aim of reducing the exchange size involved while rising the capacity, or to mitigate the temperature difference. Such an approach could better help reduce the fuel consumption (e.g. of aeronautic/aerospace and other vehicles. Moreover, it turned out that nanoparticles' addition in a base fluid (e.g. water) improves the rate of heat transfer in these systems. Thereby, this technique is increasingly taken up in aerospace, nuclear, biomedical and electronic applications. Table 1 gathers some relevant studies dealing with heat transfer improvement via nanofluids.

Table 3. 1. References' synthesis on thermal transfer via nanofluids.

Reference	Arrangement	Highlights	Main findings
Bahrami et al. [28]	Microchannel	Effect of the Reynolds number (Re) on the thermal field and the Nusselt number (Nu).	Rising Re reduces the effect of the percentage of facing discrete heat sources and the mean Nu.
Tighchi and Esfahani [29]	Square cavity	Effect of Rayleigh number, extinction coefficient and scattering albedo on dynamic and thermal fields.	The effect has been demonstrated and the numerical approach used (LBM) has turned out to be adequate in terms of the computation time.
Hoseinpour et al. [30]	Porous cavity	Rayleigh number (Ra), porosity and Darcy number (Da)effects.	The entropy generation decreases with the volume fractions of the nanofluid and increases with Ra, porosity and Da.
Sivasankaran and Pan [31]	Lid-driven cavity	Effect of Ra number and nanoparticles' volume fraction.	Heat transfer rate rises proportionally with nanoparticles' volume fraction.
D'Orazio and Karimipour[32]	Microchannel	Effect of Knudsen (Kn) and Grashof (Gr) numbers.	Nu number increases strongly with Gr number du to buoyancy forces.
Azizi et al. [33]	Cylindrical microchannel heat sink.	Effect of Re number and water's concentration.	Obtaining an optimum Re value and a water's fraction.
Reference	Arrangement	Highlights	Main findings
Bahrami et al. [28]	Microchannel	Effect of the Reynolds number (Re) on the thermal field and the Nusselt number (Nu).	Rising Re reduces the effect of the percentage of facing discrete heat sources and the mean Nu.

This non-exhaustive investigation points that the use of nanofluids as a heat transfer medium has been pierced over recent decades. To the best of our knowledge, in the perusal of literature fulfilled, simulating nanofluid forced flows and heat transfer in an open-ended porous channel with the REV-multi-distribution functions(MDF)-TLB method remain scarce. To fill out this gap, it is the latter approach which was considered herein to simulate the flow in forced convection within a porous channel saturated with a Cu/water mixture as nanofluids via the Brinkman-Forchheimer-Darcy (BFD) model. Such a model leans on momentum equation supplemented with the term friction due to macroscopic shear, which reduces to the traditional Navier-Stokes equation of a viscous fluid when the permeability is infinite and to the Darcy's equation when it is zero. The originality of the current study is to take-up of the REV-lattice Boltzmann method to handle the single phase model of flow of nanofluid with particles concentration less than 4% through an open-ended macroporous channel and to analyze the irreversibility of the considered system through the entropy generation rate and the Bejan number under various effects of relevant parameters. It should also be pointed out that, despite the extensive research undertaken on heat transfer in macrochannels, the system‘s instability study and the viscous dissipation effect on convective heat transfer and laminar flow of nanofluids should still be addressed. In addition, to our knowledge and from the open literature review, studies on system’s irreversibility and entropy generation in a nanofluid-filled macrochannel subjected to forced convection using Brinkman-Forchheimer-Darcy model are developed through this chapter. To sum up, through the findings obtained, the proposed numerical simulation contributes to establishing the confidence premises required for thermal laminar flows of forced convective heat transfer in nanofluid-filled macrochannels.The layout of this chapter is as follows. In Section 2, the problem statement and simplifying assumptions are described. In section 3, the mathematical modeling of the dimensionless governing equations at the REV scalein a saturated porous fluid is presented for the local thermal equilibrium **(**LTE)condition. The calculation of the entropy generation through relevant parameters is briefly filled in. Section 4 introduces LBM for nanofluid flow in porous media adopted herein, and code validation is reported in Section 5. Section 6 comments on the obtained outcomes, and the last section sums up the main findings of this analysis.

2. Problem statement and assumptions

Figure 1depicts the nanofluid forced flow and heat transfer in an open-ended porous channel along with relevant geometric parameters. It displays a 2D channel of length L and height H filled with Cu/water as a nanofluid. This enters into the channel with a constant and uniform

velocity(U_0) and a uniform temperature (T_{in}) and leaves and leaves it while being fully developed, so that Neumann Boundary conditions (BCs) are imposed at exit. The laminar nanofluid flow exchanges heat through its upper and lower walls, which are assumed to be isothermal (at constant temperature T_w) and no-slip. The channel being straight, the Cartesian coordinate system is used to describe the fluid flow whose -axis represents the streamwise direction.

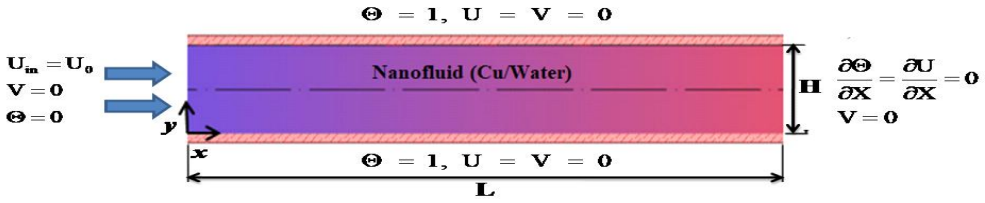

Figure 3. 1. Sketch of the envisioned problem with geometrical parameters and boundary conditions associated.

The assumptions that match to the subsequent mathematical model (Eqs. (1)-(3)) are:

•The forced convective flow is laminar;

• The flow in the porous medium is considered as Brinkman-Forchheimer-Darcy (BFD) flow;

• The Cu/water nanofluid is assumed to be homogeneous, isotropic Newtonian, viscous and incompressible (Ref. [34]);

• The no-slip boundary condition is used for the top and bottom walls;

• The effects of viscous dissipation are significant

• Cu-nanoparticles and water are in local thermal equilibrium (LTE): this results in a single transport energy equation;

• Both phases have constant thermophysical properties (see Table 2).

Table 3. 2.The mixture (Cu/water) thermophysical properties at $T = 298K$.

Properties	Water	Cu
$\lambda\left(W.m^{-1}.K^{-1}\right)$	0.613	400
$\rho\left(Kg.m^{-3}\right)$	997.1	8933
$C_p\left(J.kg^{-1}.K^{-1}\right)$	4179	385
$\mu(Pa.s)$	$8.92\text{x}10^{-4}$	-

3. Mathematical modeling

3.1 REV governing equations

Recall that here it is the Cu/water nanofluid flow and forced heat transfer in a porous channel that are investigated. With related assumptions and conditions up-stated, the governing equations (mass, momentum and energy conservations) at the REV scale for a convective nanofluid flow saturating a porous channel read [35-40]:

$$\vec{\nabla}.\vec{V}=0 \tag{3.1}$$

$$\frac{\rho_{nf}}{\varepsilon}\frac{\partial \vec{V}}{\partial t}+\frac{\rho_{nf}}{\varepsilon^2}\left(\vec{V}.\nabla\vec{V}\right)=-\nabla p+\nabla.\left(\mu_e\nabla\vec{V}\right)-\frac{\mu_{nf}}{K}\vec{V}-\frac{\mu_{nf}F_\varepsilon}{\sqrt{K}}\left\|\vec{V}\right\|\vec{V} \tag{3.2}$$

$$\left(\rho C_p\right)_{nf}\left(\frac{\partial T}{\partial t}+\vec{V}.\vec{\nabla}T\right)=\lambda_e\nabla^2T+\psi_1+\psi_2 \tag{3.3}$$

Where $\vec{V}(u,v)$, p and T are the fluid's volume-averaged velocity, pressure and temperature, respectively. ε is the porosity, and K and F_ε are the permeability and adjusted Forchheimer shape factor of porous medium, respectively. And μ_{nf} and ρ_{nf} depict the nanofluid dynamic viscosity and density, respectively. C_p denotes nanofluid specific heat capacity. Moreover, μ_e and λ_e are the effective dynamic viscosity and thermal conductivity, respectively, and ultimately the source term $\psi_1+\psi_2$ corresponding to the dissipation function is specified below using relationship (8).

It is more appropriate to consider the dimensionless transport equations instead to facilitate outcomes interpretation using dimensionless variables indicated by uppercase letters. These can be obtained through the following parameters:

$$(U,V)=\left(\frac{u}{u_0},\frac{v}{u_0}\right),\ (X,Y)=\left(\frac{x}{H},\frac{y}{H}\right),\ \tilde{t}=t\frac{U_0}{H},\ P=\frac{p}{\rho u_0^2},\Theta=\frac{T-T_{in}}{T_w-T_{in}} \tag{3.4}$$

Regarding the other characteristic dimensionless parameters, the Reynolds number is $Re(=HU_0/\nu_f)$, the Prandtl number is $Pr(=\nu_f/\alpha_f)$, the Darcy number is $Da(=K/H^2)$, the Eckert number is $Ec(=U_0^2/c_p/\Delta T)$, the heat capacity ratio is $R_c(=(\rho C_p)_s/(\rho C_p)_f)$, and the thermal conductivity ratio is $R_k(=\lambda_s/\lambda_f)$, respectively.Hence , according to these parameters considered, the resulting dimensionless equations can be written as :

$$\nabla.\vec{V}=0 \tag{3.5}$$

$$\frac{\partial \vec{V}}{\partial t}+U.\nabla\left(\frac{\vec{V}}{\varepsilon}\right)= -\vec{\nabla}(\varepsilon P)+\frac{1}{\mathrm{Re}(1-\varphi)^{2.5}\left(1-\varphi+\varphi\left(\frac{\rho_{np}}{\rho_f}\right)\right)}\nabla^2\vec{V}-\frac{\varepsilon}{\mathrm{Re}(1-\varphi)^{2.5}\left(1-\varphi+\varphi\left(\frac{\rho_{np}}{\rho_f}\right)\right)Da}\vec{U}-\frac{F_\varepsilon\varepsilon}{\sqrt{Da}}\left\|\vec{V}\right\|\vec{V} \quad (3.6)$$

$$\left(\varepsilon+(1-\varepsilon)\frac{R_c}{R_{c_{nf}}}\right)\frac{\partial\Theta}{\partial\tilde{t}}+U.\nabla\Theta= \frac{\varepsilon R_{\lambda_{nf}}+(1-\varepsilon)R_k}{RePr\left(1-\varphi+\varphi\frac{(\rho c_p)_{np}}{(\rho c_p)_f}\right)}\nabla^2\Theta+\frac{Ec}{Re\left(1-\varphi+\varphi\frac{(\rho c_p)_{np}}{(\rho c_p)_f}\right)}(\psi_1+\psi_2) \quad (3.7)$$

With

$$\left.\begin{aligned}\psi_1&=\varepsilon\left(\frac{1}{Da(1-\varphi)^{2.5}}+\frac{F_\varepsilon Re\left(1-\varphi+\varphi\frac{\rho_{np}}{\rho_f}\right)}{\sqrt{Da}}|\vec{V}|\right)\left\|\vec{V}\right\|^2\\ \psi_2&=\frac{1}{(1-\varphi)^{2.5}}\left(2\left[(\frac{\partial U}{\partial X})^2+(\frac{\partial V}{\partial Y})^2\right]+\left[\frac{\partial U}{\partial Y}+\frac{\partial V}{\partial X}\right]^2\right)\end{aligned}\right\} \quad (3.8)$$

The permeability K and the shape factor F_ε may be rated using the following relationships [41]:

$$K=\varepsilon^3 d_p^2/\left(150(1-\varepsilon)^2\right) \text{ and } F_\varepsilon=1.75\left(150\varepsilon^3\right)^{-0.5} \quad (3.9)$$

d_p (=10 nm [23]) being the nanoparticles diameter.

The thermo-physical properties of the mixture Cu/water (up-involved in Equations (5)-(8)) are calculated via the following classical relationships coming from Maxwell and Brikmann (Einstein model extended up to 4% volume concentration) theories predictions for solid/fluid mixtures [34], to name a few:

$$\begin{cases}\rho_{nf}=(1-\varphi)\rho_f+\varphi\rho_{np}\\ \mu_{nf}=\mu_f/(1-\varphi)^{2.5}\\ \lambda_{nf}/\lambda_f=\dfrac{\lambda_{np}+2\lambda_f-2\varphi(\lambda_f-\lambda_{np})}{\lambda_{np}+2\lambda_f+\varphi(\lambda_f-\lambda_{np})}\\ (\rho c_p)_{nf}=(1-\varphi)(\rho c_p)_f+\varphi(\rho c_p)_{np}\end{cases} \quad (3.10)$$

Where φ is the nanoparticles' volume fraction. Note that here the indices *f* and *np* stand for thermophysical properties of the base fluid and nanoparticles (Cu), respectively. Recall that

indices *f* and *np* respectively refer to the thermophysical properties of base fluid and nanoparticles (Cu).

It should be emphasized that these correlations do not take into account either Brownian motion or the mutual forces between particles, thereby evading correlations use which may prove to be complicated to implement.

3.2 Initial and boundary conditions (I & BCs)

Knowing that the implementation of the initial (I) and boundary conditions (BCs) plays an essential

role in any flow problem to obtain a proper solution, dimensionless initial and boundary conditions (I & BCs) associated with the pre-formulated equations are:

- $U(\tilde{t}) = V(\tilde{t}) = \Theta(\tilde{t}) = 0$ (Initial conditions) ;
- $U = 1$; $V = 0$; $\Theta = 0$, at $X = 0$ and $0 \le Y \le 1$ (inlet) ;
- $\frac{\partial U}{\partial X} = \frac{\partial V}{\partial X} = \frac{\partial \Theta}{\partial X} = 0$; at $X = L/H$ and $0 \le Y \le 1$ (outlet) ;
- $U = 0$; $V = 0$ and $\Theta = 1$ at $0 \le X \le L/H$ and Y=1(top) ;
- $U = 0$; $V = 0$ and $\Theta = 1$ at $0 \le X \le L/H$ and $Y = 0$ (bottom).

Note that the LBM context, these macroscopic boundary conditions have to be translated using mesoscopic distribution functions without their physical meaning being altered (see § IV.Bhereinafter).

3.3 Entropy generation for LTE condition

Entropy is generated due to the existence of temperature and velocity gradients. In terms of dimensionless variables, the local entropy generation rate (sometimes called entropy generation number) for the porous system mentioned above can be depicted via the dimensionless following relationship [42, 43]:

$$Ns = \underbrace{\frac{\varepsilon R_{k,nf} + (1-\varepsilon) R_k}{(\Theta + \Pi)^2}\left[\left(\frac{\partial \Theta_f}{\partial X}\right)^2 + \left(\frac{\partial \Theta_f}{\partial Y}\right)^2\right]}_{\textit{Heat transfer irreversibility (HTI)}} + \underbrace{\frac{Ec.Pr}{(\Theta + \Pi)}(\psi_1 + \psi_2)}_{\textit{Nanofluid friction irreversibility (FFI)}} \qquad \textbf{(3.11)}$$

From this relationship, it looms that HTI and FFI are the two ingredients of total entropy generation whereby the irreversibility could be assessed. It is noteworthy that the average total entropy generation (Ns_{av}) of the system is obtained by averaging Eqution (11) over the entire channel.

Irreversibility within the system (or its performance) is assessed using the Bejan number [14],which is defined as follows:

$$Be = HTI / Ns \quad \textbf{(3.12)}$$

The local Nusselt number (Nu) along the bottom wall is evaluated as:

$$Nu = -\frac{\varepsilon\lambda_{nf} + (1-\varepsilon)\lambda_s}{\varepsilon\,\lambda_f}\left(\frac{\partial\Theta}{\partial Y}\right)_{Y=0} \quad \textbf{(3.13)}$$

Spatial averaged Nusselt number is obtained by integrating the local Nusselt number along the bottom wall as :

$$Nu_{av} = \frac{1}{L/H}\int_0^{L/H} Nu\, dX \quad \textbf{(3.14)}$$

4. LBM for nanofluid flow in porous media

4.1 Single relaxation time lattice Boltzmann model (SRT-LBM)

The LB model at the REV scale for the flow field in porous media (viz. the governing equations. (5)-(7)) is adopted in this study. To avoid pointless repetitions, such an equations' system is not listed in this section. Heat transfer within a channel is often a forced convection problem where the Reynolds number is one of the key parameters.

To handle the problem aimed herein, it is the thermal lattice Boltzmann method (TLBM) at the REV scale based on two distribution functions, f and g , respectively for the flow and temperature fields which is taken up here. So, the macroscopic flow characteristics are obtained by the link between macroscopic flow variables and the distribution density function. Simply put, in LBM, each cell is a fluid particles cluster (represented by distribution functions) that can move in different directions. Thereby, the spatial and temporal evolvement of the fluid particle distribution function is described via the following SRT-based LB evolving equation [25, 44, 45]:

$$f_i\left(x + e_i\Delta t, t + e_i\Delta t\right) - f_i\left(x,t\right) = -\Delta t\tau_e^{-1}\left[f_i\left(x,t\right) - f_i^{eq}\left(x,t\right)\right] + \Delta t F_{e_i} \quad \textbf{(3.15)}$$

In Eq. (4.15), $\tau_e\ (=3\nu_{nf}+0,5)$ is the dimensionless relaxation time for pseudo particles' density distribution $f_i(x,t)$ at space x and time t; e_i and Δt are the discrete lattice velocities and the time step, while $f_i^{eq}(x,t)$ is the equilibrium distribution function (EDF), which for the D2Q9 model (see **Figure 2**) is defined as :

$$f_i^{eq} = \rho\omega_i\left[1 + \frac{e_i.u}{c_s^2} + \frac{uu:\left(e_i.e_i - c_s^2 I\right)}{2c_s^4\varepsilon}\right] \quad \textbf{(3.16)}$$

Where ω_i is the weight factor for distribution functions and $c_s\ (=c/\sqrt{3})$ is the sound speed. The lattice velocities e_i used for D2Q9 model are given by:

$$e_i = \begin{cases} (0,0) \\ c\left[\cos\left((i-1)\pi/2\right), \sin\left((i-1)\pi/2\right)\right], i = 1-4 \\ \sqrt{2}c\left[\cos\left((2i-9)\pi/4\right), \sin\left((2i-9)\pi/4\right)\right], i = 5-8 \end{cases} \quad \textbf{(3.17)}$$

$c\,(=\Delta x/\Delta t)$ being the lattice speed and the weights are $\omega_0 = 4/9$, $\omega_{1-4} = 1/9$, $\omega_{5-9} = 1/36$. It is worthy to mention that the order numbers i= 1- 4 and i =5 -8 respectively indicate upright, streamwise and the diagonal directions of the lattice (**Figure. 3.2**).

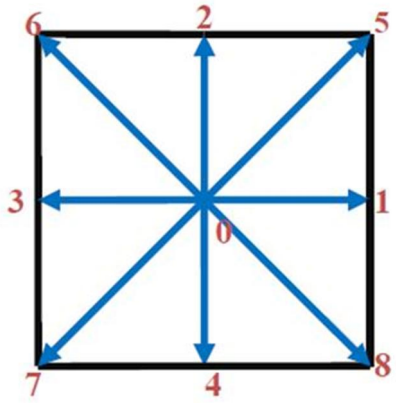

Figure 3. 2.Lattice structure (unit cell) for particle velocity vectors e_i for D2Q9 model.

The last quantity F_{ei} of Equation. (3.15) is the total force due to the porous medium and other external forces which can be expressed as [34, 46]:

$$F_{ei} = -\left(\left(\frac{\varepsilon \upsilon_{nf}}{K}u + \frac{\varepsilon F_\varepsilon}{\sqrt{K}}|u|u\right)\frac{(e_i - u)^2 f_i^{eq}}{RT_0}\right) \quad \textbf{(3.18)}$$

At last, fluid density ρ and temporary velocity v are determined from the moment of the distribution function as follows:

$$\rho = \sum_i f_i, \quad \mathrm{v} = \sum_{\mathrm{i}} \mathrm{f_i e_i} / \rho + \Delta \mathrm{t F_{ei}} / 2 \quad \textbf{(3.19)}$$

Given the nanoparticles presence, the actual velocity u is computed according to the following relationship [47]:

$$\mathrm{u} = \frac{\mathrm{v}}{\mathrm{c_0} + \sqrt{\mathrm{c_0}^2 + \mathrm{c_1}|\mathrm{v}|}} \quad \textbf{(3.20)}$$

With $$c_0 = \frac{1}{2}\left(1 + \varepsilon\frac{\Delta t}{2}\frac{\upsilon}{K}\right), c_1 = \varepsilon\frac{\Delta t}{2}\frac{F_\varepsilon}{\sqrt{K}} \quad \textbf{(3.21)}$$

As up-mentioned, the thermal part is simulated by using a different g distribution function for temperature. Herewith, the SRT-based LB evolving equation for temperature can be written as follows [43, 48]:

$$g_i\left(x+e_i\Delta t,t+\Delta t\right)-g_i\left(x,t\right)=-\Delta t\tau_g^{-1}\left(g_i\left(x,t\right)-g_i^{eq}\left(x,t\right)\right)+\Delta tG_i \qquad \textbf{(3.22)}$$

Where g_i is the temperature distribution function, τ_g is the lattice relaxation time, which can be defined as:

$$\tau_g=3Pr\frac{R_{c,nf}}{R_{k,nf}}\frac{(1-\varphi)^{-2.5}}{(1-\varphi)+\varphi\dfrac{\rho_p}{\rho_f}}(\tau_e-0.5)C+0.5 \qquad \textbf{(3.23)}$$

With
$$C=\frac{\varepsilon+(1-\varepsilon)R_k/R_{k,nf}}{\varepsilon+(1-\varepsilon)R_c/R_{c,nf}} \qquad \textbf{(3.24)}$$

Also, equilibrium distribution function for temperature field, g_i^{eq} for D2Q9 can be expressed as [39, 49]:

$$g_i^{eq}=\omega_i\Theta\left(1+e_iu/c^2{}_s\right) \qquad \textbf{(3.25)}$$

The term G_i appearing in Eq. (4.22) can be expressed by :

$$G_i=\omega_i.Ec.Re^{-1}\frac{\left(1+\dfrac{e_iu}{c_s^2}\left(\dfrac{\tau_g-0.5}{\tau_g}\right)\right)}{\left(1-\varphi+\varphi\dfrac{(\rho c_p)_{np}}{(\rho c_p)_f}\right)}\left(\psi_1+\psi_2\right) \qquad \textbf{(3.26)}$$

In final step, the temperature is given by [39]:

$$\left(\varepsilon+\left(1-\varepsilon\right)\frac{R_C}{R_{C,nf}}\right)\Theta=\sum_{i=0}^{8}g_i \qquad \textbf{(3.27)}$$

It is worth mentioning that, for the sake of simplicity and implementation, we opted for a simple and first-order accurate strategy unlike that of He et al. [50] which is second-order.

4.2 Dynamic and thermal LB-BCS

It is worth noting that implementation of BCs in LBM is different from other common grid-based numerical solving methods. Naturally, the leading role of boundary conditions (BCs) in the LBM formalism is translated by the microscopic distribution functions to establish a connection between the macroscopic-prescribed BCs, such as velocity and/or temperature and the microscopic BCs for of the LBM. Herein, these are computed using the following relationships [51- 54] to cite a few:

•Flow part

The inlet density and the distribution functions can be expressed as follows :

$$\left.\begin{aligned} &\rho_{in} = \left(f_0 + f_2 + f_4 + 2\left(f_3 + f_6 + f_7\right)\right)/\left(1 - U_0\right) \\ &f_1 = f_3 + 2\rho_{in}U_0/3 \\ &f_5 = f_7 - \left(f_2 - f_4\right)/2 + \rho_{in}U_0/6 \\ &f_8 = f_6 + \left(f_2 - f_4\right)/2 + \rho_{in}U_0/6 \end{aligned}\right\} \quad \textbf{(3.28)}$$

The corner node at the inlet requires some special treatment. For instance, the bottom node at the inlet is taken. f_3, f_4 and f_7 are known where ρ is specified and u=0 after the streaming process. By applying the bounce back rule for the non-equilibrium part of the particle distribution normal to the inlet and the boundary, $f_1 = f_3$, $f_2 = f_4$, $f_5 = f_7$ and $f_6 = f_8$. A similar procedure can be applied to the top inlet node and outlet nodes [51].

$$\left.\begin{aligned} &f(n,j,3) = 2f(n-1,j,3) - f(n-2,j,3) \\ &f(n,j,6) = 2f(n-1,j,6) - f(n-2,j,6) \\ &f(n,j,7) = 2f(n-1,j,7) - f(n-2,j,7) \end{aligned}\right\} \quad \textbf{(3.29)}$$

n being the node number in the streamwise direction. The bounce back condition is used to handle boundary conditions at the channel solid walls via the relationship:

$$f_{\bar{i}}(x_{nf}) = f_i(x_{nf}) \quad \textbf{(3.30)}$$

Where $e_{\bar{i}} = -e_i$ and x_{nf} is the fluid node at the lower and upper walls of the canal.

Through this bounce-back relationship, it is the quantities f_4, f_7 and f_8 (respectively f_2, f_5 and f_6) which are unknown at the upper wall (respectively at the lower wall).

•**Thermal part** (Refs. [53, 54])

At the channel input, the following BCs are imposed as

$$g_1 = -g_3 \; ; g_5 = -g_7 ; \; g_8 = -g_6 \quad \textbf{(3.31)}$$

For the exit (east), the boundary conditions were set as follows:

$$g_{3,n} = -g_{3,n-1} ; g_{6,n} = -g_{6,n-1} ; g_{7,n} = -g_{7,n-1} \quad \textbf{(3.32)}$$

At north and south walls, the following conditions are fixed:

$$\left.\begin{aligned} &g_4 = T_w(\omega_2 + \omega_4) - g_2 \qquad g_2 = T_w(\omega_2 + \omega_4) - g_4 \\ &g_7 = T_w(\omega_5 + \omega_7) - g_5 \text{ and } \; g_5 = T_w(\omega_5 + \omega_7) - g_7 \\ &g_8 = T_w(\omega_6 + \omega_8) - g_6 \qquad g_6 = T_w(\omega_6 + \omega_8) - g_8 \end{aligned}\right\} \quad \textbf{(3.33)}$$

As a solving method, the SRT-TLBM approach at the REV scale is herein used to solve the governing equations along with specified boundary and initial conditions.

5. Grid independency and validation

As up-mentioned, an in-house parallel SRT-TLBM code has been developed for this numerical investigation. To ensure the validity of this numerical solver, validation has been

done and, the results achieved are compared with those of Santra et al. [55] and Mahmud and Fraser [56]. Table 3.3 gathered the maximum errors (%) for the model validation. Previously, grid independence for code was performed for three sizes, namely (1122x51), (1320x60) and (1518x69) to find the grid independent outputs (see **Figure 3a**).

Table 3. 3.Model validation errors (%)

Error (%)/ Fig. 3 b	**Error (%)/ Fig. 3 c**
0.98 (Re=200)	0.81 (Da=0.01)
0.91 (Re=100)	0.47 (Da=0.05)
0.87 (Re=50)	0.42 (Da=0.1)

As depicted **in Figures. 3b-c,** results are presented in terms of average Nusselt profiles set by and dimensionless temperature (Θ) set by Da at the streamwise station $X = 6$ from which the flow becomes fully developed. The outcomes obtained corroborate Refs.'s results [55, 56] with an outstanding agreement. Accordingly, the code outcomes are reliable, thereby, demonstrating that the solver can be implemented to deal with the deemed problem. Note that, due to the small difference between the results of the last two grid sizes (0.18%), the 1320x60 grid was selected to handle the further simulations.

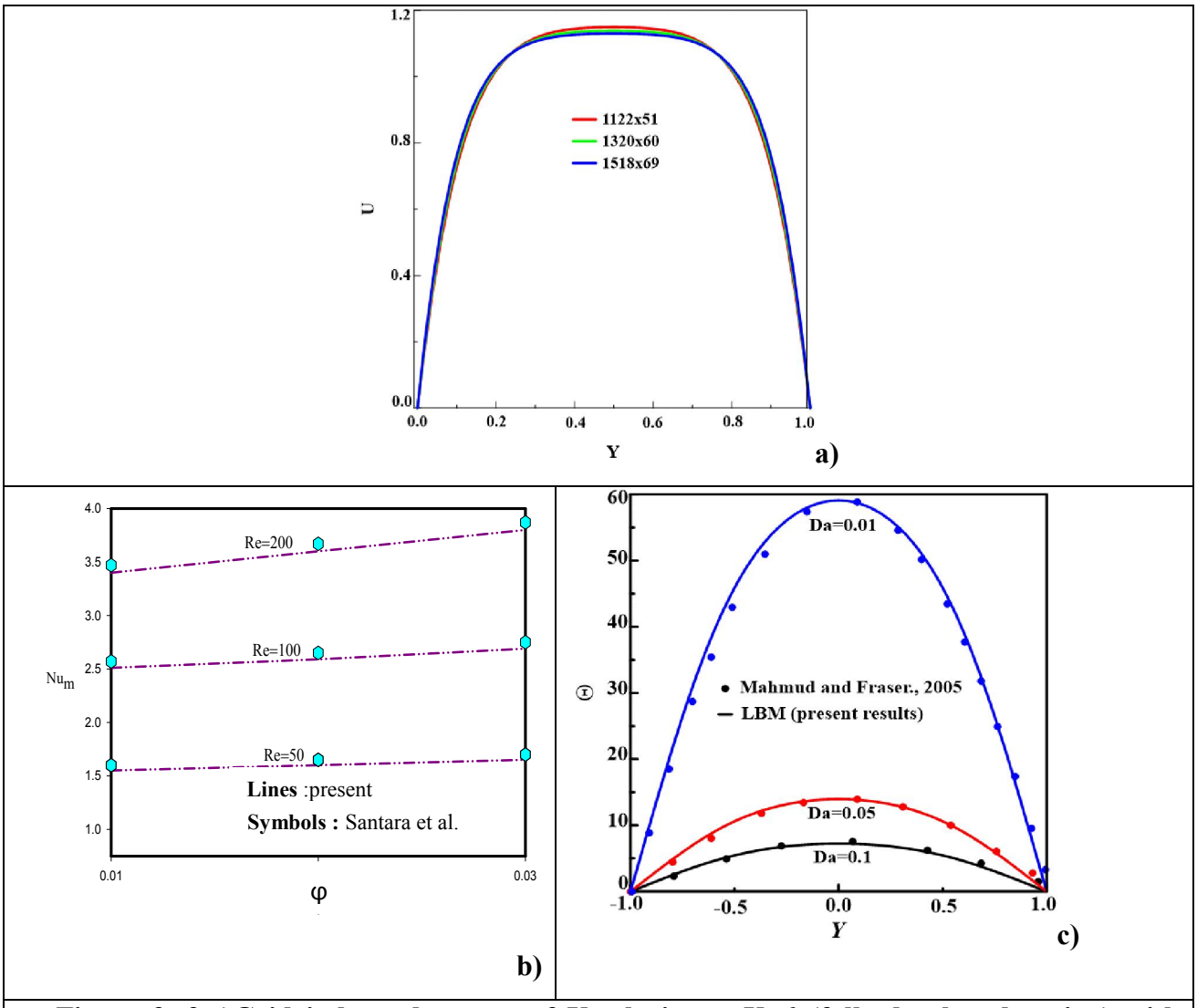

Figure 3. 3.a)Grid independent test of U-velocity at X=6 (fully-developed region) with Da=0.01, ε = 0.7 and φ = 0; b) Nu av-profiles and c) Θ -profiles = 0.6, Ec = 10, and Pr = 1. (Comparison with Santra et al. [55] and Mahmud and Fraser results [56].

6. Results and discussion

Recall that computations have been performed to handle the unsteady forced convective flow in a filled channel with Cu/water nanofluid under LTE as sketched in **Figure 1.3**. The targeted goal of this investigation is to explore the effects of the volume fraction of nanoparticles, Darcy number, porosity, heat capacity ratio and thermal conductivity ratio on heat transfer, entropy generation, the mean Nusselt number and the Bejan number. These effects have been assessed through Re = 200, Pr = 6, ε = 0.6, the nanoparticles volume fraction (φ= 0.0 - 0.04), Darcy number (Da=10^{-3}-1), Ec number (Ec = 1-10), the thermal conductivity ratio (Rk = 10-30), and heat capacity ratio (Rc = 10-20).

Figure3.4 depicts the dimensionless horizontal velocity U as a function of the upright coordinate Y at the streamwise distance X = 6, for the Da ranging from 10^{-3} to 1. It appears that this velocity exhibits a parabolic profile as Da increases. Thereby, the permeability of the porous medium increases with Da number by reducing the velocity profile flatness Likewise, low Da numbers involves a drop in maximum velocity.

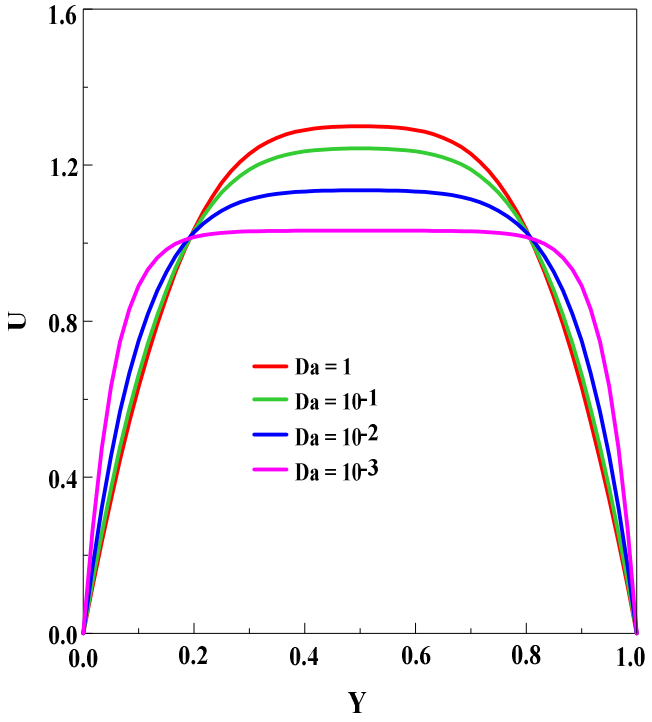

Figure 3. 4.U-velocity profile of Cu/water nanofluid vs. the upright coordinate Y at X = 6 for Re = 200, φ = 0.04, ε = 0.6, $R_c = 15$, $R_k = 10$, $E_c = 1$ and different Da numbers.

Figure 3.5 presents the dynamic U-contours for two Da numbers. It can be seen and confirming (comments of **Figure 3.4**) that as Da increases the flatness of the velocity shape decreases which indicates the role of the porous structure permeability.

a) **b)**

Figure 3. 5.Dimensionless U-velocity contour of Cu/water nanofluid for Re = 200, φ = 0.04, ε = 0.6, R_c = 15, R_k = 10, E_c = 1 and a) Da = 10^{-2} ; b) Da=1.

Figures 3.6-3.10 show the effects of Da, φ , R_k , R_c and E_c on dimensionless temperature

(Θ) vs. the upright coordinate Y at X = 6. These figures depicted that temperature profiles are highly sensitive to changes in the parameters considered. It is observed that as the number of Darcy increases, the Θ's maximum drops more and more (**Figure 3.6 and 3.7**).It can be noted that the permeability mitigates and slows the heat transfer rate, and thereby, the temperature distribution. Interestingly, the maximum of is reached around the center of the channel due to the imposed thermal boundary conditions which generates a high temperature gradient.

Moreover, it can be seen that the increase in rises that of the local maximum (**Figure 3.8**). Besides, as expected, it is observed that the temperature of the nanofluid is always higher than a fluid devoid of any nanoparticle. An in-depth examination of **Figure 3.9** shows that the temperature increases when R_c and R_k decrease indicating that the nanofluid actively participates in heat transfer. As for **Figure 3.10**, it clarifies viscous dissipation contribution on temperature demonstrating that a high Ec number amply increases the temperature. This points that viscous dissipation is indeed a heat generation source because it causes high fluid friction forces. On another aspect, it appears that undeniably influences . Despite the profiles shape similarity, the maxima exhibited are higher with φ = 0.04 (**Figure 3.10b**), the highest value deemed herein.

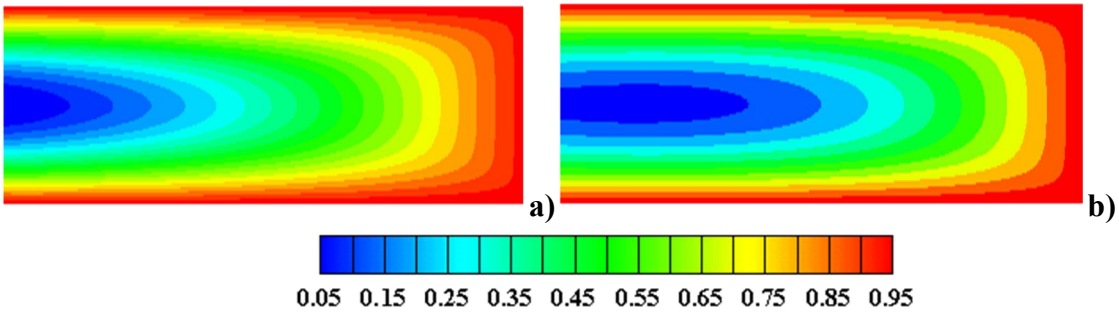

Figure 3. 6. Dimensionless temperature (Θ) contour of Cu/water nanofluid for Re = 200, φ = 0.04, = ε 0.6, R_c = 15, R_k = 10, E_c = 1 and a) Da =10^{-2} ; b) Da=10^{-3} .

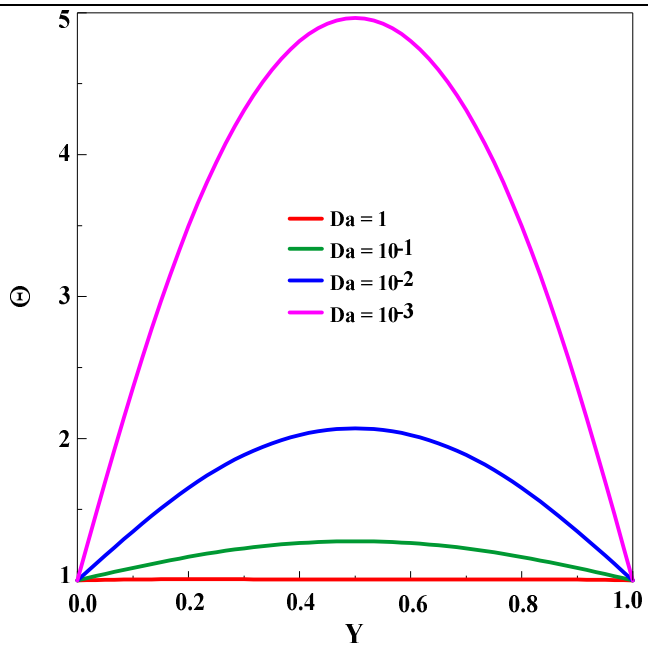

Figure 3. 7. Θ -profile of Cu/water nanofluid vs. the upright coordinate Y at X = 6 for Re=200, Ec=1, φ = 0.04, ε = 0.6, R_c = 15, R_k = 10 and different Da numbers.

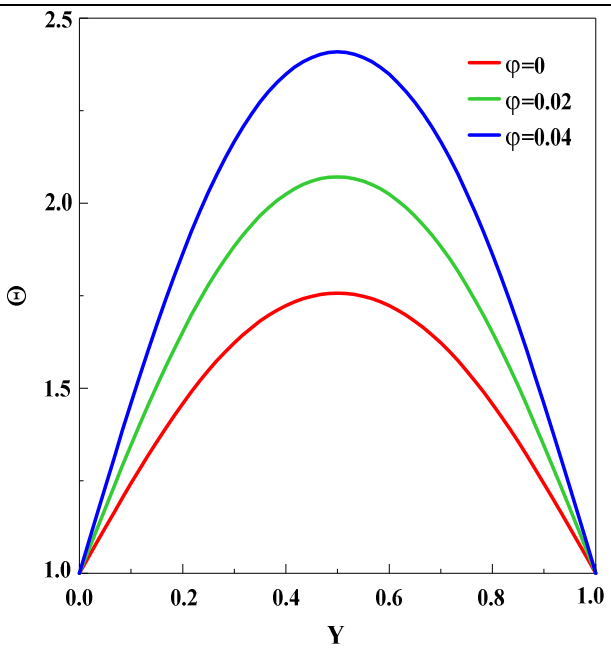

Figure 3. 8. Θ -profile of Cu/water nanofluid vs. the upright coordinate Y at X = 6 for, Re = 200, Ec = 1, Da=0.01, ε = 0.6 , R_c = 15, R_k = 10 and diverse φ (0.0, 0.02 and 0.04).

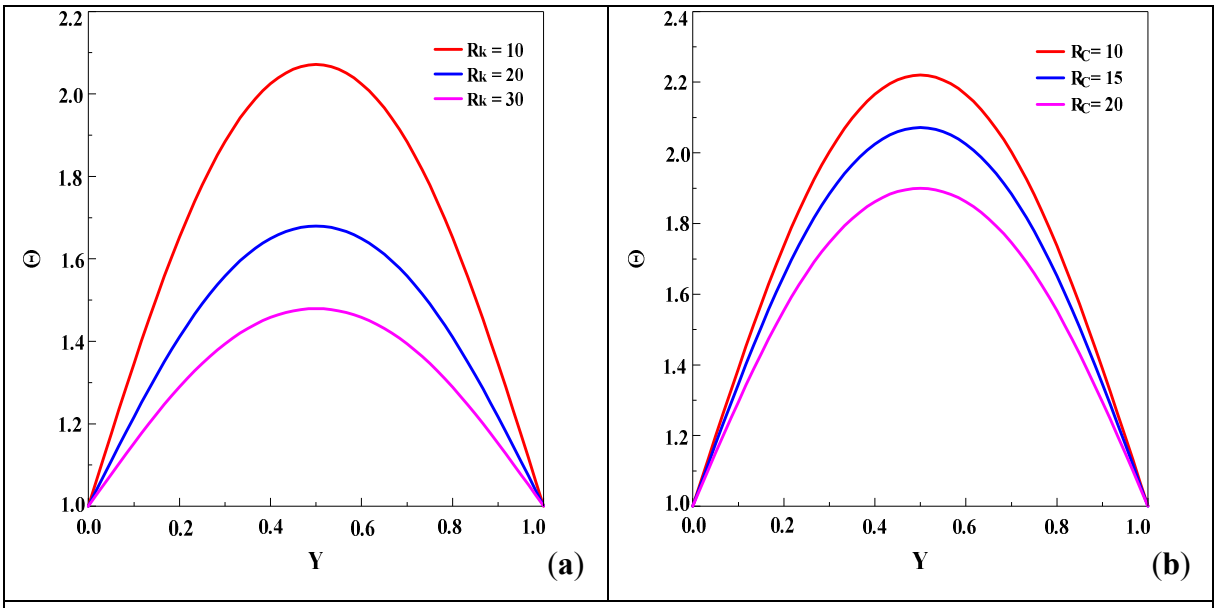

Figure 3. 9 . Θ **-profile of Cu/water nanofluid vs. the upright coordinate Y at X = 6 for** $E_c = 1$ **Re = 200, Da = 0.01,** ε **= 0.6 ,** $\varphi = 0.02$ **and diverse parameters** R_k **(a) and** R_c **(b).**

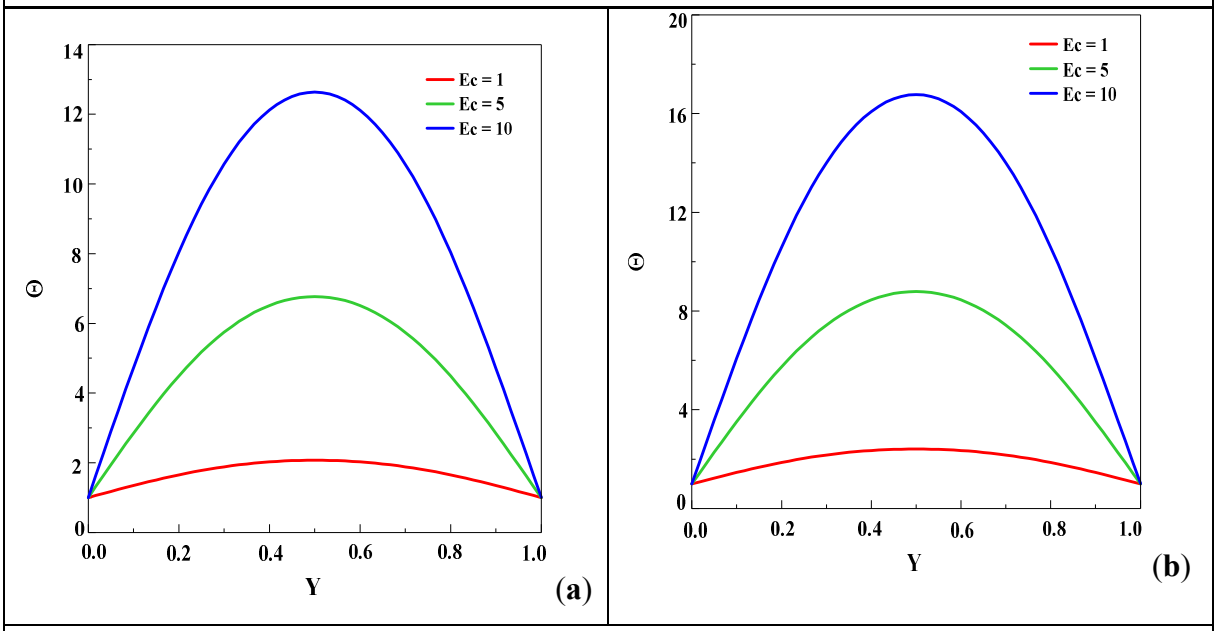

Figure 3. 10. Θ **-profile of Cu/water nanofluid vs. the upright coordinate Y at X = 6 for Re = 200, Da = 0.01,** ε **= 0.6 ,** R_c **= 15,** R_k **= 10 and two φ-values (0.02 (a) and 0.04 (b)).**

Figure 3.11 examines the effect of the parameters *Da, Ec,* R_k and R_c on Nu_{av} evolvement vs. over a wide range while keeping the other parameters constant. It is worthy to mention that Nu_{av} is a key factor to assess the improvement portion or not of the heat transfer by nanoparticles addition to the pure fluid. It exhibits that, the average Nusselt number (i.e. the global heat transfer) escalates and non-linearly regardless of nanoparticles volume fraction except at large Da and low Ec numbers (**Figures 3.11a and 3.11b**). As up-mentioned, the

Darcy and Eckert numbers reflect the relative permeability effect of a porous medium and the ratio of advective mass transfer to the heat dissipation potential, respectively. So, Figures **3.11a** and **3.11b** show their respective effects. It is found that increasing the Darcy number causes a monotonic decrease in the mean Nusselt number, while the reverse occurs when *Ec* number increases indicating that large viscous forces accentuates the forced heat convection.

As can be inferred from **Figures 3.11c** and **3.11d**, parameters R_k and R_c have an opposite effect. Explicitly, it can be concluded that using a nanofluid with high thermal conductivity (respectively, high thermal capacity) requires less time (respectively more time) to exchange the total energy. To sum up, an observation of these figures indicates that the nanofluid considered can be used as an efficient working fluid in cooling systems.

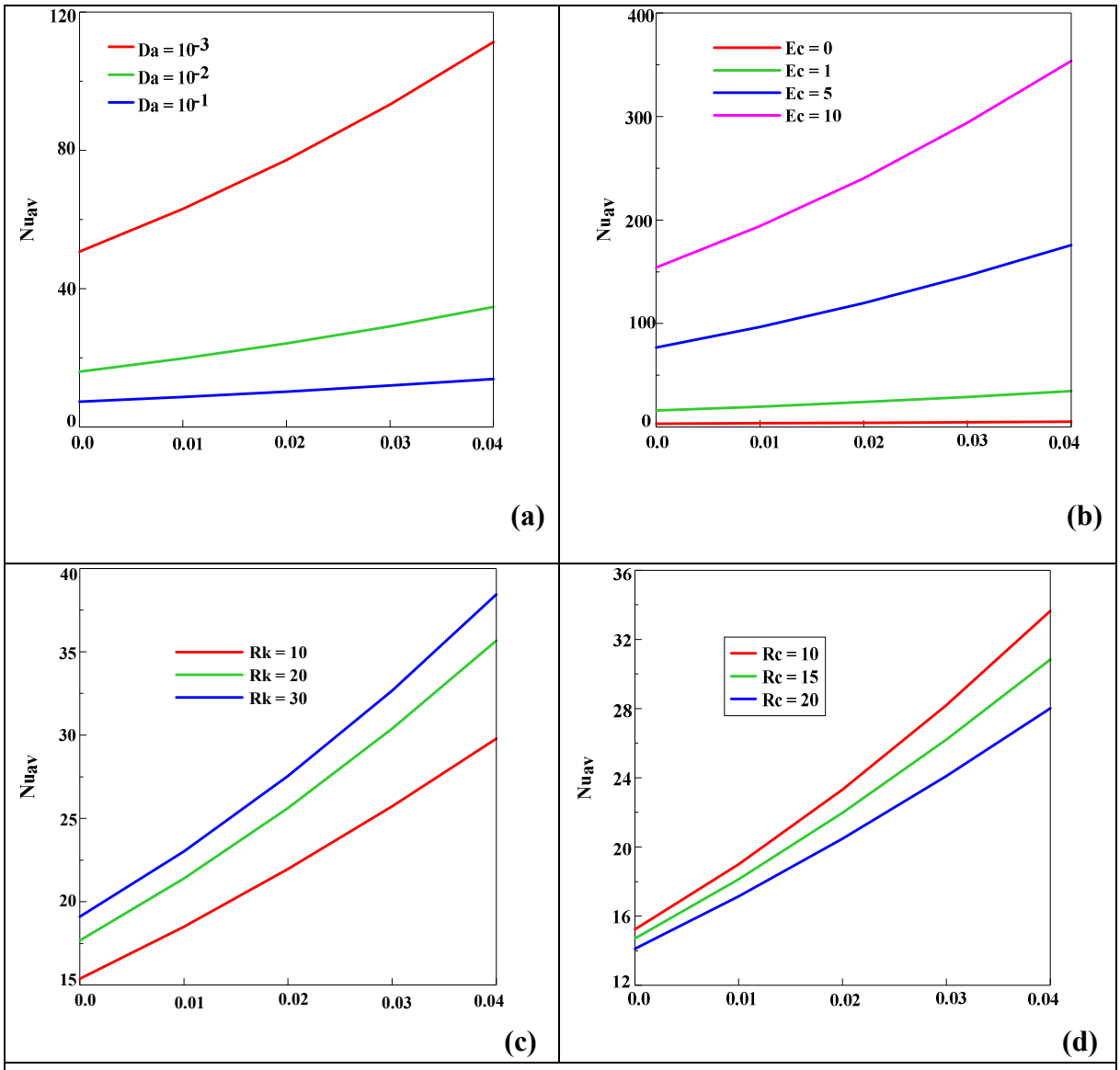

Figure 3.11 From left to right and top to bottom, plots of average Nusselt number (Nu_{av}) vs. nanoparticles volume fraction (φ) along the bottom wall: Effect of a) Da, b) Ec, c) R_k and d) R_c .

Figures 3.12a-b indicate the effects of *Da* and φ on the dimensionless entropy generation number (N_s). According to **Figure 3.12a**, this number exhibits two extrema (maximum) near walls at low Darcy number indicating that the permeability of the medium affected the fluid friction forces. As for **Figure 3.12b**, it reveals that the more increases, the higher this number is, in particular at the channel center. This trend explains that the nanoparticles addition increases the thermal conductivity of the medium and thereby viscous effects augment.

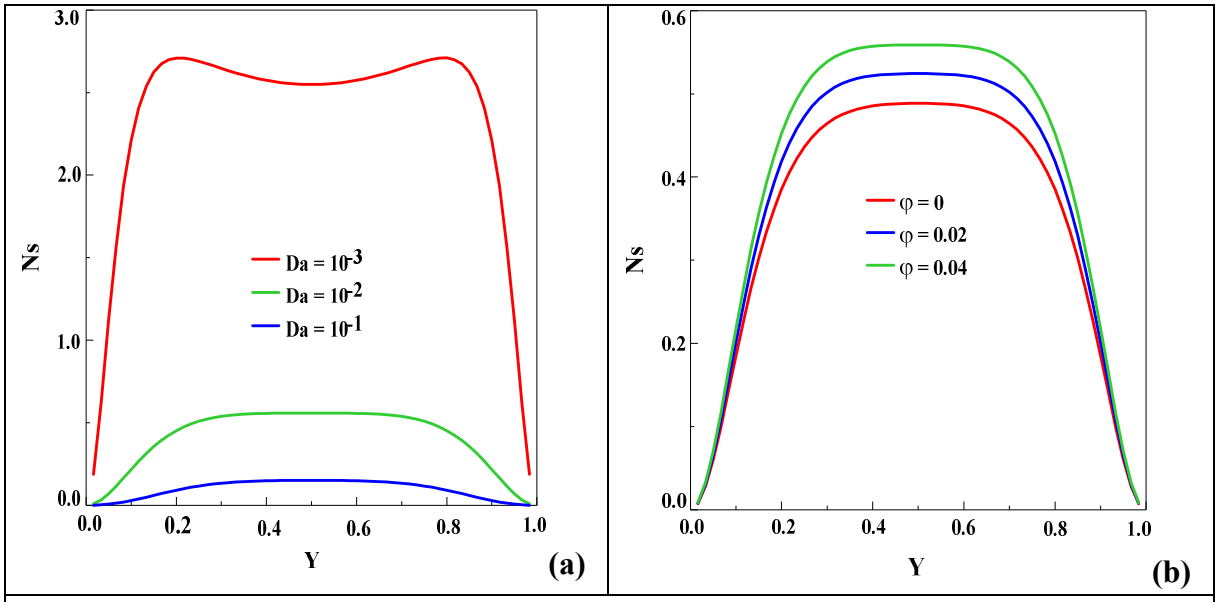

Figure 3. 12. Local entropy generation (Ns)'s upright evolution for different Da (a) and φ (b) at the streamwise distance with Re = 200, ε = 0.6 , R_c = 15, R_k = 10 and Ec =1.

The effect of Eckert's number on Ns is brought out in **Figure 3.13** along the upright coordinate *Y* at *X* = 6 for which *Da* = 0.01, φ = 0.02 and ε = 0.6.As shown, Ns increases with increasing Eckert number. This is expected because for high *Ec*, momentum advection outweighs heat dissipation. Hence, the higher the *Ec* number, the larger the entropy generation which explains that viscous forces caused large fluid friction forces which generates a heat source. As can be seen, such a figure demonstrates that, whatever the Eckert number, N_s presents a symmetrical profile over the entire height of the channel with two maxima and one minima which become more and more apparent as *Ec* increases.

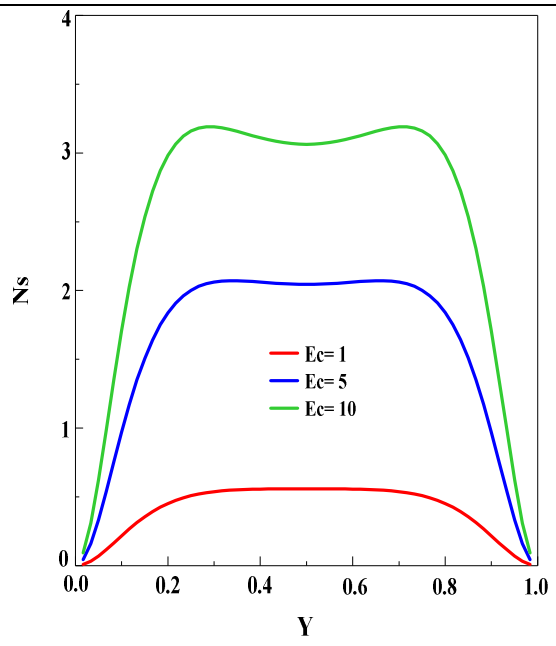

Figure 3.13. Local entropy generation (Ns)'s upright evolution for different Ec numbers at the streamwise distance X= 6 with Da = 0.01, φ = 0.02 and ε = 0.6, , R_c = 15 and R_k = 10

Figure 3.14 reveals any change in the parameter Rk in no way affects Ns for Da=0.01, φ= 0.02 and ε = 0.6. Note that from R_k=10, Ns's amplitude reaches a local maximum depending on the thermal conductivity of the medium and thereby indicates the effects of the nanofluid dispersion under viscous effects and heat transfer propagation.

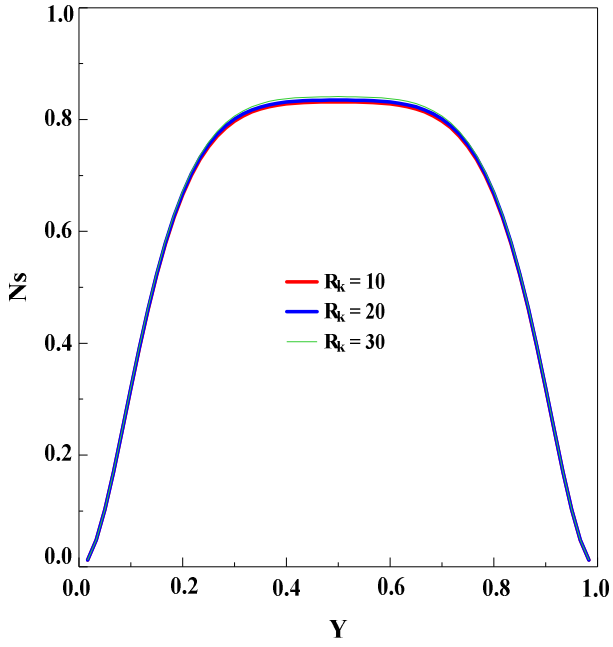

Figure 3. 14. Upright evolution of the local entropy generation (Ns) for different R_k

values at the streamwise distance X= 6 with Da = 0.01, φ = 0.02 , ε = 0.6, R_c = 15, and Ec =1

Figure 3.15 illustrates the N_s number along the channel height for various values of R_c parameter when *Da*, and have the values considered herein, viz. 0.01, 0.02 and 0.6, respectively. It appears that the R_c parameter has a slight influence on *Ns*. It turns out that the Rc increase improves the entropy generation rate (*Ns*) due to the viscous effects dominance which accentuate the irreversibility.

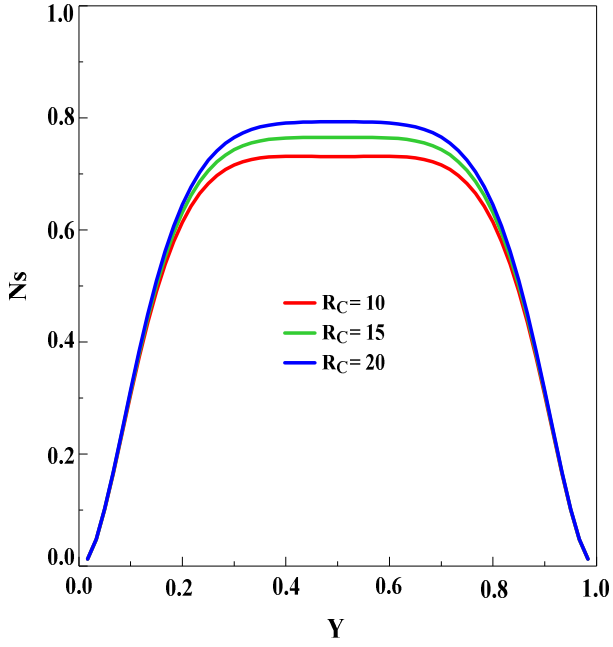

Figure 3. 15. Upright evolution of the local entropy generation (Ns) for different R_c values at the streamwise distance X = 6 with Da = 0.01, φ = 0.02n ε = 0.6, R_k = 10, and Ec =1.

Figure 3.16 illustrates the effect of *Da, Ec,* R_k and R_c on the average entropy generation rate (Ns_{av}) due to nanofluid flow. It is found that this quantity varies monotonically when varying *Da* and *Ec* (see **Figures 3.16a-b**). It decreases when Da increases, while it increases with *Ec*. Thereby high permeability affected the heat transfer and fluid friction irreversibly dominates the entropy generation rate. As for the effects of thermophysical characteristics on the generation of global entropy, it can be stated that Ns_{av} increases linearly with the volume fraction whatever the values of R_c and R_k (see **Figures 3.16c-d**) indicating that the nanoparticles addition accentuates the viscous effects and the convective heat transfer . Therefore, the nanoparticles rise the thermal conductivity of the medium which generates a

heat source inside the channel due to the fluid friction and porous medium forces. Moreover, it can be observed that this quantity (Ns_{av}) is improved for the large values of R_c and of R_k. To sum up, the nanoparticles addition in the base fluid improves the rate of heat transfer and fluid friction forces while inducing more irreversibility.

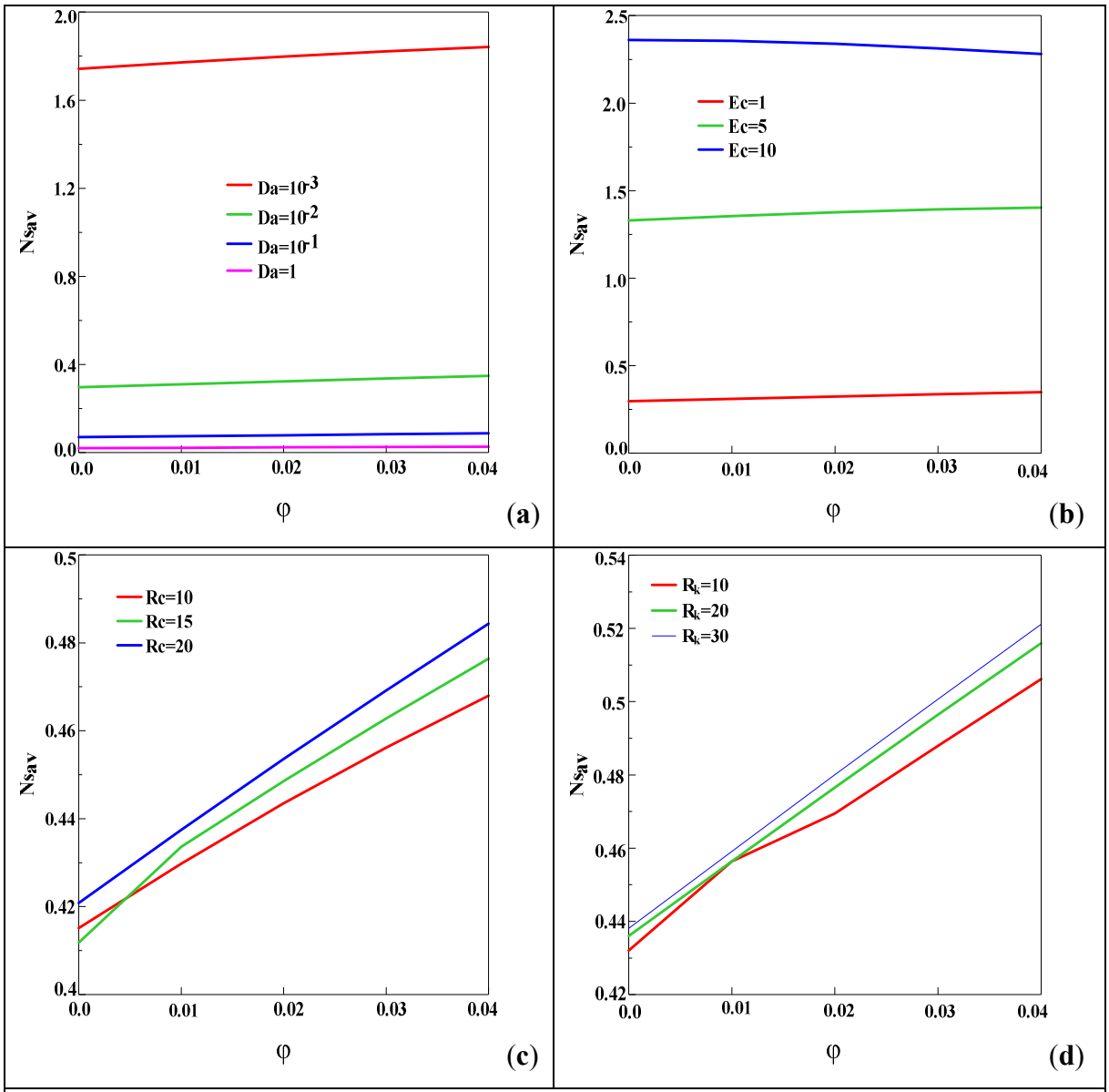

Figure 3. 16. Plots of average entropy generation (Ns_{av}) vs. nanoparticles volume fraction φ: Effect of a) Da ; b) Ec c) R_k and d) R_c, respectively (left to right and top to bottom).

Ultimately, to illuminate the effects of the key numbers *Da, Ec,* R_k and R_c on the irreversibility within the system, the Bejan number (*Be*) is plotted in **Figures 17a-e**.All these

figures show that it is the second ingredient of entropy generation (FFI) which dominates over the entire height of the canal due to shearing, indicating that it is the conduction mode that clearly prevails (Be<<0.5). For this case, it is worth noting that viscous forces resulting high fluid friction forces dominate the irreversibility of the system. This is due to the thermal boundary conditions imposed on the walls which induce temperature gradients at these locations throughout the channel. Likewise, it turned out that all the parameters considered, viz *Da, Ec,* R_k and R_c have a negligible effect at the channel center in the considered range.

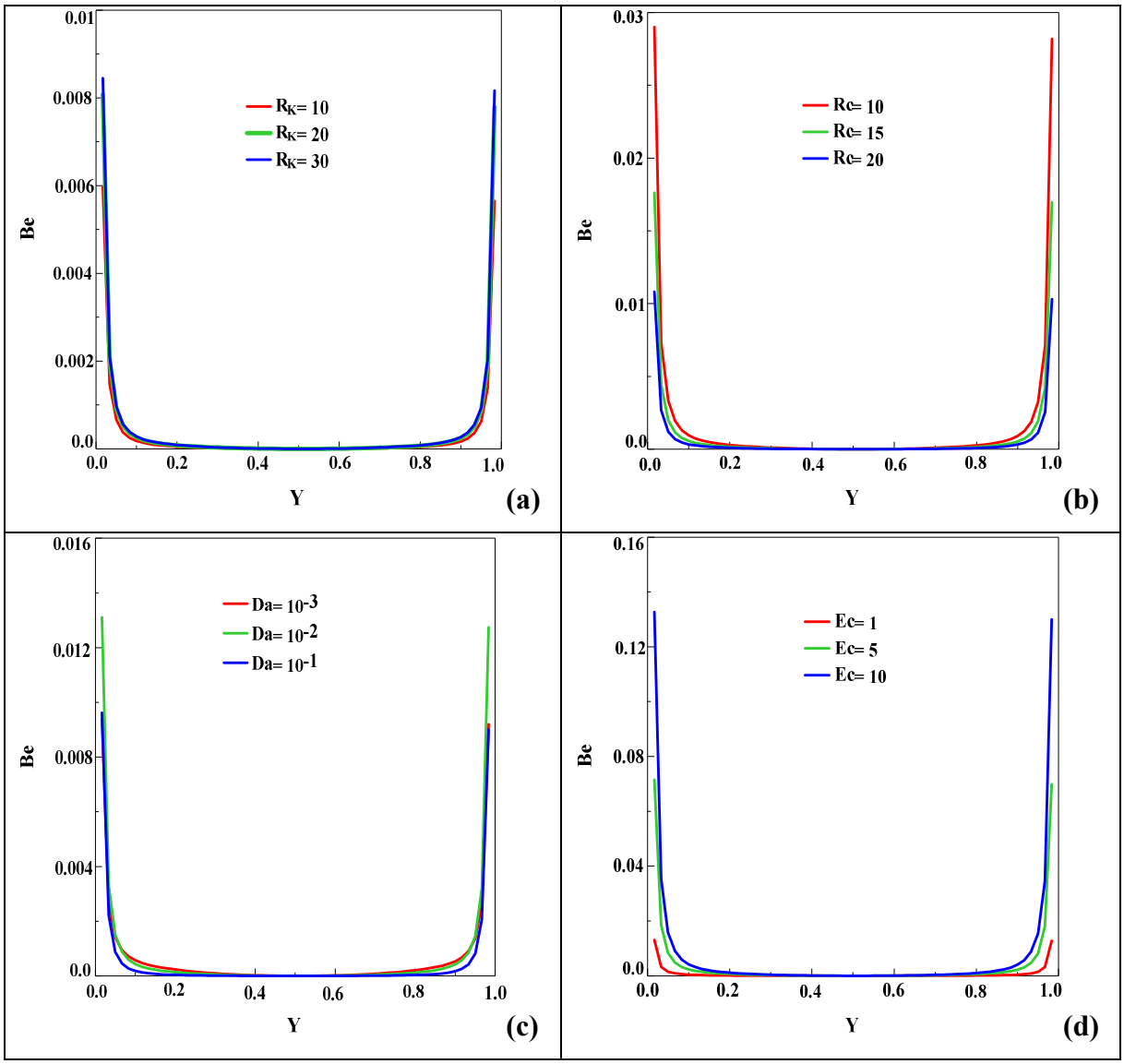

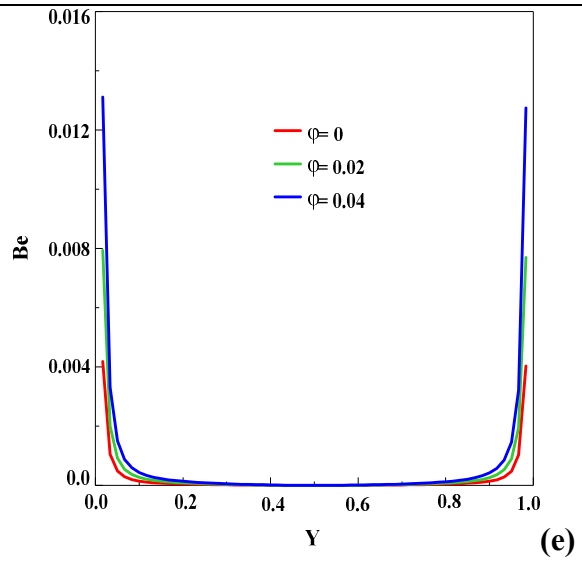

Figure 3.17. Bejan's upright evolution parametrized by a) R_k, b) R_c, c) Da, d) Ec, and e) φ at the streamwise distance X =6

7. Conclusion

In this study, the unsteady convective nanofluid (Cu/water) flow in an open-ended porous channel is demonstrated via a MDF-thermal lattice Boltzmann method and the Brinkman-Forchheimer-Darcy model. Although only the SRT-LB model is considered herein, it is relevant to opt for a MRT counterpart in a near future. Through the various flow control parameters (Re, Ec), the permeability (Da), the medium's porosity (ε), conductivity and thermal capacity ratios (Rk and Rc), and nanoparticles volume concentration (φ), the underlying physics of this problem is systematically explored. This investigation is filled up by exhibiting the average Nusselt number, the local and average entropy generation rates and the local Bejan number to highlight the irreversibilities that prevail in the present configuration of the problem. Based on the numerical results, the salient outcomes of this study can be drawn as follows:

- The volume fraction of the nanoparticles leads to a rise in heat transfer and entropy generation while being reinforced by the porous medium permeability.
- Heat transfer rate rises by dropping Darcy number whatever the nanoparticles volume fraction. In addition, such an effect is more important at high intensity of viscous dissipation.
- Adding nanoparticles increases the average entropy generation rate ($N_{s_{av}}$) as the heat capacity (R_c) and thermal conductivity (R_k) ratios increase, while increasing the Da number has the opposite effect.

- Increasing the nanoparticles volume fraction (φ) improves the nanofluid thermal conductivity and, thereby, the overall heat transfer.
- Irreversibilities within the heat transfer system (HTI) predominate only in the immediate vicinity of the channel walls due to the imposed thermal boundary conditions.

To sum up, obtaining less entropy generation and high system efficiency requires a suitable combination of the various key parameters of the flow deemed. Likewise, the MDF-TLBM approach has been shown to be effective in dealing with nanofluids flow in a porous medium with acceptable accuracy, which is of great importance to further deepen our understanding of the flow and the heat transfer process of nanofluids.

References

[1] Qi. Zhao, Y. Zhang, D. Zhou, Y. Huang, M. Xu, Y. Tian, Lattice Boltzmann method for nanofluid forced convection heat exchange in a porous channel with multiple heated sources, *Numer. Heat Transf. A: Appl.* 79 (1) (2021) 21-39. https://doi.org/10.1080/10407782.2020.1814590

[2] M.A. Mansour, S. Elsayed, A.J Chamkha, Entropy generation optimization for MHD natural convection of a nanofluid in porous media-filled enclosure with active parts and viscous dissipation, *Int. J. Numer. MethodsHeat Fluid Flow* 27(2) (2017) 379-399. https://doi.org/10.1108/HFF-10-2015-0408

[3] M. Torabi, M. Torabi, S.M. Ghiaasiaan, G.P. Peterson, The effect of Al2O3-water nanofluid on the heat transfer and entropy generation of laminar forced convection through isotropic porous media, *Int. J. Heat Mass Transf.* 111 (2017) 804-816. https://doi.org/10.1016/j.ijheatmasstransfer.2017.04.041

[4] A. Kasaeian, R. Daneshazarian, O. Mahian, L. Kolsi, A.J. Chamkha, S. Wongwises, I. Pop, Nanofluid flow and heat transfer in porous media: A review of the latest Developments, Int. *J. Heat Mass Transf.* 107 (2021) 778-791. https://doi.org/10.1016/j.ijheatmasstransfer.2016.11.074

[5] S. Chakraverty, U. Biswal, Modeling and Simulation of Nanofluid Flow Problems, Synth. Lect. Mech. Eng.5 (2020)1-89. https://doi.org/10.2200/S00978ED1V01Y201912MEC025

[6] Z. Alhajaj, A.M. Bayomy, M.Z. Saghir, A comparative study on best configuration for heat enhancement using nanofluid, *Int.J.Thermofluid*. 7-8 (2020) 100041. https://doi.org/10.1016/j.ijft.2020.100041

[7] M. J. Maghrebi, M. Nazari, T. Armaghani, Forced Convection Heat Transfer of Nanofluids in a Porous Channel, *Transp Porous Med*. 93 (2017) 401-413. https://doi.org/10.1007/s11242-012-9959-2

[8] H. Maleki, M. R. Safaei, A. A. A. A. Alrashed, A. Kasaeian, Flow, and heat transfer in non-Newtonian nanofluids over porous Surfaces, *J. Therm. Analysis Calorim*. 135 (2019) 1655-1666. https://doi.org/10.1007/s10973-018-7277-9

[9] A.T. Akinshilo, Geometry Shape Effects of Nanoparticles on Fluid Heat Transfer Through Porous Channel, *AUT J. Mech. Engineering*. 4 (2020) 41-50. https://doi.org/10.22060/AJME.2019.14684.5738

[10] M. Mahdavi, M. Saffar-Avval, Saeed Tiari, Zohreh Mansoori, Entropy generation and heat transfer numerical analysis in pipes partially filled with porous medium, *Int. J. Heat Mass Transf*. 79 (2014) 496-506. https://doi.org/10.1016/j.ijheatmasstransfer.2014.08.037

[11] H.Xu, L. Gong, S. Huang, M.Xu, Flow and heat transfer characteristics of nanofluid flowing through metal foams, *Int. J. Heat Mass Transf.* 83 (2015) 399-407. https://doi.org/10.1016/j.ijheatmasstransfer.2014.12.024

[12] S. Alihosseini, A. Jafari, The effect of porous medium configuration on nanofluid heat transfer, *Applied Nanosc.* 10 (2020) 895-906. https://doi.org/10.1007/s13204-019-01192-1

[13] A. Bejan, Entropy Generation Minimiszation,CRC Press, Boca Raton, 1996.

[14] R. Ellahi, Sadiq M. Sai, N. Shehzad, Z. Ayaz, A hybrid investigation on numerical and analytical solutions of electro-magnetohydrodynamics flow of nanofluid through porous media with entropy generation, *Int. J. Numer. Meth. Heat Fluid Flow* 30 (2020) 834-854. https://doi.org/10.1108/HFF-06-2019-0506

[15] Z. Shah, M. Sheikholeslami, Ikramullah, P. Kumam, Simulation of entropy optimization and thermal behavior of nanofluid through the porous media, *Int. Com. Heat Mass Transf*. 120 (2021) 105039. https://doi.org/10.1016/j.icheatmasstransfer

[16] Z.H. Chai, C.S. Huang, B.C. Shi, Z.L. Guo, A comparative study on the lattice Boltzmann models for predicting effective diffusivity of porous media*, Int. J. Heat Mass Transfer*. 98 (2016) 687-696. https://doi.org/10.1016/j.ijheatmasstransfer.2016.03.065

[17] Z.H. Chai, B.C. Shi, Z.L. Guo, A multiple-relaxation-time lattice Boltzmann model for general nonlinear anisotropic convection-diffusion equations*, J. Sci. Comput*. 69 (2016) 355-390. https://doi.org/10.1007/s10915-016-0198-5

[18] L. Wang, Z.H. Chai, B.C. Shi, Regularized lattice Boltzmann simulation of double diffusive convection of power-law nanofluids in rectangular enclosures, *Int. J. Heat Mass Transf.* 102 (2016) 381-395. https://doi.org/10.1016/j.ijheatmasstransfer.2016.06.041

[19] O. Aliu, H. Sakidin, J. Foroozesh, N. Yahya, Lattice Boltzmann application to nanofluids dynamics-A review, *J. Mol. Liq*. 300 (2020) 112284. https://doi.org/10.1016/j.molliq.2019.112284

[20] K. Ghasemi, M. Siavashi, Lattice Boltzmann numerical simulation and entropy generation analysis of natural convection of nanofluid in a porous cavity with different linear temperature distributions on side walls, *J. Mol. Liq.* 233 (2017) 415-430. http://dx.doi.org/10.1016/j.molliq.2017.03.016

[21] H. Tahmooressi, A. Kasaeian, A. Tarokh, R. Rezaei, M. Hoorfar, Numerical simulation of aggregation effect on nanofluids thermal conductivity using the lattice Boltzmann method, *Int. Com. Heat Mass Transf*. 110 (2020) 104408. https://doi.org/10.1016/j.icheatmasstransfer.2019.104408

[22] T. Seta, E. Takegoshi, K. Okui, Lattice Boltzmann simulation of natural convection in porous media, *Math. Comput. Simul*. 72 (2006) 195-200. https://doi.org/10.1016/j.matcom.2006.05.013

[23] R. Mohebbi, M.M. Rashidi, M. Izadi, N.A.C. Sidik, H.W. Xian, Forced Convection of Nanofluids in an Extended Surfaces Channel Using Lattice Boltzmann Method, *Int. J. Heat Mass Transf.*117 (2018) 1291-1303. https://doi.org/10.1016/j.ijheatmasstransfer.2017.10.063

[24] Q. Zhao, Y. Zhang, D. Zhou, Y. Huang, M. Xu, Y. Tian, Lattice Boltzmann method for nanofluid forced convection heat exchange in a porous channel with multiple heated sources, *Numer. Heat Transf. Part A: Applications.* 79 (2021) 21-39. http//doi.org/10.1080/10407782.2020.1814590

[25] S. Hammouda, B. Amami, H. Dhahri, Viscous Dissipation Effects on Heat Transfer for Nanofluid Flow Over a Backward-Facing Step Through Porous Medium Using Lattice Boltzmann Method, *J. Nanofluids*. 7 (2018) 668-682. http//doi.org/10.1166/jon.2018.1491

[26] Z. Mehrez, A. El Cafsi, Forced convection magnetohydrodynamic Al 2O3-Cu/water hybrid nanofluid flow over a backward-facing step, *J. Therm. Analysis Calorim*. 135 (2019) 1417-1427. https://doi.org/10.1007/s10973-018-7541-z

[27] D. Kashyap, A.K. Dass, Two-phase lattice Boltzmann simulation of natural convection in a Cu-water nanofluidfilled porous cavity: Effects of thermal boundary conditions on heat transfer and entropy generation, *Adv. Powder Technol*. 29 (2018) 2707-2724. https://doi.org/10.1016/j.apt.2018.07.020

[28] R. Rabhi, A. Yahya, B. Amami, H. Dhahri, Influence of magnetohydrodynamic viscous flow on entropy generation within porous micro duct using the Lattice Boltzmann Method, *RSC Adv*. 7 (2017) 30673-30686. https://doi.org/10.1039/C7RA03563B

[29] G. R. Kefayati, H. Tang, MHD thermosolutal natural convection and entropy generation of Carreau fluid in a heated enclosure with two inner circular cold cylinders, using LBM, *Int. J. Heat Mass Transf*, 126 (2018) 508-530. https://doi.org/10.1016/j.ijheatmasstransfer.2018.06.026

[30] Z. Guo, T.S. Zhao, A lattice Boltzmann model for convection heat transfer in porous media, Numer. Heat Transf. Part B. 47 (2005) 157–177. https://doi.org/10.1080/10407790590883405

[31] S. Chen, B. Yang, C.G. Zheng, A lattice Boltzmann model for heat transfer in porous media, Int. J. Heat Mass Transf. 111 (2017) 1019-1022. https://doi.org/10.1016/j.ijheatmasstransfer.2017.04.054

[32] K. Vafai, Convective flow and heat transfer in variable porosity media, Int. J. Fluid mech. 147 (1984) 223-259. https://doi.org/10.1017/S002211208400207X

[33] H. Dhahri, A. Boughamoura, S. B. Nasrallah, Entropy generation for pulsating flow in a cylinder filled with porous media including viscous dissipation effects, *J. Porous Media*. 16 (2013) 69-87. https://doi.org/10.1615/JPorMedia.v16.i1.70

[34] M. Siavashi, H. Reza T. Bahrami, H. Saffari, Numerical investigation of flow characteristics, heat transfer and entropy generation of nanofluid flow inside an annular pipe partially or completely filled with porous media using two-phase mixture model, *Energy.* 93 (2015) 2451-2466. https://doi.org/10.1016/j.energy.2015.10.100

[35] A. Bejan, Entropy Generation Minimisation, CRC Press, Boca Raton, FL, 1996.

[36] Z. Guo, B. Shi, C. Zheng, A coupled lattice BGK Model for the Boussinesq equations, *Int. J. Numer.Methods Fluids.* 39 (2002) 325-342. https://doi.org/10.1002/fld.337

[37] R. Mabrouk, H. Dhahri, H. Naji, S. Hammouda, Z. Younsi, Lattice Boltzmann simulation of forced convection melting of a composite phase change material with heat dissipation through an open-ended channel, *Int. J. Heat Mass Transf*. 153 (2020) 119606. https://doi.org/10.1016/j.ijheatmasstransfer.2020.119606

[38] Z. L. Guo, T. S. Zhao, Lattice Boltzmann model for incompressible flows through porous media, *Phys. Rev. E*. 66 (2002) 036304.https://doi.org/10.1103/PhysRevE.66.036304

[39] A. Yehya, H. Naji, L. Zalewski, Experimental and numerical characterization of an impure phase change material using a thermal lattice Boltzmann method, *Appl. Therm. Eng*. 154 (2019) 738-750. https://doi.org/10.1016/j.applthermaleng.2019.03.026

[40] Z.L. Guo, T.S Zhao, Lattice Boltzmann simulation of natural convection with temperature dependent viscosity in a porous cavity, *Prog. Comput. Fluid Dyn*. 5 (2005b) 110-117. https://doi.org/1 0.1504/PCFD.2005.005823

[41] Q. Zou, X. He, On pressure and velocity boundary conditions for the lattice Boltzmann BGK model, *Int. J. Phys. Fluids*. 9 (1997) 1591. https://doi.org/10.1063/1.869307

[42] R. Mabrouk, H. Naji, H. Dhahri, Numerical Investigation of Metal Foam Pore Density Effect on Sensible and Latent Heats Storage through an Enthalpy-Based REV-Scale Lattice Boltzmann Method, *Processes*. 9 (2021) 1165. https://doi.org/10.3390/pr9071165

[43] C. S. Kumar, S. Mohankumar, M. Geier, A. Pattamatta, Numerical investigations on convective heat transfer enhancement in jet impingement due to the presence of porous media using Cascaded Lattice Boltzmann method. *Int. J. Therm. Sci*. 122 (2017) 201-217. https://doi.org/10.1016/j.ijthermalsci.2017.08.020

[44] A.A. Mohamad, Lattice Boltzmann Method: Fundamentals and Engineering Applications with Computer Codes, 2nd ed. Springer: London, UK, 2011.

[45] S. Mahmud, R.A. Fraser, Flow, thermal, and entropy generation characteristics inside a porous channel with viscous dissipation, *Int. J. therm. Sci*. 44 (2005) 21-32. https://doi.org/10.1016/j.ijthermalsci.2004.05.001

Chapter 4: Mixed convection heat transfer in a rectangular inclined microchannel totally filled with nanofluid

1. Introduction

Recent miniaturization techniques have led to an increasing development of Micro Electro Mechanical Systems (MEMS) used in different sectors (medicine, biology, industry,..). MEMS are mechanical systems comprising at least one micrometer-sized component. This component can be a conduit, a seat of a flow, whose dimension is of the order of a few microns. However, to design and manufacture such systems, it is necessary to understand and characterize the flow and heat transfer in these small scales [1-4]. The effects of gravity are ignored in the investigation of forced convection and are taken into account for natural convection. Therefore, numerous intermediate situations between forced convection and free convection coexist with comparable orders of magnitude, called mixed convection. Among the examples of this diversity, we can cite: slow flows in pipes (as in water radiators) or along a wall, isotherm jets (heating air conditioning of local ...), and atmospheric flows and currents (more generally a lot of highly isotherm flows). Heat transfer by mixed convection in micro channels has been treated for several decades [5-6]. In this context, Khanafer et al. [7] simulated mixed convection heat transfer in a differentially heated cavity of the cylinders speed. They found that the average Nusselt number increased for high values of the rotation speed of the cylinder, the Reynolds number (Re) and the Richardson number (Ri). This simulation also showed that the heat transfer rate was comparable to the values of the cylinder speed for high Ri. Kang and John [8] studied slip effects on mixed convective heat transfer in a vertical plate. They stated that in gas flows, heat transfer would decrease as the flow became more rarefied. This behavior took place because the temperature jump condition reduced the heat transfer more than that improved by the slip velocity. Naizmand and Rahimi [9] simulated the mixed convection of slip flows in a vertical parallel plate microchannel in symmetric and asymmetric wall heat fluxes. The top-bottom walls of the microchannel were subjected to constant heat fluxes. They pointed out that the increase in Gr/Re would enhance the heat transfer rate and the friction losses. Tavakoli et al.[10] numerically investigated mixed convection heat transfer inside rectangular microchannels with two-phases. The obtained results showed that an improvement in Re, the slip coefficient number, Grashof number (Gr) and the volume fraction of nanoparticles would enhance the heat transfer rate.

The recent considerable development of research dealing with nanofluids, as it is possible for some applications, has significantly increased heat transfer by introducing a low concentration of nanoparticles into a pure fluid. Nanofluids are a mixture of liquid and dispersed solid nanoparticles. Their characteristics are different from the traditional solid–liquid mixtures in milli or micro-meter particle's size. For low values of concentrations, some of these solutions

have been shown to be very effective in enhancing heat transfer under certain conditions. Masoud et al.[11] presented an experimental study dealing with nanofluid thermal conductivity composed of MWCNT-CuO/ Water. Xu and sun [12] conducted a model of a hybrid nanofluid in a vertical microchannel under mixed convection. They stated that the nanoparticle volumetric fractions strongly affected the dynamic and thermal behaviors. Additionally, they demonstrated that the increase in Ri and the nanoparticles volume fractions would enhance the average heat transfer rate. Manay and Mandev [13] investigated the mixed convection of nanofluids in circular microchannels. They found that the suspension of the volume fraction of silicon dioxide nanoparticles enhanced the heat transfer rate. Therefore, it would decrease regardless Re. Naphon et al. [14] experimentally studied the performance of heat transfer for jet impingement in a micro-channel heat sink for the flow of laminar nanofluids. They found that convective heat transfer went up from 18.56% to 0.015% by volume fraction. Bowers et al.[15] experimentally studied the thermal behavior of the flow of laminar nanofluids in micro channels. They proved that convective heat transfer intensified for both nanofluids (silica and alumina) at low particle concentrations. The improvement in heat transfer grew with the rise of Re and the hydraulic diameter of microchannels.

Generally, the Lattice Boltzmann Method (LBM) is a new tool for the numerical simulation of the flows of nanofluids. The LBM has also been successfully applied to simulate microchannel flows. Unlike classical numerical methods based on the discretization of macroscopic conservation equations, this method is based on microscopic models. It should be noted that several investigations have used the LBM as a reliable process to deal with nanofluid models inserted in microchannels [16-17]. However, the slip velocity effects on the mixed convection are scarcely treated. Mozaffari et al. [18] investigated numerically the effects of gravity on the flow in a microchannel using the LBM. They also studied the effect of varying slip flow parameters such as Gr and the slip coefficient on the hydrodynamic and thermal properties of the fluid flow.Karimipour et al. [19] investigated mixed convection in a microchannel while considering the gravitational effects and using the LBM. They noted that for small values of slip velocity, the effects of the buoyancy force on the heat transfer rate were important. D'Orazio and Karimipour [20] studied the same problem with top-bottom walls subjected to a constant heat flux. Based on the above literature, the use of the LBM to simulate forced mixed convection in inclined microchannels for the flow of laminar nanofluids has been scarce. Thereby, this chapter uses such an approach to further understand the effect of gravity on heat transfer for mixed convection in inclined micro channels for the flow of laminar nanofluids. Therefore, we report here a numerical study of heat transfer for the flow of laminar nanofluids in an inclined

microchannel subjected to a constant heat flux. Attention is focused on the effects of the emerging parameters on streamlines, isotherms, slip velocity, wall temperature and Nusselt number.

2. Physical problem

The proposed physical model with the cartesian coordinate system considered in this study is depicted in (**Figure 4.1)**. It is an open-ended inclined micro-channel with length is ten times longer than its width (L/H = 10) completely filled with a Al2O3/Water nanofluid maintained under mixed convection heat transfer. The top-bottom walls are subjected to a constant heat flux, q. The uniform velocity and the temperature of the fluid at the channel entrance are chosen to be U_i and T_i, and the output conditions are assumed to be fully developed, where the geometry is two-dimensional. It is well known that the characteristic length is chosen as the hydraulic length (D_H) in a channel flow, which means $D_H = 2H$ have a small amount in a micro flow inside a microchannel due to the fact of low value of microchannel width (H). Hence it's corresponded Reynolds number ($R_e = \rho_i u_i D_H / \mu$) will have a low value. The temperature of inlet cold nanofluid (T_i) will increase through the microchannel due to heat exchange with hot walls. Effects of buoyancy forces on slip velocity and temperature domain at different values of nanoparticles volume fraction (φ= 0, φ=2%, φ= 4%) are investigated. To do this, four different case studies as no-gravity, Ri=1, Ri=5 and Ri=10 at Re=1 are considered while the dimensionless liquid slip coefficient changes from B=0.005 to B=0.01 and B=0.02. Double population distribution functions of ''f'' and ''g'' in thermal lattice Boltzmann method are used for the hydrodynamic and thermal domains.

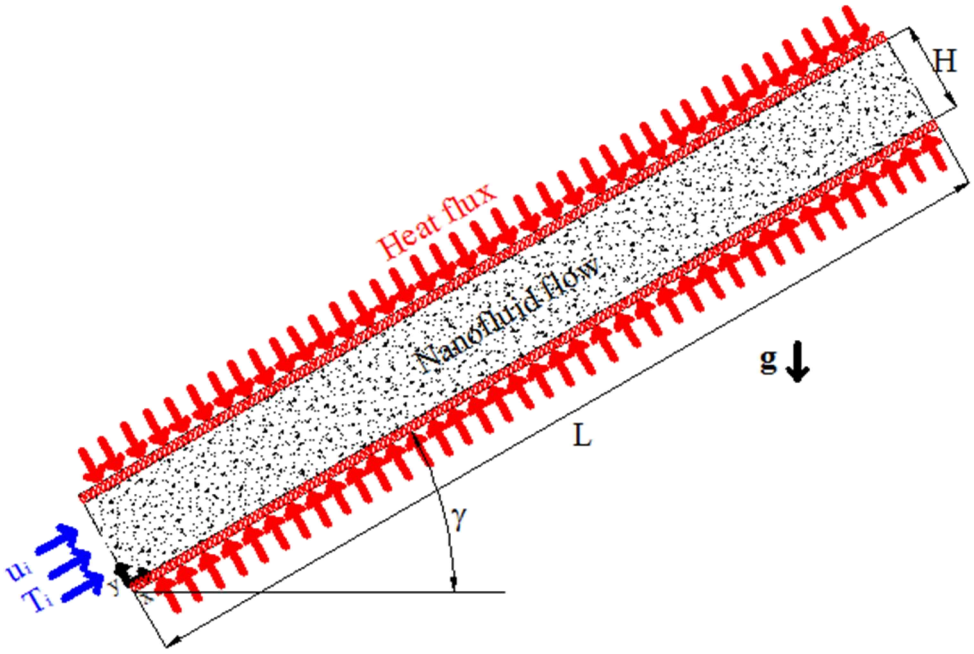

Figure 4. 1. Mixed convection of Al2O3/Water nanofluid flow in an inclined microchannel

To simulate a laminar nanofluid flow through an inclined microchannel, the nanoparticles are assumed to be suspended uniformly in the base fluid (water). Furthermore, the flow of the nanofluid field is assumed to be uniform, incompressible and laminar.The thermo-physical properties are kept constant, and the viscous dissipation effects are included in the energy equation.

3. Mathematical formulation

3.1 Nanofluids

Nanofluids represent a dispersion of particles in a nanometric size, called nanoparticles, in a basic fluid in order to improve their properties.

Effective density can be given by [21]:

$$\rho_{nf}=\varphi\rho_s+(1-\varphi)_{\rho_f} \tag{4.1}$$

Where φ is the nanoparticle volume fraction.

The thermal diffusivity of the nanofluid can be given by [22]:

$$(\rho c_p)_{nf}=\varphi(\rho c_p)_s+(1-\varphi)(\rho c_p)_f \tag{4.2}$$

$$\alpha_{nf}=k_{nf}/(\rho c_p)_{nf} \tag{4.3}$$

Using the Brinkman model [23], the effective dynamic viscosity used with the nanoparticles with higher represent concentration is [24]

$$\mu_{nf}=\mu_f/(1-\varphi)^{2.5} \tag{4.4}$$

Eq. (5) given by [25], is used to determine the thermal conductivity of the nanofluid:

$$\frac{k_{nf}}{k_f} = 1 + 64.7 \times \phi^{0.7460} \left(\frac{d_f}{d_p}\right)^{0.3690} \times \left(\frac{k_s}{k_f}\right)^{0.7476} \times \left(\frac{\mu}{\rho_f \alpha_f}\right)^{0.9935} \times \left(\frac{\rho_f B_c T}{3\pi\mu^2 l_{BF}}\right)^{1.2321} \quad \textbf{(4.5)}$$

with

$$\mu = A \times 10^{\frac{B_c}{T-C}}, \; T = 247.8K, \; A = 2.414 \times 10^{-5} Pa.s \quad \textbf{(4.6)}$$

B_c : the Boltzmann constant $\left(1.3807 \times 10^{-23} J/K\right)$

L_{BF} : the base fluid mean free path

3.2 Modified Lattice Boltzmann method

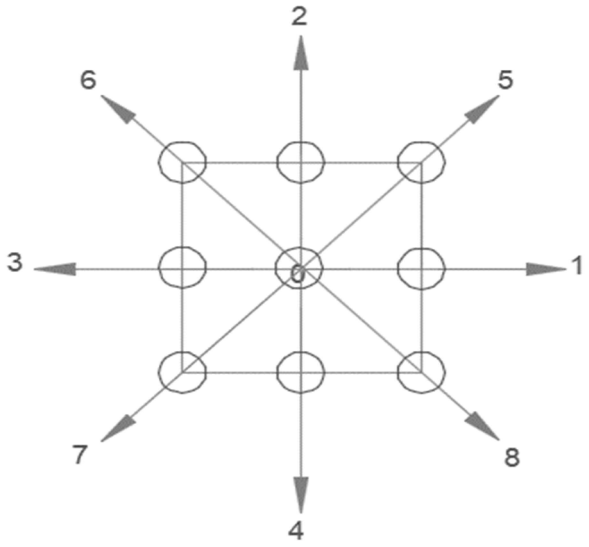

Figure 4. 2. a. The schematic lattice of D2Q9

Recently, the LBM has known remarkable progress to simulate complex phenomena in various engineering applications and has been successfully applied to simulate transport phenomena microchannels [26]. Accordingly, in this paper the LBM in a two- dimensional configuration (D2Q9, **Figure 4.2.a**) based on the BGK approximation (Bhatnagar et al.[27]) is used to simulate the mixed convection in an inclined microchannel for a laminar nanofluid with the associated boundary conditions. The LBM domain is discretized in uniform cartesian cells which hold a fixed number of distribution functions. These distribution functions are calculated by solving the lattice Boltzmann equation, which is the special discretization of the kinetic Boltzmann equation. Therefore, the lattice Boltzmann equations relative to different macroscopic fields are (Guo and Zhoa, [28] ; Mussa et al.,[29]) : equation.

$$\tilde{f}_i = f_i + \frac{dt}{2\tau_f}\left(f_i - f_i^e\right) \tag{4.7}$$

$$\tilde{g}_i = g_i + \frac{dt}{2\tau_g}\left(g_i - g_i^e\right) + \frac{dt}{2} f_i Z_i \tag{4.8}$$

Symbols $\tilde{f}_i$ and $\tilde{g}_i$ define the modified distribution functions (all details can be found in [30]). However, they indicate the momentum and internal energy distribution functions, respectively (He et al., 1998), and f and g their densities. f^e and g^e indicate the equilibrium distribution functions.[31].

In the BGK formulation, this new distribution function can be expressed as follows [31]:

$$\tilde{f}_i\left(\vec{x}+\vec{c}_i dt, t+dt\right) - \tilde{f}_i\left(\vec{x},t\right) = -\frac{dt}{\tau_f + 0.5dt}\left(\tilde{f}_i - f_i^e\right) \tag{4.9}$$

$$\tilde{g}_i\left(\vec{x}+\vec{c}_i dt, t+dt\right) - \tilde{g}_i\left(\vec{x},t\right) = -\frac{dt}{\tau_g + 0.5dt}\left(\tilde{g}_i - g_i^e\right) - \frac{\tau_g dt}{\tau_g + 0.5dt} f_i Z_i \tag{4.10}$$

$$Z_i = \left(\vec{c}_i - \vec{u}\right).D_i\vec{u} \tag{4.11}$$

with the material derivative $D_i = \partial_t + \vec{c}_i.\nabla$

Where τ_f and τ_g are the relaxation times, and f_i^e and g_i^e indicate the equilibrium distribution functions. Zi are the heat dissipation term. The microscopic particle velocities are [19] :

$$\vec{c}_o = (0,0).$$

$$\vec{c}_i = \left(\cos\frac{i-1}{2}\pi, \sin\frac{i-1}{2}\pi\right)c, i = 1,2,3,4$$

$$\vec{c}_i = \sqrt{2}\left(\cos\left(\frac{i-5}{2}\pi + \frac{\pi}{4}\right), \sin\left(\frac{i-5}{2}\pi + \frac{\pi}{4}\right)\right)c, i = 5,6,7,8 \tag{4.12}$$

The equilibrium distributions functions are chosen in the quadratic expansion of Maxwellian [31]

$$f_i^e = \omega_i\rho\left[1 + \frac{3\vec{c}_i.\vec{u}}{c^2} + \frac{9\left(\vec{c}_i.\vec{u}\right)^2}{2c^4} - \frac{3\left(u^2+v^2\right)}{2c^2}\right] \tag{4.13}$$

$$g_0^e = -\omega_0\left[\frac{3\rho e\left(u^2+v^2\right)}{2c^2}\right]$$

$$g_{1,2,3,4}^e = \omega_i\rho\left[1.5 + 1.5\frac{\vec{c}_i.\vec{u}}{c^2} + 4.5\frac{\left(\vec{c}_i.\vec{u}\right)^2}{c^4} - 1.5\frac{\left(u^2+v^2\right)}{c^2}\right] \tag{4.14}$$

$$g_{5,6,7,8}^e = \omega_i\rho\left[3 + 6\frac{\vec{c}_i.\vec{u}}{c^2} + 4.5\frac{\left(\vec{c}_i.\vec{u}\right)^2}{c^4} - 1.5\frac{\left(u^2+v^2\right)}{c^2}\right]$$

Where

$\vec{u} = (u,v)$, $\vec{x} = (x,y)$, $\rho e = \rho RT$, the mass functions are chosen as $\omega_0 = 4/9$, $\omega_i = 1/9 \; for \; i = 1,2,3,4$, $\omega_i = 1/36 \; for \; i = 5,6,7,8$

Finally, the hydrodynamic variables can be obtained via the given expressions [19]:

$$\rho = \sum_i \tilde{f}_i \tag{4.15}$$

$$\rho \vec{u} = \sum_i \vec{c}_i \tilde{f}_i$$

$$\rho e = \sum_i \tilde{g}_i - \frac{dt}{2} \sum_i f_i Z_i \tag{4.16}$$

We can write [20]:

$$\tau_f = \sqrt{\frac{6}{\pi k}} D_H . B \tag{4.17}$$

And

$$\tau_g = \frac{\tau_f}{\Pr} \tag{4.18}$$

Where K is the heat capacity ratio of gas, and for diatomic ideal gas this number is equal to 7/5.

3.3 Boundary conditions

3.3.1 Open boundary conditions

Here the LBM- boundary conditions deal with microscopic distribution functions f and g. A non-equilibrium bounce back model is adopted, for the hydrodynamic boundary conditions at duct extremities [32]. In this model, distribution functions secure the equilibrium conditions and enhance accuracy [33].

The hydrodynamic entrance and exit boundary conditions are discretized using the non-equilibrium bounce back model [32-33]:

$$\begin{aligned} \tilde{f}_1 &= \tilde{f}_3 + \frac{2}{3}\rho_{in} u_{in} \\ \tilde{f}_5 &= \tilde{f}_7 + \frac{1}{2}\left(\tilde{f}_4 - \tilde{f}_2\right) + \frac{1}{6}\rho_{in} u_{in} \\ \tilde{f}_8 &= \tilde{f}_6 - \frac{1}{2}\left(\tilde{f}_4 - \tilde{f}_2\right) + \frac{1}{6}\rho_{in} u_{in} \end{aligned} \tag{4.19}$$

$$\tilde{f}_3 = \tilde{f}_1 - \frac{2}{3}\rho_{out}u_{out}$$
$$\tilde{f}_7 = \tilde{f}_5 - \frac{1}{2}\left(\tilde{f}_4 - \tilde{f}_2\right) - \frac{1}{6}\rho_{out}u_{out} - \frac{1}{2}\rho_{out}v_{out} \qquad \textbf{(4.20)}$$
$$\tilde{f}_6 = \tilde{f}_8 + \frac{1}{2}\left(\tilde{f}_4 - \tilde{f}_2\right) - \frac{1}{6}\rho_{out}u_{out} - \frac{1}{2}\rho_{out}v_{out}$$

The unkhnowc thermal distribution functions at these areas (extremities) are computed using the known thermal input conditions and the non-equilibrium bounce back model as [35-37]:

$$\tilde{g}_5 = \frac{6\rho_{in}e_{in} + 3dt\sum_i\left[f_iZ_i - 6\left(\tilde{g}_0 + \tilde{g}_2 + \tilde{g}_3 + \tilde{g}_4 + \tilde{g}_6 + \tilde{g}_7\right)\right]}{2 + 3u_{in} + 3u_{in}^2}\left[3 + 6u_{in} + 3u_{in}^2\right]\frac{1}{36}$$
$$\tilde{g}_1 = \frac{6\rho_{in}e_{in} + 3dt\sum_i\left[f_iZ_i - 6\left(g_0 + \tilde{g}_2 + \tilde{g}_3 + \tilde{g}_4 + \tilde{g}_6 + \tilde{g}_7\right)\right]}{2 + 3u_{in} + 3u_{in}^2}\left[1.5 + 1.5u_{in} + 3u_{in}^2\right]\frac{1}{9} \qquad \textbf{(4.21)}$$
$$\tilde{g}_8 = \frac{6\rho_{in}e_{in} + 3dt\sum_i\left[f_iZ_i - 6\left(\tilde{g}_0 + \tilde{g}_2 + \tilde{g}_3 + \tilde{g}_4 + \tilde{g}_6 + \tilde{g}_7\right)\right]}{2 + 3u_{in} + 3u_{in}^2}\left[3 + 6u_{in} + 3u_{in}^2\right]\frac{1}{36}$$

$$\tilde{g}_0 = \frac{6\left(\tilde{g}_1 + \tilde{g}_5 + \tilde{g}_8\right) - 3dt\sum_i\left(\frac{c_{ix}}{c}\right)f_iZi - 6\left(\rho eu_{out}\right)}{2 - 3u_{out} + 3u_{out}^2}\left[3 - 6u_{out} + 6v_{out} + 3\left(u_{out}^2 + v_{out}^2\right) - 9u_{out}v_{out}\right]\frac{1}{36}$$
$$\tilde{g}_3 = \frac{6\left(\tilde{g}_1 + g_5 + \tilde{g}_8\right) - 3dt\sum_i\left(\frac{c_{ix}}{c}\right)f_iZi - 6\left(\rho eu_{out}\right)}{2 - 3u_{out} + 3u_{out}^2}\left[1.5 - 1.5u_{out} + 3u_{out}^2 - 1.5v_{out}^2\right]\frac{1}{9}$$
$$\tilde{g}_7 = \frac{6\left(\tilde{g}_1 + g_5 + \tilde{g}_8\right) - 3dt\sum_i\left(\frac{c_{ix}}{c}\right)f_iZi - 6\left(\rho eu_{out}\right)}{2 - 3u_{out} + 3u_{out}^2}\left[3 - 6u_{out} - 6v_{out} + 3\left(u_{out}^2 + v_{out}^2\right) + 9u_{out}v_{out}\right]\frac{1}{36}$$

(4.22)

3.3.2 Top-Bottom walls boundary conditions

In The no-slip regimes, the boundary conditions used are:

unkhnowc thermal distribution functions at these areas (extremities) are computed using the known thermal input conditions and the non-equilibrium bounce back model as [34-36]:

$$u_w = u_{liquid}\big|_w \qquad \textbf{(4.23)}$$

$$T_w = T_{liquid}\big|_w \qquad \textbf{(4.24)}$$

Where u_w is the velocity of the wall, and u_{liquid} represents the velocity of the liquid at the wall. Similar definitions can be considered the temperature field.

Thompson and Troian [37] show the slip flow on the walls using molecular method.

$$\Delta u_w = u_{fluid}\left(y \to wall\right) - u_w = L_s \frac{\partial u_{fluid}}{\partial y}\Big|_w \quad \textbf{(4.25)}$$

Where L_s is the constant slip length.

Ngoma and Erchiqui [38] considered The slip length coefficient (β) and the slip velocity for the liquid in the microchannel are written as (Ngoma and Erchiqui [38]):

$$u_s = \pm\beta \frac{\partial u_{fluid}}{\partial y}\Big|_{y=0,h} \quad \textbf{(4.26)}$$

Where u_s is the slip velocity of the liquid on the wall. The dimensionless form is written as:

$$U_s = \pm B \frac{\partial U}{\partial Y}\Big|_{\mathrm{Y=0,1}} \quad \textbf{(4.27)}$$

To write the slip velocity using eq. (27) in the LBM, U_s was calculated by using the specular reflective bounce back and diffuse-scattering boundary condition [39] is applied in this study. The hydrodynamic distribution functions at the lower wall are given as [34]:

$$\tilde{f}_2 = \tilde{f}_4 \quad \textbf{(4.27.1)}$$

$$\tilde{f}_{5,6} = r\tilde{f}_{7,8} + \left(1-r\right)\tilde{f}_{8,7} \quad \textbf{(4.27.2)}$$

Where r= is the accommodation factor (r < 1).

Thereby, the hydrodynamic distribution functions at the top wall are:

$$\tilde{f}_4 = \tilde{f}_2 \quad \textbf{(4.28.1)}$$

$$\tilde{f}_{7,8} = r\tilde{f}_{5,6} + \left(1-r\right)\tilde{f}_{6,5} \quad \textbf{(4.28.2)}$$

By analogy with eq. (26), we can write the temperature jump in the microchannel walls [40]:

$$\Delta T_w = T_{fluid}\left(y \to wall\right) - T_w = \zeta \frac{\partial T_{fluid}}{\partial y}\Big|_w \quad \textbf{(4.29)}$$

Where ζ is the temperature jump distance. The dimensionless form of eq. (29) is written as:

$$\theta - \theta_w = \frac{B}{\mathrm{Pr}} \frac{\partial \theta}{\partial y}\Big|_{\mathrm{Y=0,1}} \quad \textbf{(4.30)}$$

For the thermal boundary condition in the microchannel, the general-purpose thermal boundary condition (GPTBC) (D'Orazio et al.) heat flux model is considered in this chapter [31].

4. Effects of gravity

The model proposed under a mixed convection nanofluid in an inclined microchannel is studied by using the approximation of Boussinesq, where the buoyancy force is

$\vec{G} = \beta \vec{g}\left(T - \overline{T}\right)$ .Taking into consideration the influence of "F" (external force), and the lattice Boltzmann equation is given as [19]:

$$\partial_t f + (c.\nabla) f = -\frac{f - f^e}{\tau} + F \tag{4.31}$$

With

$$\vec{F} = \frac{G(\vec{c} - \vec{u})}{RT} f^e$$

Therefore,

$$\widetilde{f}\left(\vec{x} + \vec{c_i}dt, t + dt\right) - \widetilde{f}\left(\vec{x}, t\right) = -\frac{dt}{\tau_f + 0.5dt}\left(\widetilde{f_i} - f_i^e\right) + \left(\frac{\tau_f dt}{\tau_f + 0.5dt}\frac{3G\left(c_{ix} - u\right)}{c^2} f_i^e\right)\sin\gamma + \left(\frac{\tau_f dt}{\tau_f + 0.5dt}\frac{3G\left(c_{iy} - v\right)}{c^2} f_i^e\right)\cos\gamma \tag{4.32}$$

$$f_i = \frac{\tau_f \tilde{f}_i^e + 0.5 f_i^e dt}{\tau_f + 0.5dt} + \frac{0.5\tau_f dt}{\tau_f + 0.5dt} F \tag{4.33}$$

$$f_i = \frac{\tau_f \tilde{f}_i + 0.5dt f_i^e}{\tau_f + 0.5dt} + \left(\frac{0.5dt\tau_f}{\tau_f + 0.5dt}\frac{G\left(c_{ix} - u\right)}{RT} f_i^e\right)\sin\gamma + \left(\frac{0.5dt\tau_f}{\tau_f + 0.5dt}\frac{G\left(c_{iy} - v\right)}{RT} f_i^e\right)\cos\gamma \tag{4.34}$$

Accordingly, the hydrodynamic variables can be written as follows:

$$\rho = \sum_i \tilde{f}_i \tag{4.35.1}$$

$$u = \frac{1}{\rho}\sum_i \tilde{f}_i c_{ix} + \frac{dt}{2} G\sin\gamma \tag{4.35.2}$$

$$v = \frac{1}{\rho}\sum_i \tilde{f}_i c_{iy} + \frac{dt}{2} G\cos\gamma \tag{4.35.3}$$

As it was said before, the lower and upper walls were affected by a constant heat flux by the following equation [20]:

$$q = \left(\sum_i c_i \tilde{g}_i - \rho e u - \frac{dt}{2}\sum_i c_i f_i Z_i\right)\frac{\tau_g}{\tau_g + 0.5dt} \tag{4.36}$$

Using the last equation for the upper wall leads to:

$$\sum_i c_i \tilde{g}_i = \frac{dt}{2}\sum_i c_{iy} f_i Z_i + \rho e_N V_w + \frac{\tau_g + 0.5dt}{\tau_g} q_y \tag{4.37}$$

5. Results and comments

To achieve the grid-mesh test, simulation is performed for three sizes, which are (350x35), (400x40) and (450x45), for the slip velocity in the absence of gravity. The results of the slip velocity remain independent beyond the grid size (400x40). The results of the slip velocity remain independent beyond the grid size (400x40). As it can be seen, the predicted values are almost similar. As illustrated, the maximal difference between the first two meshes is approximately 0.8%. Then, it shrinks to reach a deviation of 0.2% between the last two grids. This suggests that the solution becomes independent of the (400x40) grid. Therefore, such a grid is selected for the rest of the later computations. (See table 4.1)

Table 4. 1Grid independency in absence of buoyancy force for two values of B

	Grids		
	350x35	400x40	450x45
B=0.02	0.124	0.125	0.125
B=0.01	0.125	0.073	0.073

Present work achievements by LBM versus analytical ones of Kandlikar et al. [1] are compared in **Figure.2.b** corresponded to a plane flow between two parallel plates at width of 2h. The slip velocity is involved analytically as $u^+ = 1 - y^{*2} + 8Kn$, where $u^+ = u/\left(\left(-h^2/2\mu\right)\left(dp/dx\right)\right)$ and $y^* = y/h$. Suitable agreements are seen between them.

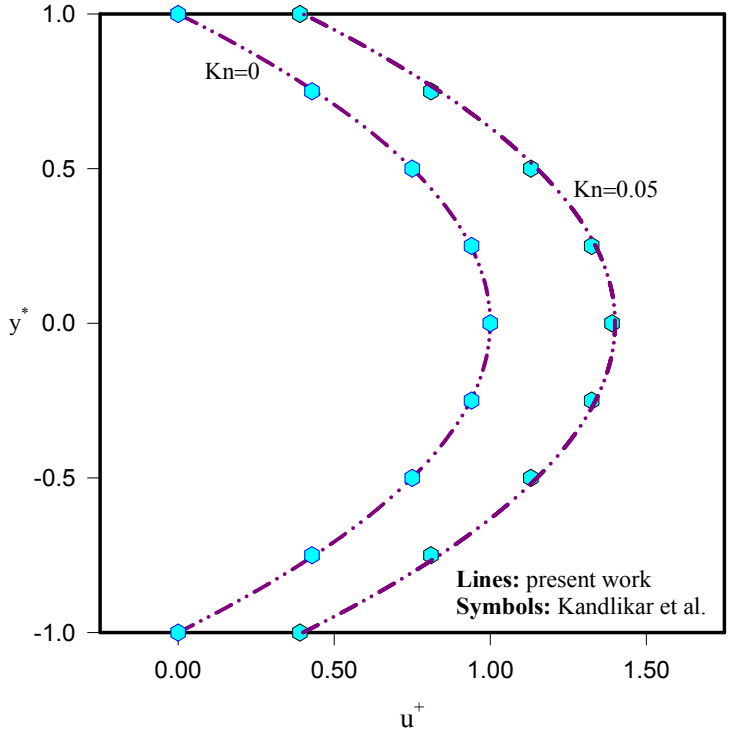

Figure 4 .2.b. Fully developed velocity profiles of preset work vs. analytical solution of Kandlikar et al. [1]

This work reports on heat transfer for the flow of laminar nanofluids in inclined microchannels with top-bottom walls subjected to a constant heat flux considering the gravitational effects. The used nanofluid is Al2O3, which is the nanoparticle chosen for this study, as given in Table 4.2. Re is chosen to be 1. Numerical simulation is completed by presenting the effect of emerging parameters, such as the buoyancy force (Ri =1, 5, 10), the slip coefficient (B=0.005, 0.01, 0.02), the nanoparticle volume fraction (φ=0, 2%, 4%) and the micro-channel inclination angle (γ= 0°, 30°, 60°), on the dynamic and thermal behaviors.

Figure 4.3.a, b displays the streamlines (a) and isotherms (b) for B=0.01 and φ=4% without gravity. The horizontal streamlines occur from the entrance left side along the walls. The isotherms are symmetrical with respect to the central line due to the existence of the heat flux at the top-bottom walls. For the same condition, velocity reaches a maximum at the centerline of the microchannel depending on X. Far from the entrance, where X = 0.08L, the velocity becomes developed with a maximum of less than 1.5 (**Figure 4.3.c)**. The obtained symmetry in the streamlines and isotherms is strongly affected by the buoyancy force and disappears at high values of Ri whatever the inclination angle, as shown in **Figure 4.4.** This figure depicts the existence of a rotational long cell generated near the upper half of the domain. For higher

γ, this trend disappears for each value of Ri. Due to the gravitational effects, obvious descending flows are detected along the inclined microchannel. As a result, the inclination angle strongly affects the buoyancy force for large values of Ri.

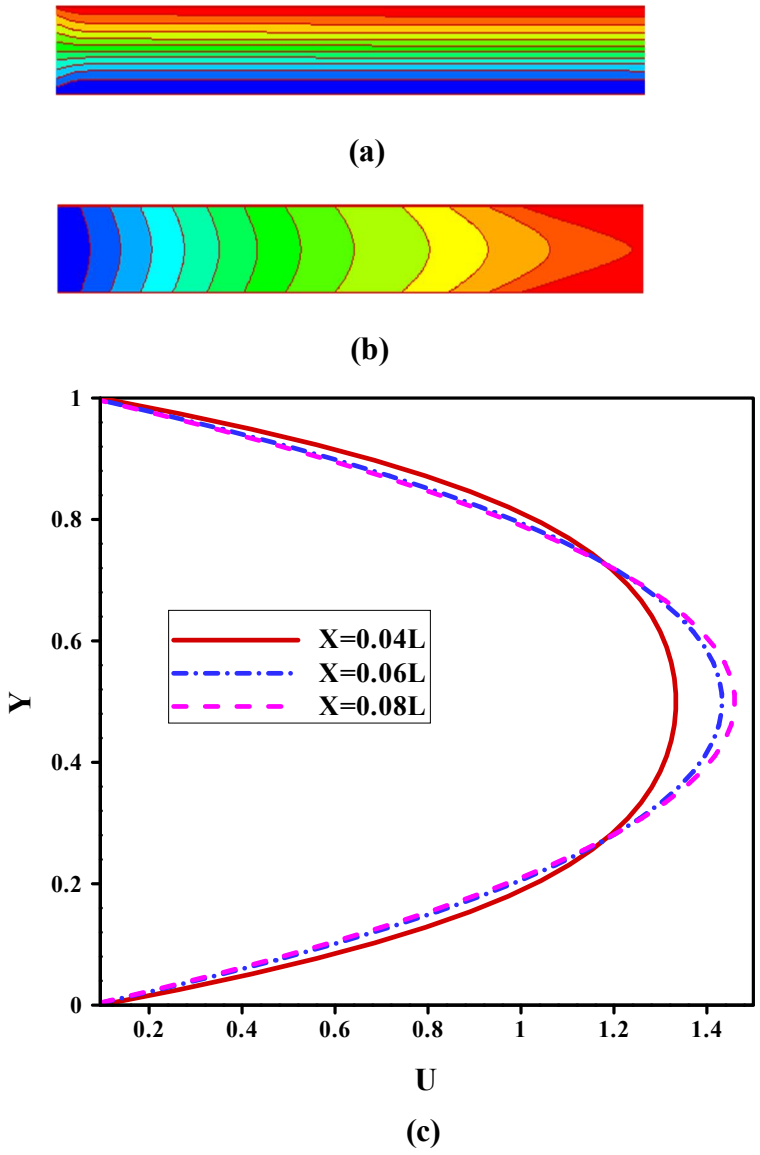

Figure 4. 3. a, b Streamlines, isotherm contours, velocity profles and temperature profles for φ=4% and B=0.01. in the absence of gravity. c Dimensionless velocity profles for no gravity

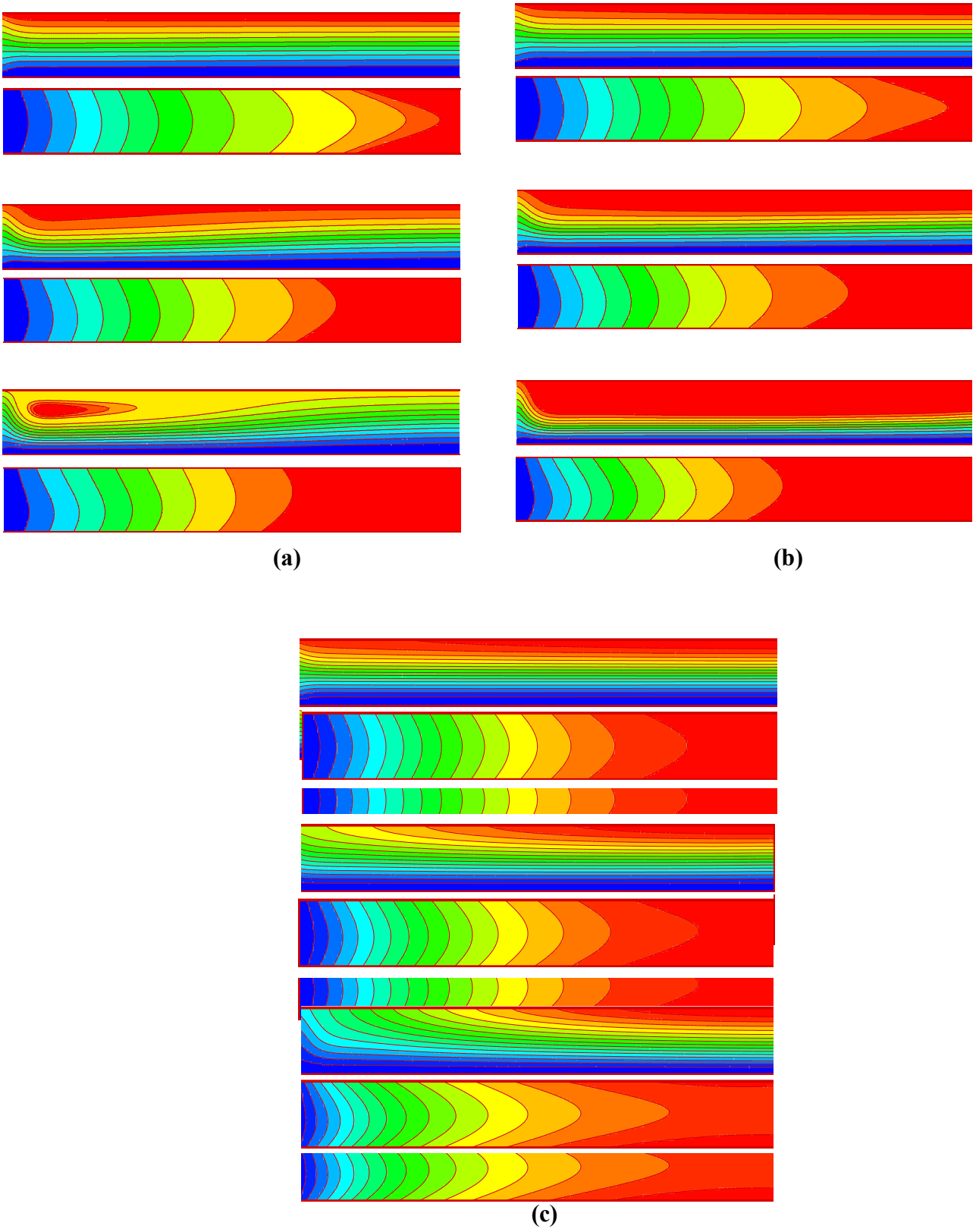

Figure 4. 4. Streamlines (upper) & isotherms (lower) at B=0.01 and φ =4% for a : γ= 0° ; b : γ=30° and c: γ= 60° at Ri=1 (top), Ri=5 (middle) & Ri=10 (bottom)

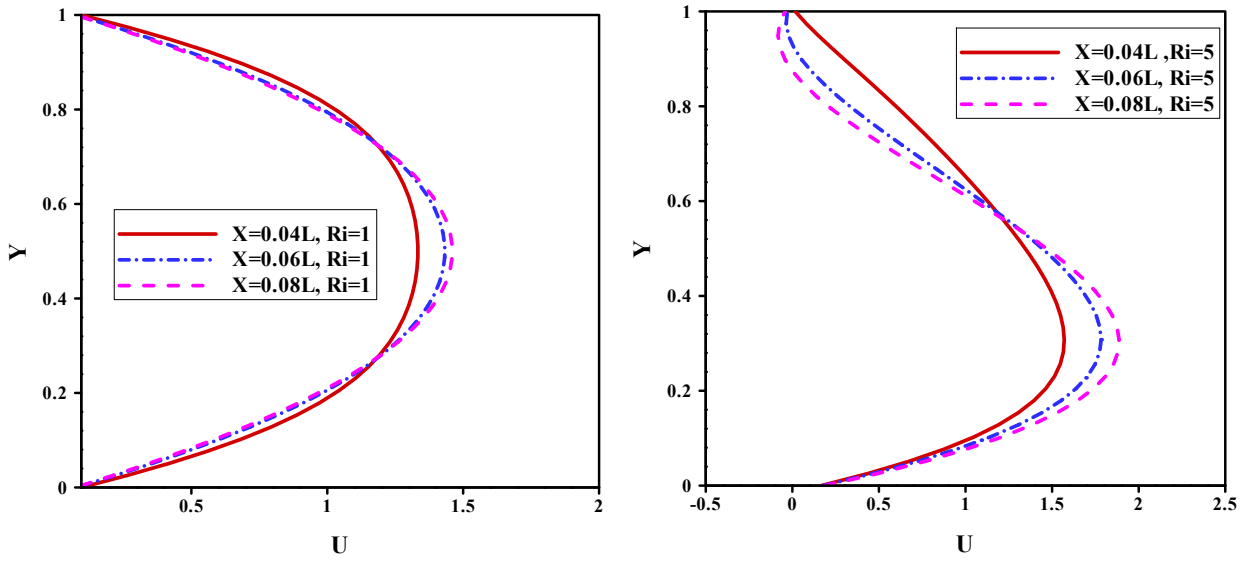

(a) (b)

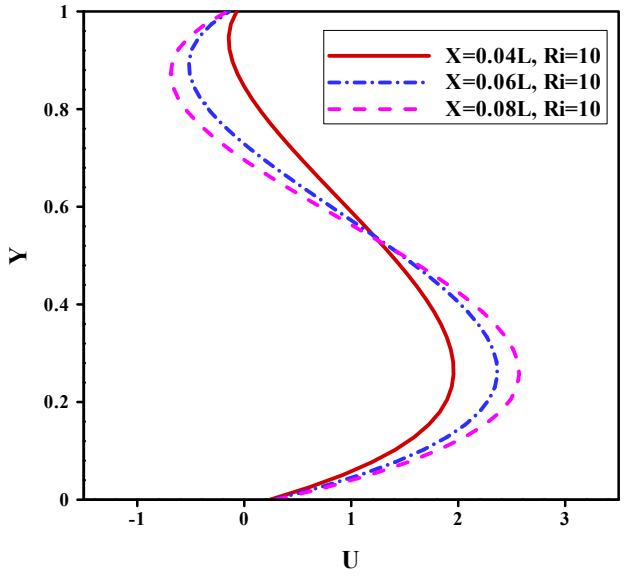

(c)

Figure 4. 5.Dimensionless horizontal velocity profiles vs X for φ =4%, B=0.01 and γ = 0°.

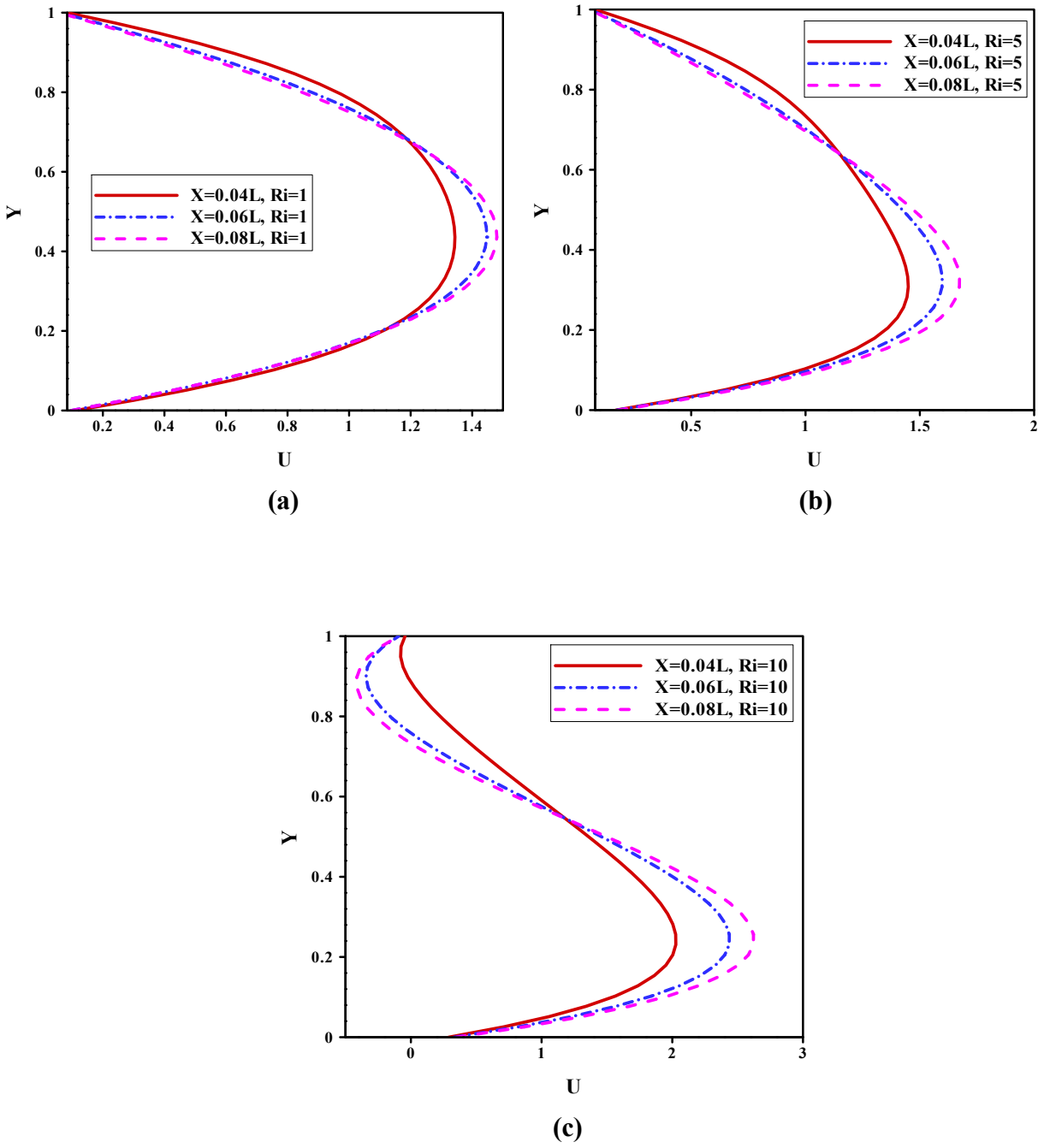

Figure 4. 6. Dimensionless horizontal velocity profiles vs. X for B=0.01, φ =4% and γ=30°

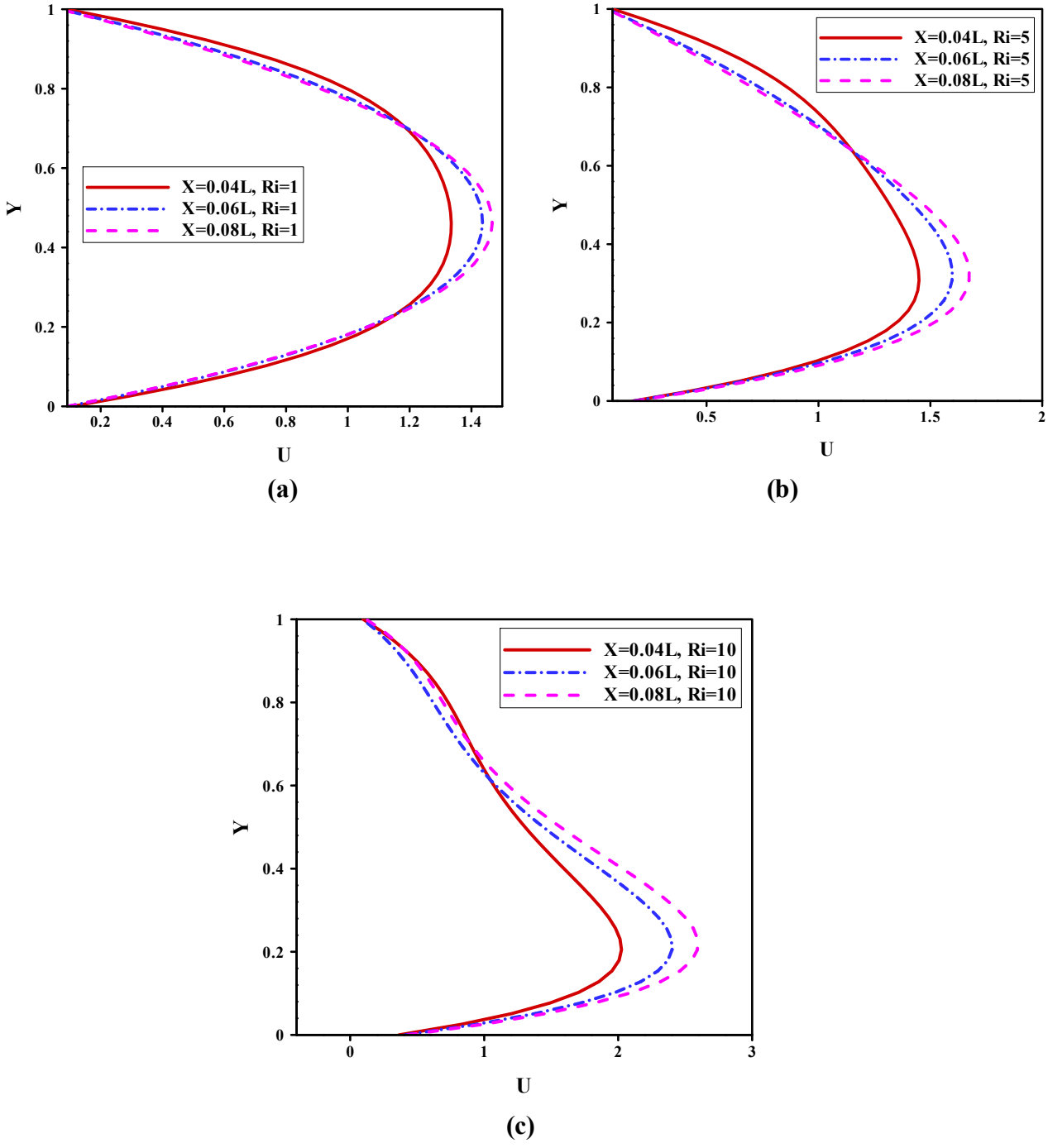

Figure 4. 7. Dimensionless horizontal velocity profiles vs. X for B=0.01 and φ=4% and γ=60°.

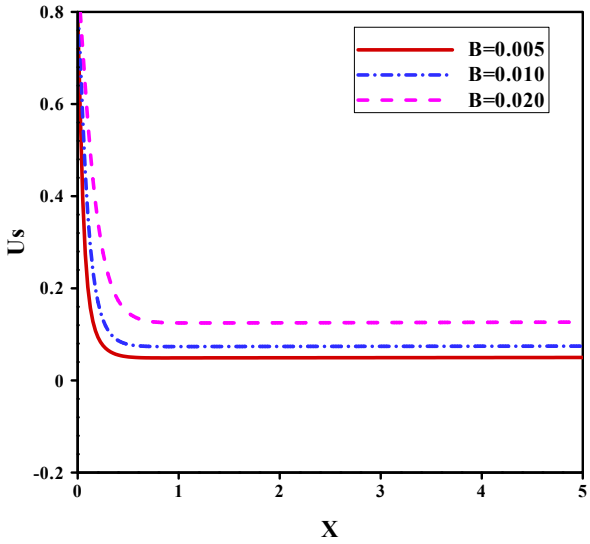

Figure 4. 8. Slip velocity at the wall of microchannel without gravity (no-gravity) and for φ =4%

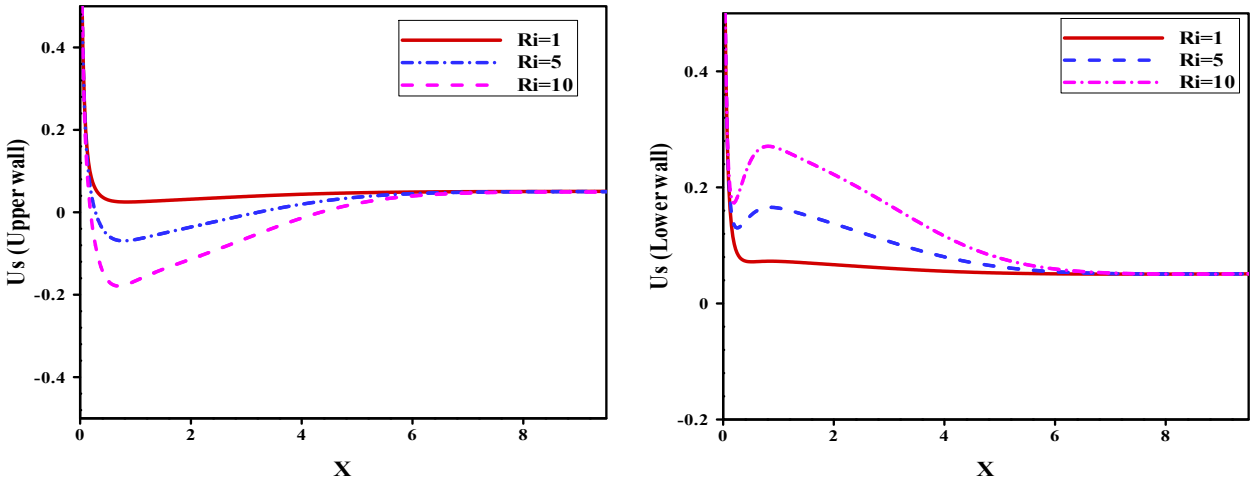

(a)

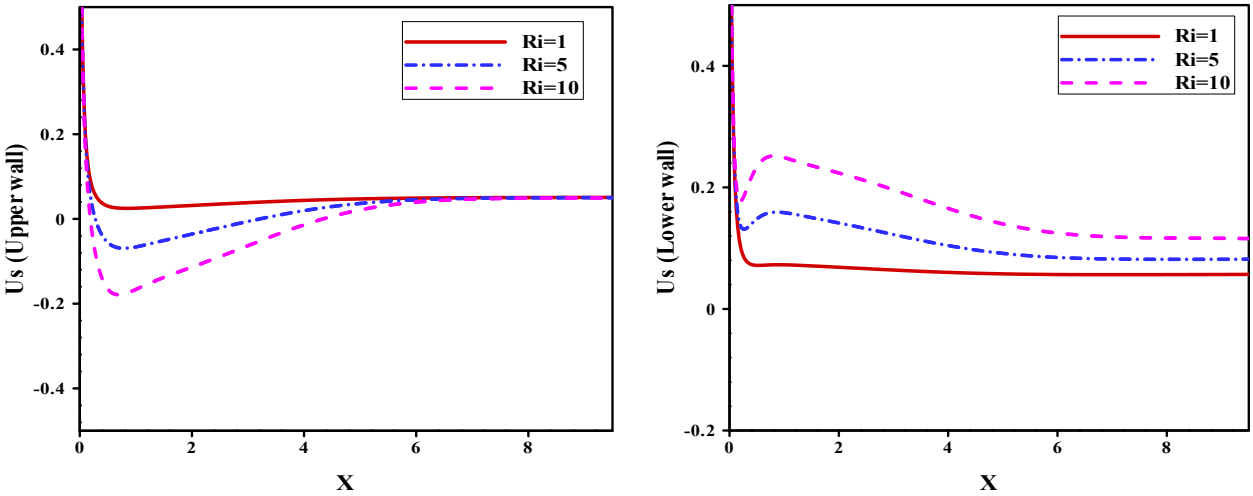

(b)

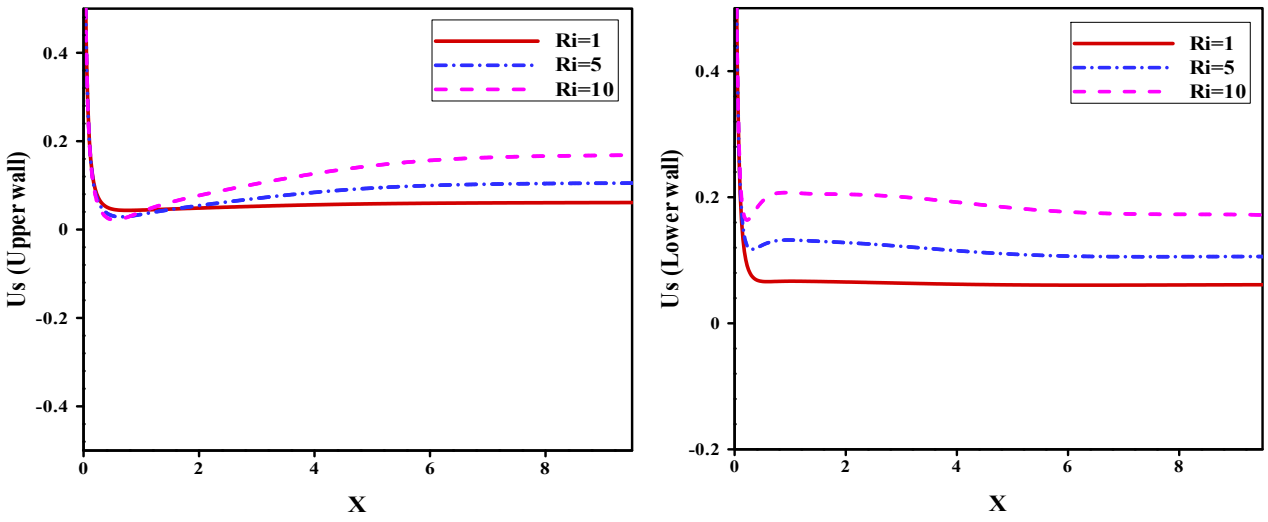

(c)

Figure 4. 9. Slip velocity at the walls of inclined microchannel (a: γ=0°; b: γ= 30° and c: γ=60°) at B=0.005 and φ =4%

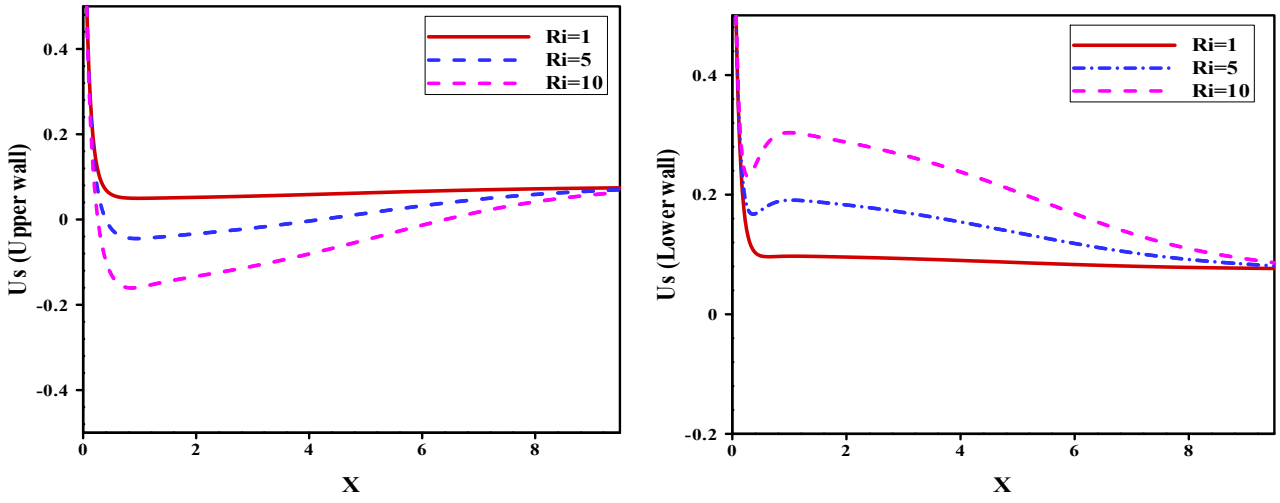

(a)

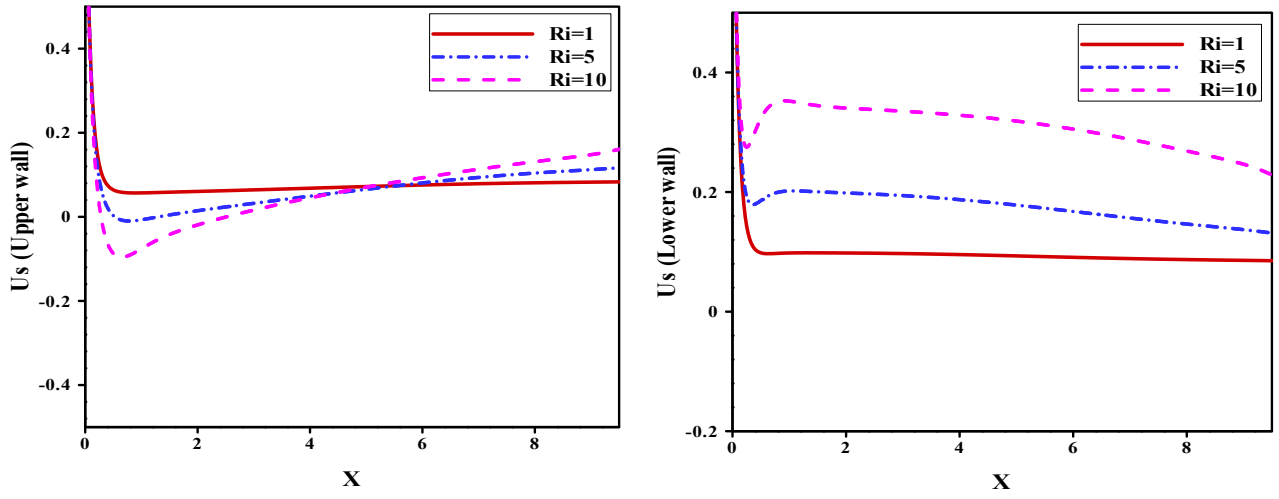

(b)

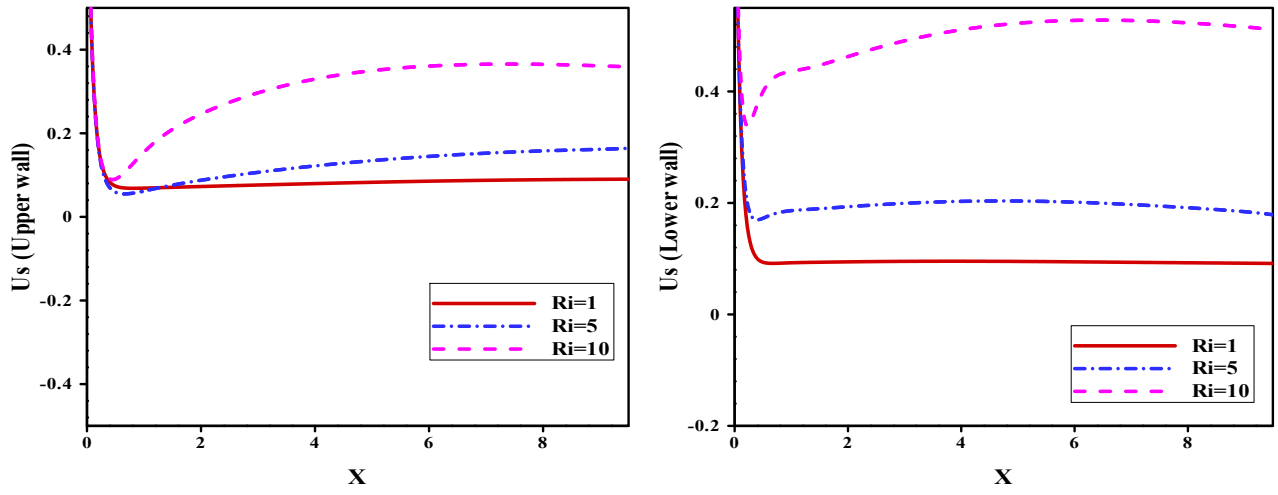

(c)

Figure 4. 10. Slip velocity at the walls of inclined microchannel (a : γ=0°; b: γ= 30° and c: γ=60°) at B=0.01 and φ =4%

5.1 Dynamic field

Figure 4.5 shows the profiles of dimensionless velocity, along the wall of the microchannel at B = 0.01, γ=0 and φ = 0.04 for different Ri. The wholly developed profile is illustrated in Figure (3.5.a). at X = 0.08L near the entrance region (X = 0.04 L andX = 0.06 L). Thereby, according to the rule of forced convective heat transfer (Ri = 1), the presence of the slip velocity at Y = 0 and Y = 1 is clear in this figure and attains its maximal value at the microchannel input. Then, it decreases with movement along the microchannel and eventually establishes. By increasing Ri and generating the buoyancy force, the flow moves towards the mixed convection heat transfer (**Figure 4.5.b**) and **4.5.c**). Therefore, a rotational cell appears with the growth of Ri, and its size is strongly affected by the buoyancy force. **Figures 4.6** and **4.7** show that the shape of the velocity profile depends on both Ri and γ. The intensity of the velocity goes up for high values of γ (**figure 4.7**). It is stated again that the rotational cell disappears for γ = 60°. Then, the inclination effect dominates the Ri effects. **Figure 4.8** presents the slip velocity profile along the microchannel without gravity. At the top-bottom walls, the nanofluid velocity is nil due to the slip boundary conditions. Then, it rises for higher values of the slip factor. In addition, near the entrance region, the slip velocity reaches almost equal maximal values. The profile of this velocity decreases and tends to be asymptotic with the increase in X. In other words, for large values of B or a decreasing resistance of the solid wall, the fluid motion reduces the velocity gradients which make the velocity magnitude closer to that at the inlet of the microchannel. It becomes constant for a critical value of X. **Figure**

4.9 shows the effect of the inclination angle on the slip velocity at the top-bottom walls. It can be stated firstly that this velocity does not have the same shape for both walls due to the slip boundary condition imposed at these walls. From the behavior of the velocity profiles at the upper wall, no variation is seen in its shape for Ri = 1. The same trend concerning the slip velocity observed in **Figure 4.8** is deduced here. It is interesting to note that the upper slip velocity close to the wall at the entrance initially reaches a maximum, but falls after a short distance from the entrance region. Ultimately, it reaches negative values for X, ranging between 0.5 and 6, before the flow attains the developed regime (X ≥6). By increasing Ri, the size of the detected rotational cell grows, confirming the trend given by **Figure 4.6**. This velocity builds up with Ri, proving the effect of the buoyancy force. In fact, the lower slip velocity occurs at two local maxima: the first one at the entrance region and the second one at a critical value of X, depending on Ri. For X ≥6, the lower slip velocity rises with Ri. To examine the effects of the inclination angle on the upper-lower slip velocities, it can be noted that the intensity of the upper velocity increases, but that of the lower velocity goes down due to inclination. Then, the critical value of X for which the developed region occurs is strongly affected by γ. This critical value grows with γ. Then, the inclination effect is dominated the Ri effects.

Figure 4.10 illustrates the effects of a slip condition given by B on the upper-lower velocity. By increasing B = 0.01, the shape of both velocity values changes. The same tendency is observed for the upper velocity. In fact, it decreases from a maximum at the entrance to reach a minimum and rise again, attaining positive values for a critical value of X, depending on Ri. The observed trend is accentuated with γ. However, the lower slip velocity remains positive whatever the value of Ri, and its amplitude is more pronounced for $\gamma = 60°$.

5.2 Thermal field

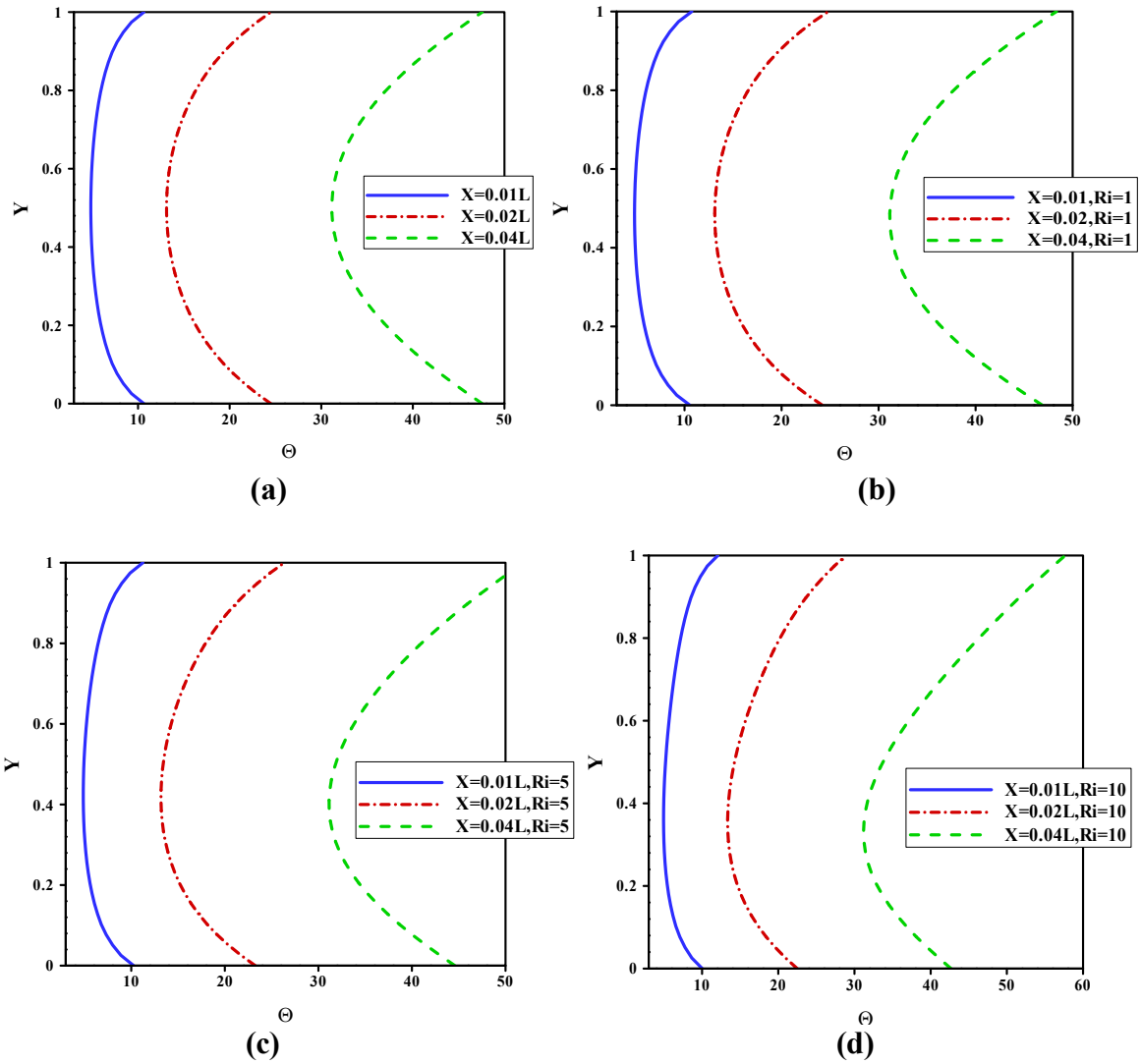

Figure 4. 11. Dimensionless temperature profiles profiles at various vertical cross sections of the horizontale microchannel for, a: nogravity ,b:Ri=1,c:Ri=5,d:Ri=10, at ϕ=4%, B=0.01 and γ =0°.

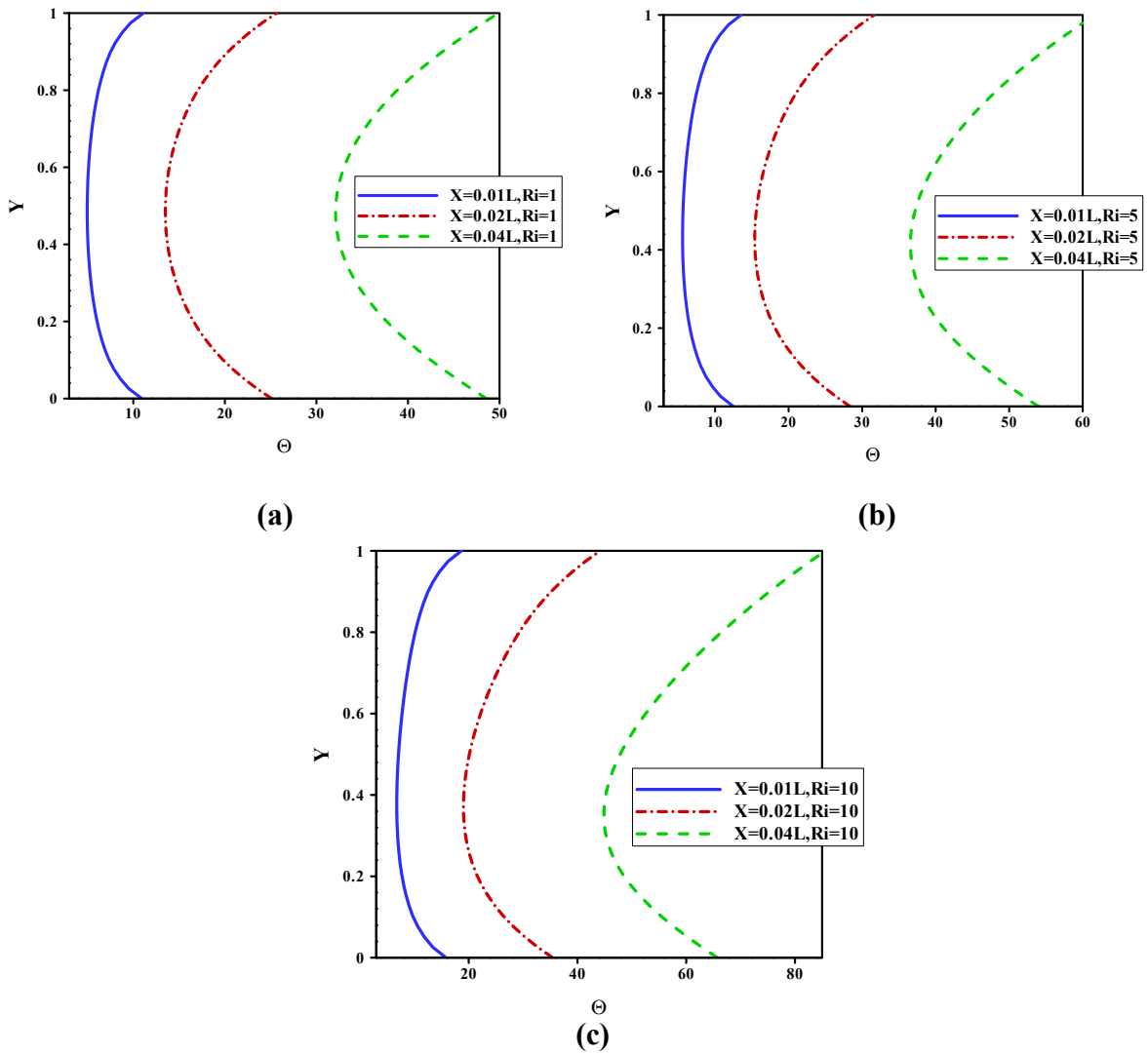

Figure 4. 12. Dimensionless temperature profiles profiles at various vertical cross sections of the horizontale microchannel for φ =4%, B=0.01 and γ = 30°.

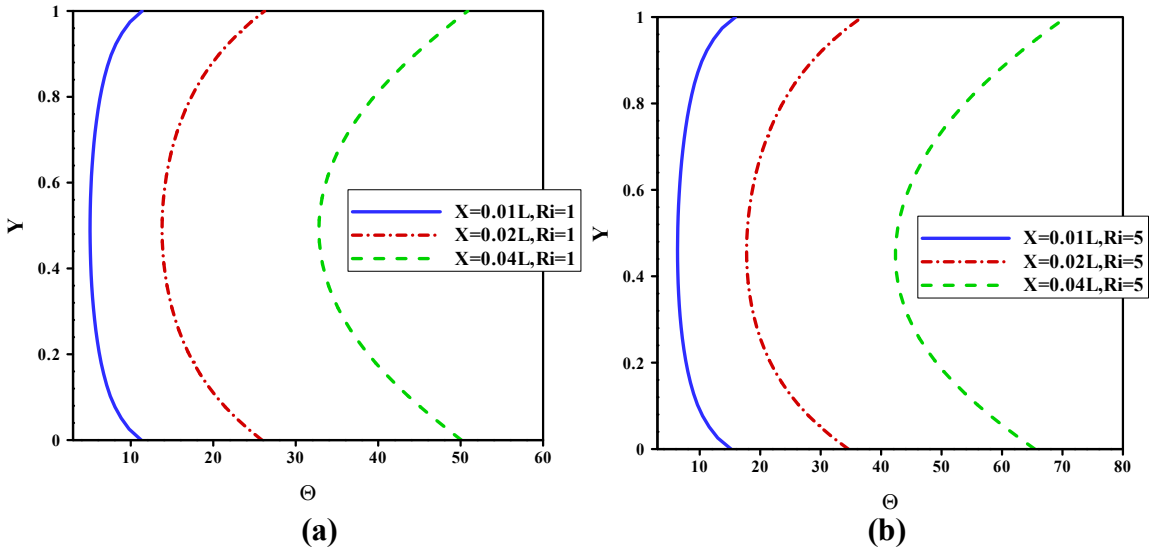

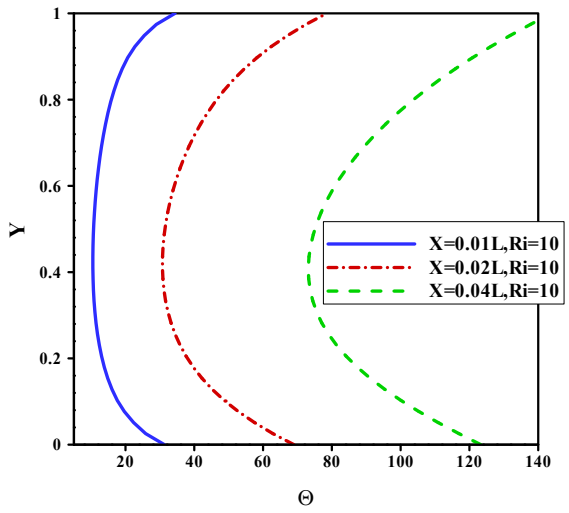

(c)

Figure 4. 13. Dimensionless temperature profiles profiles at various vertical cross sections of the horizontale microchannel for φ =4%, B=0.01 and γ = 60°.

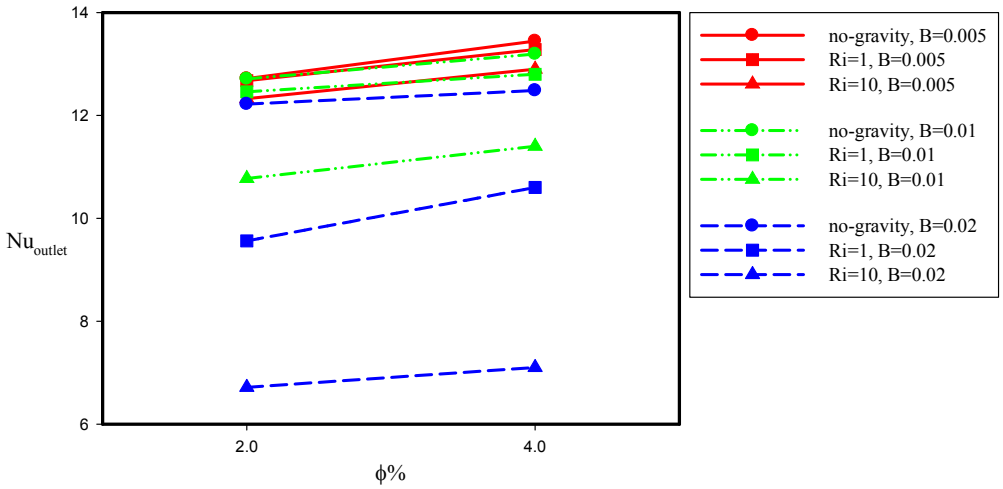

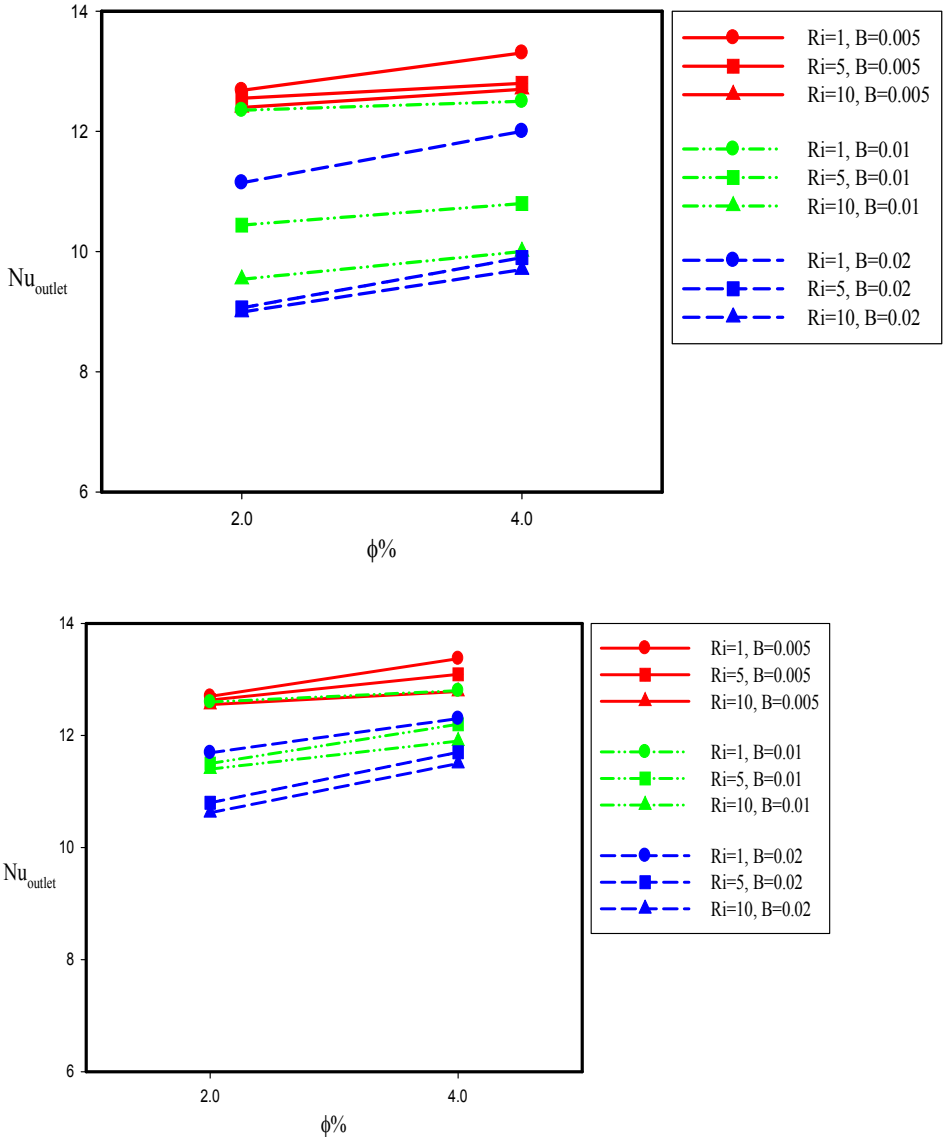

Figure 4. 14. Outlet Nusselt number along the microchannel bottom wall for γ=0°(upper plot) γ=30°(middle plot) andγ=60°(lower plot)

According to GPTBC model which are the developed forms of Dorazio et al. heat flux model, Nusselt number equation based on the constant heat flux is written as[21]:

$$Nu_x = \left(\frac{k_{nf}}{k_f}\right)\frac{q_y D_H}{\Delta T k} = \left(\frac{k_{nf}}{k_f}\right)\frac{D_H\left(\partial T/\partial y\right)_w}{\left(T_w - T_{bulk}\right)} \qquad \textbf{(4.38)}$$

Table 4. 2Thermo-physical properties Al2O3- Water

(if φ =2%→Prnf=5.6, Knf=0.657 & if φ =4%→Prnf=4.98, Knf=0.695) [41]

Properties	Water	Al2O3
$\lambda\left(W.m^{-1}.K^{-1}\right)$	0.62	40

$\rho\left(Kg.m^{-3}\right)$	996	3970
$C_p\left(J.kg^{-1}.K^{-1}\right)$	4179	385
$\mu(Pa.s)$	$8.92x10^{-4}$	-

Figure 4.11 shows the non-dimensional temperature profiles obtained without gravity (**a**) and for different Ri (**b**:Ri=1, **c**:Ri=5, **d**:Ri=10) at various X. The temperature of the nanofluid entering the microchannel grows with the increase in X. Due to the thermal boundary conditions, temperature rises to reach a maximum for a critical value of Y, as depicted in **Figure (4.11.a).** Including the effect of gravity, represented in **Figure** (**4.11.b-d**), the symmetric shape of the temperature observed from the entrance region is affected by the Ri values. It can be seen that the amplitude of the temperature increases with the Ri effects. The same trend corresponding to the nanofluid temperature observed in **Figures 4.12** and **4.13** is depicted with the effects of inclination. Then, the amplitude of this temperature grows with γ . It can be stated that the heat transfer rate is accentuated with the inclination, compared to the Ri effect. **Figure 4.14** illustrates the Nusselt number for different inclination angles, volume fractions, Ri and coefficients of slip velocity. For large values of nanoparticle volume fractions, the Nusselt number is enhanced for lower Ri. It can also be seen that higher B induces a lower heat transfer rate. Therefore, without gravity, the high intensity of Nusselt is obtained at B=0.005. Approaching the vertical position, the heat transfer rate is ameliorated. Thus, it is noted that a higher part of the heat transfer rate occurs for a large amount of φ and for a low amount of B.

6. Conclusion

We have presented a numerical study of mixed convection heat transfer in an inclined microchannel full of laminar Water/Al2O3 nanofluid. The top-bottom walls have been subjected to a constant heat flux. Then, a double population distribution function approach of a modified LBM has been used to simulate the effect of the buoyancy force on the dynamic and thermal fields. Among the obtained results, we can cite the following :

- The buoyancy force and the inclination angle have strongly affected the shape of the velocity profile. Then, a rotational cell has appeared with the increase in Ri, and its size has been strongly affected by the buoyancy force and disappeared for $\gamma = 60°$. Thus, it can be concluded that the inclination effect dominates the Ri effects.

- The slip velocity at the top-bottom walls has reached optimal values depending on the combination of the Ri effects, the inclination angle and the slip velocity. These velocities have the same shape for all emerging parameters without gravity. In the presence of gravity, this shape has been strongly affected by Ri and the inclination angle.
- The temperature has shown a symmetric profile without gravity. Hence, the intensification of this parameter has improved heat transfer.
- The heat transfer rate at the outlet has linearly varied with the volume fraction regardless of the emerging parameters. Then, it has improved for lower values of Ri regardless of the inclination angle, and the slip velocity has increased.

References

[1] Kandlikar S, Garimella S, Li D, Colin S, King M R. Heat transfer and fluid flow in minichannels and microchannels. first ed. NY, USA: Rochester Institute of Technology;2005

[2] Nguyen N T, Wereley N T. Fundamentals and applications of microfluidics. 2nd ed. Artech house INC, Norwood, MA 02062, 2006.

[3] Mitra S K, Chakraborty S. Microfluidics and nanofluidics handbook fabrication, implementation, and applications. London New York: Taylor & Francis Group; 2012.

[4] Gad-el-Hak M, MEMS-Applications, 2nd ed. London New York: Taylor & Francis Group; 2005.

[5] Avci M, Aydin O. Mixed convection in a vertical parallel plate microchannel With Asymmetric Wall Heat Fluxes. J.Heat transfer. 2007;129:1091-1095.

[6] Avramenko A A , Tyrinov A I ,Shevchuk I V , Dmitrenko N P , Kravchuk A V , V.I. Shevchuk I V. Mixed convection in a vertical flat microchannel. Int J Heat Mass Transf. 2017;106:1164–1173.

[7] Khanafera K , Aithal SM, Vafaid K. Mixed convection heat transfer in a differentially heated cavity with two rotating cylinders International. J Therm Sci.2019;135: 117-132.

[8] Cao K ,Baker J. Slip effects on mixed convective flow and heat transfer from a vertical plate. Int J Heat Mass Transf. 2009;52:3829–3841.

[9] Niazmand H, Rahimi B.Mixed convective slip flows in a vertical parallel plate microchannel with symmetric and asymmetric wall heat fluxes.Transactions of the Canadian Society for Mech Eng.2012;36:207-218.

[10]Mohammad RT, Omid A A, Anoushiravan M, Erfan K ,Farzad P . Numerical study of mixed convection heat transfer inside a vertical microchannel with two-phase approach. J Therm Anal Calorim,2019;135:1119–1134.

[11] Masoud Z, Davood T, Karimipour A. Developing a new correlation to estimate the thermal conductivity of MWCNT-CuO/water hybrid nanofluid via an experimental investigation. J Therm Anal Calorim, 2017;129:859–867.

[12] Xu H, Sun Qi. Generalized Hybrid Nanofluid Model with the Application of Fully Developed Mixed Convection Flow in a Vertical Microchannel. Commun. Theor. Phys, 2019;71:903-911.

[13] Manay E, Mandev E. Experimental investigation of mixed convection heat transfer of nanofluids in a circular microchannel with different inclination angles. J Therm Anal Calorim, 2019;135:887-900.

[14] Naphon P, Nakharintr L, Wiriyasart S. Continuous nanofluids jet impingement heat transfer and flow in a micro- channel heat sink. Int J HeaT Mass transf,2018,26:924-932.

[15] Bowers J, Cao H, Qiao G, QiLi, Zhang G, Mura E, Yulong D. Flow and heat transfer behaviour of nanofluids in microchannels. Progress in Natural Science: Materials International,2018;28:225–234.

[16] Ay C, Young CW, Young CF.Application of lattice Boltzmann method to the fluid analysis in a rectangular microchannel. Comput. Math. Appl, 2012; 64:1065-1083.

[17] Yang YT, Lai FH. Numerical study of flow and heat transfer characteristics of alumina-water nanofluids in a microchannel using the lattice Boltzmann method. Int Commun Heat Mass Transf, 2011;38:607-614.

[18] Mozaffari M, Karimipour A , D'Orazio A. Increase lattice Boltzmann method ability to simulate slip flow regimes with dispersed CNTs nanoadditives inside. J Therm Anal Calorim , 2019;137:229–243.

[19] Karimipour A, Nezhad A H, D'Orazio A, Shirani E.I nvestigation of the gravity effects on the mixed convection heat transfer in a microchannel using lattice Boltzmann method. Int J Therm Sci, 2012;54:142-152.

[20] D'Orazio A, A.Karimipour A. A useful case study to develop lattice Boltzmann method performance, Gravity effects on slip velocity and temperature profiles of an air flow inside a microchannel under a constant heat flux boundary condition. Int J Heat Mass Transf, 2019;136:1017-1029.

[21]Karimipour A, Nezhad AH, D'Orazio A, Esfe MH, Safaei RM, Shirani E. Simulation of copper–water nanofluid in a microchannel in slip flow regime using the lattice Boltzmann method. European J Mechan B/Fluids. 2015;49:89-99.

[22] Xuan Y, Li Q. Investigation on convective heat transfer and flow features of nanofluids. ASME J Heat Transf, 2003;125:151-155.

[23] Brinkman HC. The viscosity of concentrated suspensions and solutions. J Chem Phys, 1952;20:571-581.

[24] Azmi WH , Sharma KV , Rizalman M , Najafi G , Mohamad MS. The enhancement of effective thermal conductivity and effective dynamic viscosity of nanofluids. Renewable sustainable Enerqy Reviews,2016; 53:1046-1058.

[25] Ranjbarzadeh R, Karimipour A, Afrand, M, Isfahani AHM, Shirneshan A. Empirical analysis of heat transfer and friction factor of water/graphene oxide nanofluid flow in turbulent regime through an isothermal pipe. Applied Therm Engineering. 2017;126:538-547.

[26] Succi S.The lattice Boltzmann equation for fluid dynamics and beyond, first ed., Oxford, 2001.

[27]Bhatnagar L, P. Gross EP, Krook M. A Model for Collision Processes in Gases. I. Small Amplitude Processes in Charged and Neutral One-Component Systems. Phys. Rev.1954; https://doi.org/10.1103/PhysRev.94.511

[28] Guo Z, Zhao TS. A lattice Boltzmann model for convection heat transfer in porous media . Num Heat Transf Part B. 2005;47:157-177.

[29] Mussa MA , Abdullah S , Nor Azwadi CS , Muhamad N. Simulation of natural convection heat transfer in an enclosure by the lattice-Boltzmann method. Computers and Fluids. 2011;44:1162-168.

[30] He X, Chen S, Doolen G. A novel thermal model for the lattice Boltzmann method in incompressible limit. J Comp Phys.1998;146: 282-300.

[31] D'Orazio A, Karimipour A, Nezhad H, Shirani E. Lattice Boltzmann method with heat flux boundary condition applied to mixed convection in inclined lid driven cavity. Meccanica.2015;50: 945-962.

[32] Zou Q, He X. On pressure and velocity boundary conditions for the lattice Boltzmann BGK model. Phys. Fluids.1997;9:1591-1599.

[33] Alamyane AA, Mohamad AA. Simulation of forced convection in a channel with extended surfaces by the lattice Boltzmann method. Comput Math Appl. 2010;59:2421-2430.

[34] D'Orazio A, Corcione M, Celata GP. Application to natural convection enclosed flows of a lattice Boltzmann BGK model coupled with a general purpose thermal boundary condition. Int J Therm Sci. 2004;43:575-586.

[35] D'Orazio A, Succi S, Arrighetti C. Lattice Boltzmann simulation of open flows with heat transfer. Phys Fluids. 2003;15:2778-2781.

[36] D'Orazio A, Succi S. Simulating two-dimensional thermal channel flows by means of a lattice Boltzmann method with new boundary conditions. Future Generation Computer Systems. 2004;20:935-944.

[37] Thompson PA, Troian SM. A general boundary condition for liquid flow at solid surfaces. Phys Rev Lett. 1997;389:360-362.

[38] Ngoma GD, Erchiqui F. Heat flux and slip effects on liquid flow in a microchannel. Int J Therm Sci. 2007.46:1076-1083.

[39] Niu XD, Shu C, Chew YT. A thermal lattice Boltzmann model with diffuse scattering boundary condition for micro thermal flows. Comput Fluids. 2007;36:273-281.

[40] Akbarinia A, Abdolzadeh M, Laur R. Critical investigation of heat transfer enhancement using nanofluids in microchannels with slip and non-slip flow regimes. Appl Therm Eng. 2011;31:556–565.

[41] Santra AK, Sen S, Chakraborty N. Study of heat transfer due to laminar flow of copper–water nanofluid through two heated parallel plates isothermally. Int J Therm Sci. 2009.48:391–400.

General conclusion

The work developed in this thesis concerns the study of flows and transport in a micro-channel filled with nanofluid and flows and heat transfers in a porous macro-channel filled with nanofluid under conditions of local thermal equilibrium, taking into account the effect of viscous dissipation. The mathematical model governing these types of flow coupled with heat transfer is developed a numerical code based on the Lattice Boltzmann Method (LBM) to solve the conservation equations governing the physical problems. Firstly, convective heat flow (forced convection) and entropy generation in a porous channel filled with a nanofluid with top-bottom walls subjected to a constant heat flow is done. It was extended to simulate the flow governed by the Brinkman-Forchheimer-extended Darcy model. The incorporation velocity, temperature, entropy generation, average Nusselt number and Bejan number are investigated. The incorporation streamlines isotherms, slip velocity, wall temperature and Nusselt number has been achieved in the second case.

Numerical results obtained and those of literature show good agreement. Among these results, we can cite the following :

❖ **For the first case (porous channel)**

- The volume fraction of the nanoparticles leads to a rise in heat transfer and entropy generation while being reinforced by the porous medium permeability.
- Heat transfer rate rises by dropping Darcy number whatever the nanoparticles volume fraction. In addition, such an effect is more important at high intensity of viscous dissipation.
- Adding nanoparticles increases the average entropy generation rate (Nsav) as the heat capacity (Rc) and thermal conductivity (Rk) ratios increase, while increasing the Da number has the opposite effect.
- Increasing the nanoparticles volume fraction improves the nanofluid thermal conductivity and, thereby, the overall heat transfer.
- Irreversibilities within the heat transfer system (HTI) predominate only in the immediate vicinity of the channel walls due to the imposed thermal boundary conditions.

To sum up, obtaining less entropy generation and high system efficiency requires a suitable combination of the various key parameters of the flow deemed. Likewise, the MDF-TLBM approach has been shown to be effective in dealing with nanofluids flow in a porous medium with acceptable accuracy, which is of great importance to further deepen our understanding of the flow and the heat transfer process of nanofluids.

❖ **For the second case (micro-channel):**

- The buoyancy force and the inclination angle have strongly affected the shape of the velocity profile. Then, a rotational cell has appeared with the increase in Ri, and its size has been strongly affected by the buoyancy force and disappeared for $\gamma = 60°$. Thus, it can be concluded that the inclination effect dominates the Ri effects.
- The slip velocity at the top-bottom walls has reached optimal values depending on the combination of the Ri effects, the inclination angle and the slip velocity. These velocities have the same shape for all emerging parameters without gravity. In the presence of gravity, this shape has been strongly affected by Ri and the inclination angle.
- The temperature has shown a symmetric profile without gravity. Hence, the intensification of this parameter has improved heat transfer.
- The heat transfer rate at the outlet has linearly varied with the volume fraction regardless of the emerging parameters. Then, it has improved for lower values of Ri regardless of the inclination angle, and the slip velocity has increased.

Nomenclature

B=β/h	Dimensionless slip coefficient
Be	Bejan number
c	Lattice speed ($m.s^{-1}$)
C_p	Specific heat capacity at constant pressure ($KJ.Kg^{-1}.K^{-1}$)
c_s	Sound speed ($m.s^{-1}$)
D_H =2h	Hydrolic diameter (m)
Da	Darcy number, $Da = K / H^2$
Kn	Knudsen number
d_p	Average pore diameter (m)
Ec	Eckert number, $Ec = Uo^2 / (C_f . \Delta T_{ref})$
e_i	Discrete velocity in direction i
F_ε	Forchheimer form coefficient
F	Body force per unit mass ($N.Kg^{-1}$)
F_{ei}	Discrete body force in direction i ($Kg.m^{-3}.s^{-1}$)
f_i, g_i	Distribution function in direction i
f_i^{eq}, g_i^{eq}	Equilibrium distribution function in direction i
$\tilde{f}_i$, $\tilde{g}_i$	Modified distribution function
H	characteristic length scale (m)
L	Characteristich height scale (m)
K	Porous medium permeability (m^2)
K_R	Thermal conductivity ratio, $K_R = \lambda_s / \lambda_f$
L_s	Slip lenght (m)
l_{BF}	Mean free path of base fluid (pure water)
Ns	Entropy generation number
p	Pressure (Pa)
P	Dimensionless pressure
Pr	Prandtl number, $Pr = \nu_f / \alpha_f$
Re	Reynolds number, $Re = u_{in} H / \nu_f$
K_B	Boltzmann costant
q	Heat flux
Z_i	Heat dissipation
Nu_x	Local Nusselt number

Nu_m	Average Nusselt number
R	Gaz constant
r	Accomodation coefficient
Rc	Heat capacity ratio,
R_k	Thermal conductivity ratio
G_r	Grashof number
$Ri = G_r/\mathrm{R_e}^2$	Richardson number
T	Temperature (K)
T_m	PCM melting temperature (K)
t	Time (s)
u, v	Velocity ($m.s^{-1}$)
u_i	Inlet flow velocity ($m.s^{-1}$)
u_s	Dimensioneless slip velocity
U,V	Dimensionless velocity
x, y	Cartesiancoordinates (m)
X, Y	Dimensionless coordinates
Greek symbols	
∇	Gradient operator
$\nabla.$	Divergence operator
∇^2	Laplacian operator
Δx	Lattice step
Δt	Time step
β	Slip coefficient
α	Thermal diffusivity ($m^2.s^{-1}$)
ε	Media porosity
φ	Volume fraction
λ	Thermal conductivity ($W.m^{-1}.K^{-1}$)
μ_f	Dynamic fluid viscosity ($kg.m^{-1}.s^{-1}$)
Θ	Dimensionless temperature
ν	Kinematicviscosity ($m^2.s^{-1}$)
γ	Microchannel inclination angle
σ_T	Dynamique accomodation coefficient
σ_v	Thermal accomodation coefficient
ζ	Temperature jump distance
ψ	Total viscous dissipation
Ω	Collision operator
ρ	Density $kg.m-3$

$\tilde{t}$	Dimensionless time
$\tau_{f,g}$	Dimensionless relaxation time
w_i	Weight coefficient in direction *i*
Superscripts/subscripts	
f	Fluid
s	Solid
m	Number of network velocity
n	Space dimension
∘	Initial state
in	Inlet
out	Outlet
np	Nanoparticles
nf	Nanofluid
Ref	Reference